

**TEMPLATE-ASSEMBLED SYNTHETIC G-QUARTETS AS TARGETS FOR
ANTICANCER DRUGS**

by

Bo Liu

Bachelor of Science, Jilin University, 2010

A THESIS SUBMITTED IN PARTIAL FULFILLMENT OF
THE REQUIREMENT FOR THE DEGREE OF

MASTER OF SCIENCE

in

THE FACULTY OF GRADUATE STUDIES

(Chemistry)

THE UNIVERSITY OF BRITISH COLUMBIA

(Vancouver)

July 2012

© Bo Liu, 2012

ABSTRACT

DNA is a classic target for small-molecule ligands. In order to reduce significant toxicities of anticancer drugs resulting from unspecific interactions with DNA duplexes, it aroused great interest to investigate the specific interactions of ligands with a secondary DNA structure, G-quadruplex, formed by a guanine-rich DNA sequence. Induction and stabilization of G-quadruplex structures by ligands have been shown to inhibit telomerase activities and regulate the transcription and expression levels of oncogenes in cancer cells; therefore, the design of synthetic G-quartets under physiological conditions as minimal models of G-quadruplexes or artificial receptors of anticancer drugs has become an important and promising approach to clarify binding mechanisms, as well as to develop practical high-performance anticancer drugs. This thesis explores the recognition behavior of the second generation of hydrophilic template-assembled synthetic G-quartets (TASQs) using fluorescence spectroscopy and CD spectroscopy with PIPER, TMPyP4, AZATRUX, BSU 1051 and BRACO-19. The results show that PIPER, TMPyP4, AZATRUX can stack on top of a G-tetrad plane via π - π stacking with stoichiometries of 1:1 and high binding affinities ($K_{\text{PIPER}}=1.65\times 10^7 \text{ M}^{-1}$, $K_{\text{TMPyP4}}= 8.5\times 10^5 \text{ M}^{-1}$, $K_{\text{AZATRUX}}=2.55\times 10^6 \text{ M}^{-1}$); however, BSU 1051 and BRACO-19 have no such behavior with TASQs. All the spectra and binding mechanisms are similar to known mechanisms or computer-aided molecular simulation models, suggesting that the second generation of hydrophilic TASQs can imitate the natural terminal G-tetrad planes of G-quadruplexes. Moreover, this artificial receptor has selectivity over different ligands with an ability to

contribute to the screening of small-molecule ligands, as well as the investigations of binding mechanisms of new anticancer ligands.

The main works in this thesis are shown as follows:

1. Introduction to DNA duplexes, G-quadruplexes, template-assembled synthetic G-quartets, anticancer drugs (*i.e.* PIPER, TMPyP4, AZATRUX, BSU-1051, BRACO 19, telomestatin), and characteristic methods.
2. Synthesis of water-soluble template-assembled G-quartets (TASQ **13**), PIPER, and AZATRUX. The binding properties of these ligands with TASQ **13** were characterized by spectroscopic methods so as to show the binding abilities and binding modes of different drugs to TASQ **13**.
3. Conclusions and future work.

PREFACE

BSU 1051 and BRACO-19 were donated by Grant Bare. All the other compounds were synthesized by the author from the first step according to literature or group procedures. All optical spectra were performed by the author. All the work described in thesis chapter 2 is only in manuscript and unpublished.

TABLE OF CONTENTS

ABSTRACT	ii
PREFACE	iv
TABLE OF CONTENTS	v
LIST OF FIGURES	viii
LIST OF SCHEMES	xiii
LIST OF ABBREVIATIONS	xiv
ACKNOWLEDGEMENTS	xvi
CHAPTER 1 INTRODUCTION	1
1.1 An introduction to polymorphisms of DNA structures	1
1.1.1 DNA duplexes	1
1.1.2 Topologies of G-quadruplex	4
1.2 G-quadruplex as targets for anticancer small-ligand design	8
1.2.1 Biological functions of G-quadruplex	8
1.2.2 Biological functions of telomere and telomerase	9
1.2.3 The significance of designing ligands specifically targeting G-quadruplex	11
1.3 The interaction models between G-quadruplexes and small-molecule ligands	12
1.4 The methods to investigate the interaction between G-quadruplexes and small-molecule ligands	

.....	14
1.4.1 Circular dichroism (CD).....	15
1.4.2 Fluorescence emission spectroscopy.....	15
1.5 The small-molecule ligands based on G-quadruplexes	16
1.5.1 PIPER	17
1.5.2 Porphyrin derivatives	18
1.5.3 Triazatruxene derivatives.....	20
1.5.4 Amidoanthracene quinone derivatives	21
1.5.5 Acridine analogues.....	22
1.5.6 Telomestatin.....	23
1.6 Template-assembled synthetic G-quartets (TASQs).....	24
1.7 Thesis aims	29
CHAPTER 2 RESULTS AND DISCUSSION	32
2.1 Synopsis.....	32
2.2 Synthesis of hydrophilic template-assembled synthetic G-quartet (TASQ) and ligands	32
2.2.1 Convergent synthetic routes for TASQ 13	32
2.2.2 Synthetic routes for PIPER and AZATRUX.....	36
2.3 Ligand-binding studies	38
2.3.1 Interactions of PIPER with TASQ 13	40
2.3.2 Interactions of TMPyP4 with TASQ 13	47
2.3.3 Interactions of AZATRUX with TASQ 13	55

2.3.4 Interactions of BSU 1051 with TASQ 13.....	60
2.3.5 Interactions of BRACO-19 with TASQ 13.....	63
2.4 Experimental.....	65
2.4.1 Synthesis of hydrophilic template-assembled synthetic G-quartets (TASQs) and ligands.....	65
2.4.2 Ligand binding studies.....	75
2.4.2.1 Preparation of the sample.....	75
2.4.2.2 Fluorescence emission spectroscopy.....	76
2.4.2.3 Circular dichroism (CD).....	77
2.5 Supplementary ¹ H-NMR spectra.....	78
CHAPTER 3 CONCLUSIONS AND FUTURE WORK.....	80
REFERENCES.....	82

LIST OF FIGURES

Fig 1.1 Base pairs (C-G, T-A) and B-DNA double helix structure	2
Fig 1.2 (a) A-DNA; (b) B-DNA; (c) Z-DNA	3
Fig 1.3 (a) Hoogsteen hydrogen bond for G-quartet formation; (b) G-quartet; (c) G-quadruplex composed of the stacking of G-quartets	5
Fig 1.4 (a) Intramolecular G-quadruplex: D , E , and F ; bimolecular G-quadruplex: B and C ; tetramolecular G-quadruplex: A ; (b) Structural polymorphisms of G-quadruplexes. A : parallel tetramolecular; B : parallel bimolecular; C : antiparallel bimolecular; D : parallel propeller-type; E : antiparallel basket-type; F : hybrid-type.	6
Fig 1.5 Loop regions of a G-quadruplex: (a) lateral loop; (b) diagonal loop; (c) propeller loop	7
Fig 1.6 G-quadruplex/ligands binding modes: (a) external π - π stacking; (b) intercalation; (c) non-specific interaction	13
Fig 1.7 PIPER	18
Fig 1.8 (a) TMPyP2; (b) TMPyP4	20
Fig 1.9 AZATRUX	21
Fig 1.10 BSU 1051	22
Fig 1.11 (a) disubstituted acridine compound; (b) BRACO-19	23
Fig 1.12 Telomestatin	24
Fig 1.13 TASQs: a-c) the first generation of lipophilic TASQ; d) the first generation of hydrophilic TASQ.	26

Fig 1.14 Dimerization of first generation of lipophilic TASQ in chloroform in the presence of cesium cation.....	27
Fig 1.15 Phosphate linked TASQ in methanol.....	28
Fig 1.16 The second generation of hydrophilic TASQ	28
Fig 2.1 Fluorescence spectrum of PIPER alone (0.5 μ M) at pH 6.5 (pink), 7 (black), 7.5 (blue), and 8 (red).....	40
Fig 2.2 Job plot analysis of fluorescence binding data for PIPER and TASQ 13 . The total molar concentration ([PIPER]+[TASQ 13]) was 0.5 μ M.....	41
Fig 2.3 Scatchard plot analysis of fluorescence binding data for PIPER (0.5 μ M) in absence and presence of successive additions of TASQ 13 in the range of 0-5 μ M at 25 $^{\circ}$ C.	42
Fig 2.4 Fluorescence spectrum of PIPER (0.5 μ M) in absence and presence of successive additions of TASQ 13 in the range of 0-5 μ M at 25 $^{\circ}$ C. Arrows indicate the increasing TASQ 13 concentrations.	43
Fig 2.5 (a) Fluorescence binding plot of PIPER (0.5 μ M) on increasing TASQ 13 concentrations in the range 0-5 μ M in 0.1 mM EDTA, 10 mM Tris-HCl (black); (b) Salt-affected fluorescence binding plot of PIPER (0.5 μ M) on increasing TASQ 13 concentrations in the range 0-5 μ M in 0.1 mM EDTA, 10 mM Tris-HCl, 100 mM KCl (red).	45
Fig 2.6 (a) CD spectrum of PIPER alone (10 μ M, red); (b) TASQ 13 alone (10 μ M, black); (c) TASQ 13 and PIPER (10 μ M and 10 μ M, blue).	46

Fig 2.7 Fluorescence spectrum of TMPyP4 alone (0.5 μ M) at pH 6.5 (pink), 7 (black), 7.5 (blue), and 8 (red).....	48
Fig 2.8 Job plot analysis of fluorescence binding data for TMPyP4 and TASQ 13 . The total molar concentration ($[\text{TMPyP4}] + [\text{TASQ } \mathbf{13}]$) was 8 μ M.	49
Fig 2.9 Scatchard plot analysis of fluorescence binding data for TMPyP4 (8 μ M) in absence and presence of successive additions of TASQ 13 in the range of 0-80 μ M at 25 $^{\circ}$ C.	50
Fig 2.10 Fluorescence spectrum of TMPyP4 (8 μ M) in absence and presence of successive additions of TASQ 13 in the range of 0-80 μ M at 25 $^{\circ}$ C. Arrows indicate the increasing TASQ 13 concentrations.....	51
Fig 2.11 (a) Fluorescence binding plot of TMPyP4 (8 μ M) on increasing TASQ 13 concentrations in the range 0-80 μ M in 0.1 mM EDTA, 10 mM Tris-HCl (black); (b) Salt-affected fluorescence binding plot of TMPyP4 (8 μ M) on increasing TASQ 13 concentrations in the range 0-80 μ M in 0.1 mM EDTA, 10 mM Tris-HCl, 100 mM KCl (red).....	52
Fig 2.12 (a) CD spectrum of TMPyP4 alone (10 μ M, black); (b) TASQ 13 alone (10 μ M, red); (c) TASQ 13 and TMPyP4 (10 μ M and 10 μ M, blue).....	53
Fig 2.13 Fluorescence spectrum of AZATRUX alone (0.5 μ M) at pH 6.5 (pink), 7 (black), 7.5 (blue), and 8 (red).....	55
Fig 2.14 Job plot analysis of fluorescence binding data for AZATRUX and TASQ 13 . The total molar concentration ($[\text{AZATRUX}] + [\text{TASQ } \mathbf{13}]$) was 3.6 μ M.	56

Fig 2.15 Scatchard plot analysis of fluorescence binding data for AZATRUX (3.6 μM) in absence and presence of successive additions of TASQ 13 in the range of 0-36 μM at 25 $^{\circ}\text{C}$	57
Fig 2.16 Fluorescence spectrum of AZATRUX (3.6 μM) in absence and presence of successive additions of TASQ 13 in the range of 0-36 μM at 25 $^{\circ}\text{C}$. Arrows indicate the increasing TASQ 13 concentrations.....	58
Fig 2.17 (a) Fluorescence binding plot of AZATRUX (3.6 μM) on increasing TASQ 13 concentrations in the range 0-36 μM in 0.1 mM EDTA, 10 mM Tris-HCl (black); (b) Salt-affected fluorescence binding plot of AZATRUX (3.6 μM) on increasing TASQ 13 concentrations in the range 0-36 μM in 0.1 mM EDTA, 10 mM Tris-HCl, 100 mM KCl (red).....	59
Fig 2.18 Fluorescence spectrum of BSU 1051 alone (1 μM) at pH 6.5 (pink), 7 (black), 7.5 (blue), and 8 (red).....	60
Fig 2.19 Fluorescence spectrum of BSU 1051 (1 μM) in absence and presence of successive additions of TASQ 13 in the range of 0-10 μM at 25 $^{\circ}\text{C}$	61
Fig 2.20 (a) CD spectrum of BSU 1051 alone (10 μM , blue); (b) TASQ 13 alone (10 μM , black); (c) TASQ 13 and BSU 1051 (10 μM and 10 μM , red).....	62
Fig 2.21 Fluorescence spectrum of BRACO-19 alone (1 μM) at pH 6.5 (pink), 7 (black), 7.5 (blue), and 8 (red).....	63
Fig 2.22 Fluorescence spectrum of BRACO-19 (1 μM) in absence and presence of successive additions of TASQ 13 in the range of 0-10 μM at 25 $^{\circ}\text{C}$	64

Fig 2.23 ¹ H-NMR Spectrum of TASQ 13 in D ₂ O at 400 MHz.....	78
Fig 2.24 ¹ H-NMR Spectrum of PIPER 15 in D ₂ O at 300 MHz	79
Fig 2.25 ¹ H-NMR Spectrum of AZATRUX 19 in CDCl ₃ at 300 MHz.....	79

LIST OF SCHEMES

Scheme 2.1 Synthetic route for the tetraol cavitand 7	33
Scheme 2.2 Synthetic route for silyl deoxyguanine 10	34
Scheme 2.3 Synthetic route for TASQ 13	35
Scheme 2.4 Synthetic route for PIPER 15	37
Scheme 2.5 Synthetic route for AZATRUX 18	37

LIST OF ABBREVIATIONS

Å	angstroms
Ac	acetyl
AZATRUX	5,10,15-tris[4(1-piperidino)butyl]diindolo[3,2-a:3',2'-c]carbazole
bp	base pairs
Bu	butyl
BRACO-19	<i>N,N'</i> -(9- {[4-(dimethylamino)phenyl]amino} acridine-3,6-diyl)bis(3-pyrrolidin-1-yl)propanamide) trihydrochloride
BSU 1051	2,6-diaminoanthraquinone
CD	circular dichroism
DCM	dichloromethane
DIPEA	<i>N,N</i> -diisopropylethylamine
DMF	dimethylformamide
DMSO	dimethylsulfoxide
DNA	deoxyribonucleic acid
EB	Ethidium bromide
EDTA	ethylenediaminetetraacetic acid
ESI	electrospray ionization
Et	ethyl
h	hour
<i>i</i> -Pr	isopropyl

Ibu	isobutyryl
IC ₅₀	inhibition concentration for 50 % telomerase activity
kb	kilo bases
Me	methyl
min	minute
MALDI-TOF	matrix assisted laser desorption and ionization - time of flight
MS	mass spectrometry
NOESY	nuclear Overhauser effect spectroscopy
NMR	nuclear magnetic resonance
PIPER	<i>N,N'</i> -Bis[2-(1-piperidino)ethyl]-3,4,9,10-perylenetetracarboxylic diimide
RNA	ribonucleic acid
rt	room temperature
<i>t</i> -Bu	<i>tert</i> -butyl
TASQ	template assembled synthetic G-quartet
TBAF	tetra- <i>n</i> -butylammonium fluoride
TBS	<i>tert</i> -butyldimethylsilyl
TMPyP4	<i>meso</i> -5,10,15,20-tetrakis-(<i>N</i> -methyl-4-pyridyl)porphine tetratosylate
THF	tetrahydrofuran
Tris	tris(hydroxymethyl)aminomethane
UV/VIS	ultraviolet/visible

ACKNOWLEDGEMENTS

I would like to thank my supervisor Professor John Sherman for providing me an opportunity to carry out research in his group and for giving me a great help not only for this thesis project but also my seminar and course work. I would like to thank past and current group members for helpful discussion and support including Grant Bare, Ben Hui, Hui Yang, and Jon Freeman. Thank you to Yun Ling and Maria Ezhova for Mass spectrometry and NMR spectroscopy training.

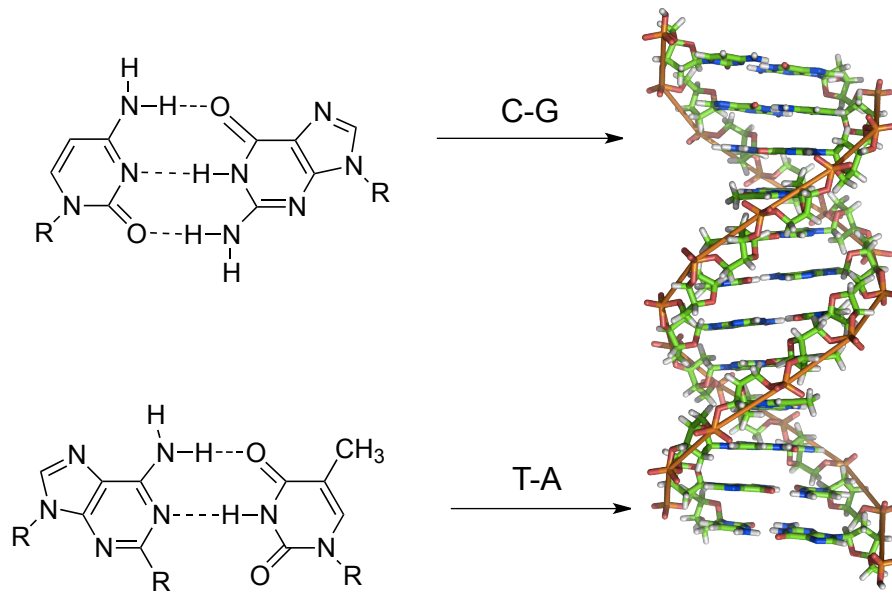
CHAPTER 1 INTRODUCTION

1.1 An introduction to polymorphisms of DNA structures

1.1.1 DNA duplexes

In 1953, Crick and Watson proposed the double helix model of deoxyribonucleic acid structure (Fig 1.1), explaining the replication of DNA templates.¹ Since then, DNA has become a major topic in molecular biology. Although the major structure of DNA is a B-type double helix, there are also other kinds of DNA structures such as A-type and Z-type double helices. The transitions between these DNA structures can influence gene transcriptions and expressions. In addition, from a classical double helical DNA to a specific G-quadruplex, the polymorphisms of DNA structures result in colorful biological functions.²

Fig 1.1 Base pairs (C-G, T-A) and B-DNA double helix structure³

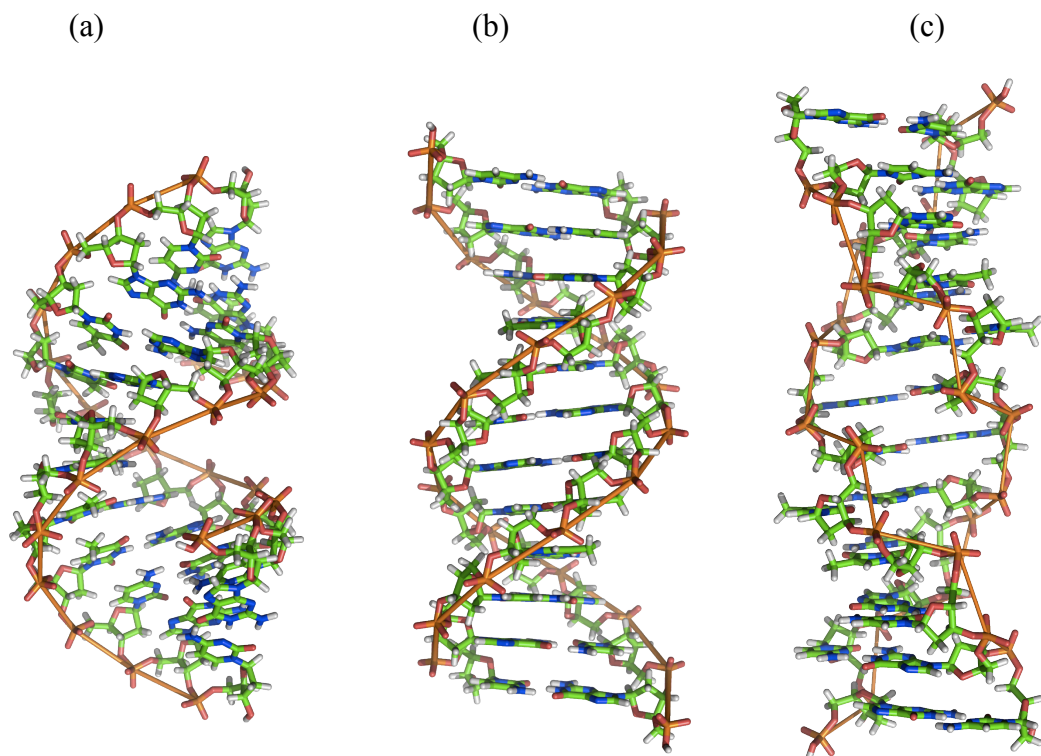


B-DNA's two main chains are both composed of deoxyriboses and phosphates. Two backbones form a right-handed helix around a common axis (Fig 1.1). The B-type double helix is normally very stable. The main forces to stabilize it are hydrogen bonds, π - π stacking between up and down aromatic nearby bases, and electrostatic interactions between negative oxygens of phosphates and metal cations.^{4,5}

However, in special situations, the molecular configuration of B-type deoxyribonucleic acid can be changed, forming an A-type DNA (Fig 1.2).^{6,7} A-DNA is still right-handed, but has a much bigger and flatter conformation than B-DNA (Fig 1.2). A-DNA double helix is formed from the association of a DNA template and an RNA strand transcribed from the corresponding DNA template chain (DNA: RNA hybrid duplexes). Moreover, if two DNA strands are replaced by two RNA strands, the double helix structure is also A-DNA (RNA: RNA hybrid duplexes).^{8,9}

On the other hand, a DNA structure will be left-handed when the sequence is arranged alternatively of guanines and cytosines, such as a self-complementary sequence d(GCGCGCGCGC). The shape of phosphates along the backbone is in a Z-like shape, so this type of DNA is called Z-DNA (Fig 1.2). The Z-DNA conformation is generally not thermodynamic stable because there is a very large electrostatic repulsion force between the two negative phosphate groups near each other; however, this unfavored conformation is still necessary in the human body, since it is a good potential site for helicase to anneal two nucleic acid strands.¹⁰

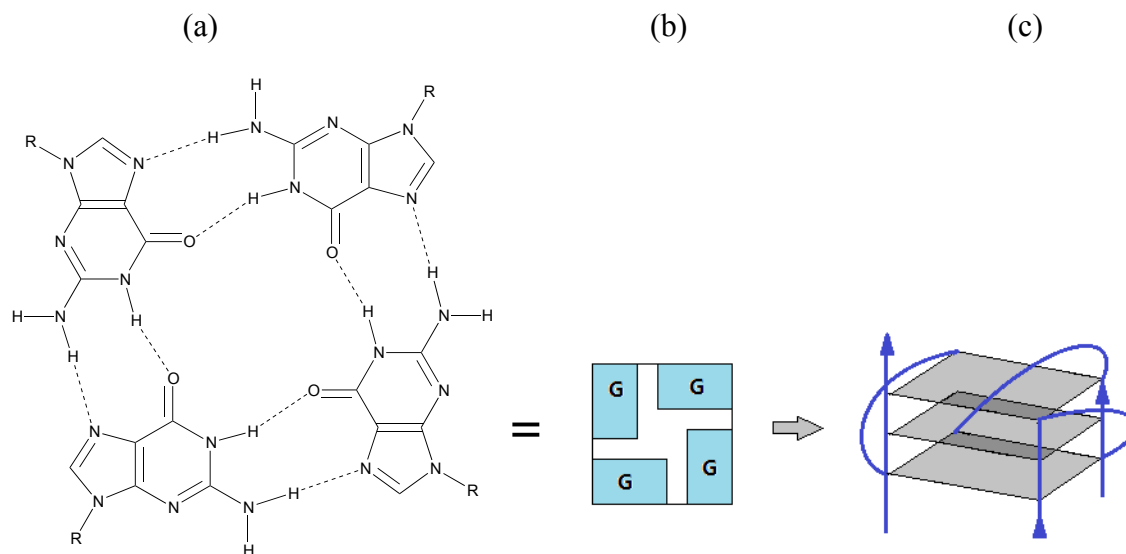
Fig 1.2 (a) A-DNA; (b) B-DNA; (c) Z-DNA¹¹



1.1.2 Topologies of G-quadruplex

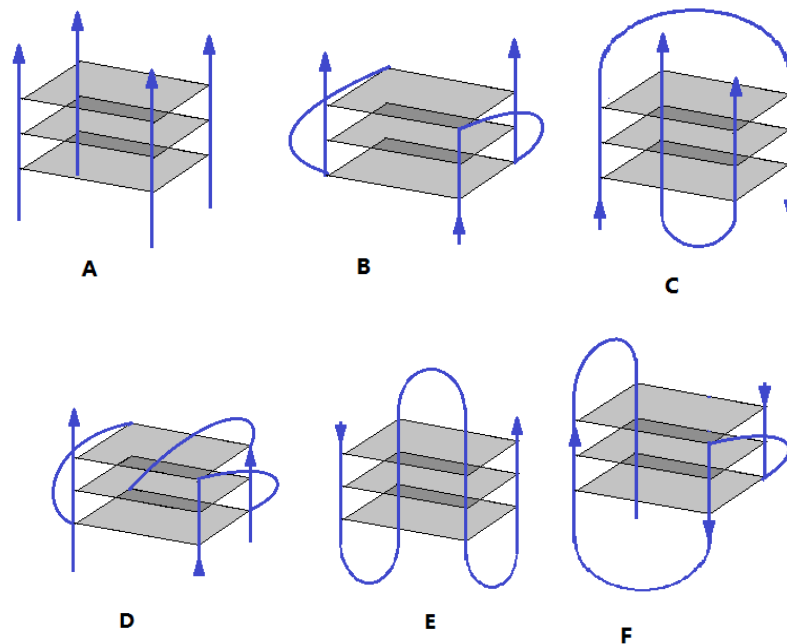
Another nucleic acid conformation is a kind of special secondary DNA structure: G-quadruplex (Fig 1.3 c). In 1962, Davies proposed this helix formation concept and suggested that a G-quartet is the basic subunit of G-quadruplex structures.¹² Different from a DNA duplex, a G-quadruplex is composed of the stacking of G-quartets (Fig 1.3 b). The four guanines can form a G-tetrad ring through the Hoogsteen hydrogen bond (Fig 1.3 a).¹³ Metal cations, small molecular ligands, and molecular crowding conditions can induce the formation of a G-quadruplex.¹⁴ In the late 1980s, *in vitro* experiments demonstrated this monovalent cation-induced G-quartet model on the G-rich sequence of a telomere end.¹⁵ A bioinformatics study predicted that 43% of the promoter regions in the human genome could form a G-quadruplex structure.¹⁶ Some important eukaryotic promoter regions (*e.g. c-myc*) have already been shown to form a G-quadruplex.¹⁷ The stabilization of G-quadruplex structures can influence the formation of tumors.¹⁸ In order to explore the feasibility of G-quadruplexes as targets for anticancer drugs, it is important to design different G-quadruplexes or G-quartets.

Fig 1.3 (a) Hoogsteen hydrogen bond for G-quartet formation; (b) G-quartet; (c) G-quadruplex composed of the stacking of G-quartets



G-rich sequences can form G-quadruplexes in two main ways: intermolecular and intramolecular G-quadruplexes (Fig 1.4 a). The intramolecular G-quadruplex is folded with one DNA molecule. The intermolecular G-quadruplex is composed of bimolecular (hairpin structure) or tetramolecular DNA (tetramer).¹⁹ The different positions of these guanines result in the diversities of G-quadruplex topologies. Four strands in a G-quadruplex are arranged as follows: 1) four strands are all parallel; 2) three strands are parallel, one strand is anti-parallel; 3) the nearby strands are parallel; 4) alternatively parallel.²⁰ From these different arrangements of strands, it forms different conformations of a G-quadruplex: 1) parallel, such as intermolecular tetramer and intramolecular propeller-type; 2) hybrid-type; 3) anti-parallel, such as basket-type and chair-type (Fig 1.4 b).²¹

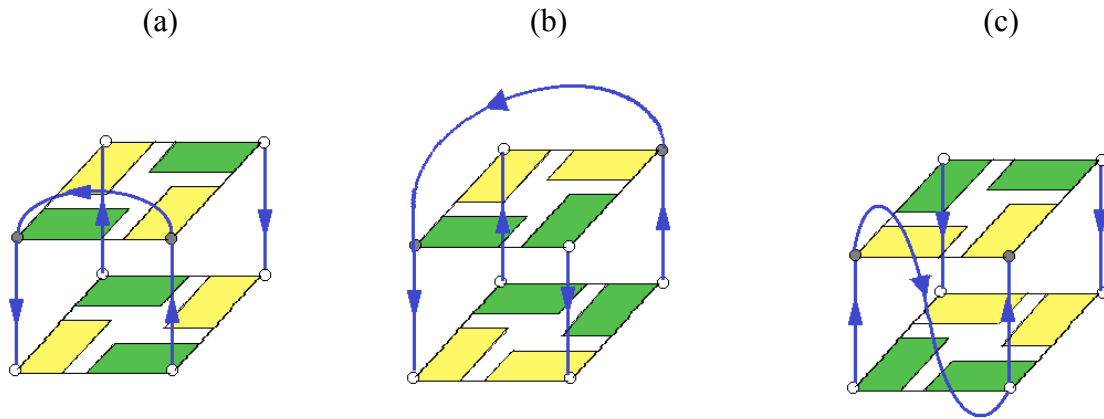
Fig 1.4 (a) Intramolecular G-quadruplex: **D**, **E**, and **F**; bimolecular G-quadruplex: **B** and **C**; tetramolecular G-quadruplex: **A**; (b) Structural polymorphisms of G-quadruplexes. **A**: parallel tetramolecular; **B**: parallel bimolecular; **C**: antiparallel bimolecular; **D**: parallel propeller-type; **E**: antiparallel baske-type; **F**: hybrid-type.



In the meanwhile, the different arrangements of G-strands induce different kinds of loops, including a propeller loop, a lateral loop, and a diagonal loop (Fig 1.5).²² In a propeller G-quadruplex, a propeller loop is formed with two inversions between top and bottom G-quartets. In an anti-parallel G-quadruplex, a propeller loop exists between the two guanines on the same G-quartet surface. When two loop-linking DNA strands are near each other, it forms a lateral loop. When two loop-linking DNA strands are in the diagonal, a diagonal loop will be formed on top of a G-tetrad surface. In general, the sequences and lengths of G-quadruplex loops will have big

influences on the topology of a G-quadruplex.²³

Fig 1.5 Loop regions of a G-quadruplex: (a) lateral loop; (b) diagonal loop; (c) propeller loop



G-quadruplex bears an important character that the stacking of G-quartets forms a cavity to selectively coordinate with certain metal cations, such as K^+ , Na^+ , Sr^+ .²⁴ This cavity has high electron density, because it is surrounded by eight-carbonyl oxygen from G-tetrads. Metal cations also have an important influence on the topology of a G-quadruplex. The positively charged ions can induce the formation of G-quartets from a G-rich sequence, increasing the stability of coordinates. The ability to stabilize G-quartets is as follows: $K^+ \gg Na^+ > Rb^+ > Cs^+ > Li^+$, and $Sr^{2+} > Ba^{2+} > Ca^{2+} > Mg^{2+}$.²⁵

Though distinctive G-rich sequences can form different G-quadruplexes, one unique sequence is also able to compose diverse G-strands, such as the sequence $d[GGG(TTAGGG)_3]$. In sodium solutions, this sequence readily forms an anti-parallel basket conformation with two lateral loops and one diagonal loop;²⁶ however, in potassium solutions, this telomeric sequence is predominantly a hybrid-type G-quadruplex conformation with two lateral loops, and one propeller loop.²⁷

Furthermore, the human telomeric G-rich sequence d[TTAGGG]_n (n>200) has potential to form a super secondary structure via the self-assembly of propeller and hybrid-type DNA tetraplexes.²⁸

In summary, a G-rich sequence can form diverse topologies of G-quadruplexes according to the quantity of G-quartets, the size and sort of loops, and the type of metal cations.

1.2 G-quadruplex as targets for anticancer small-ligand design

In the human genome, almost 376,000 kinds of G-sequences may be able to comprise G-quadruplexes, and most of these G-quadruplexes are in the dynamic process of forming and unraveling from DNA double helices.²⁹ Because of the coexistence of DNA duplex and quadruplex, it is challenging to design the functional small ligands to selectively bind to certain structures. What is more important, by studying the structures and binding mechanisms of targets (*e.g.* G-quartet's surfaces, loops, grooves), artificial anticancer drugs can be obtained by the diversity-oriented synthesis.

1.2.1 Biological functions of G-quadruplex

In the human genome, many gene regions contain G-rich sequence, such as telomeric ends.³⁰ In the cell, G-quadruplex is a vital structure to switch on/off biological functions: the stabilization of a G-quadruplex can inhibit gene transcriptions and expressions; in reverse, the unraveling of this

secondary structure will restore transcription and expression functions. Therefore, artificial designed small ligands can induce the stabilization of tetraplexes in order to inhibit gene transcriptions and expressions, resulting in the apoptosis of tumor cells. Hence, the structure and biological function of G-quadruplexes are very important for an anticancer drug design.^{31,32}

1.2.2 Biological functions of telomere and telomerase

The number of normal cell divisions in the human body is genetically fixed in a life course, according to different cell types, generally splitting 60-100 times.³³ Telomeres are composed of chromosome ends and telomere-binding proteins. The human telomere is the repeats of G-rich sequence $d[5'-TTAGGG-3']_n$ ($n>200$). The main structure of telomere is a DNA duplex (GT paired with CA); however, there is a G-overhang strand at the 3' end.³⁴ This G-overhang is turned back to the certain region of telomere as a T-loop rather than attached to the end of the double helix.³⁵ In addition, the T-loop can close a chromosome end in order to protect it from degradation by chemical modifications or ribozymes, to prevent the loss during chromosome replications, and to inhibit the unstable structure of chromosome end-end fusion.^{36,37}

Telosome/shelterin is the binding protein at the telomere end, including telomeric repeat binding factor 1 (TRF1), binding factor 2 (TRF2), protection of telomeres 1 (POT1), TRF1-interacting nuclear protein 2 (TIN2), TIN2-interacting protein 1 (TPP1), and repression and activation protein 1 (Rap1).³⁸ TRF1 can regulate the telomere length. The over-expression of TRF1 can result in shortening the telomere length. TRF2 is to protect the chromosome end, and prompting Rap1 to the

telomere. The loss of TRF2 will damage the telomere end, thus inducing the end-end fusion. POT1 can regulate telomerase activities.³⁹

The length of telomere is crucial to the growth and apoptosis of a cell. After one replication circle, the length of telomere will decrease 50-200 bp. If gene regions continue shortening, the cell will be transformed into an aging and apoptosis period. The cell death can be divided into two stages: aging cycle (M1) and crisis cycle (M2). While the telomere length is 2-24 kb, the cell will enter the M1 stage with the destabilization of chromosomes. P53 and p16 genes will regulate the cell growth. If p53 and p16 genes are deactivated, the life of the cell will enter the M2 stage. Most cells will die because of the end-end fusion of unstable chromosomes. Only minority cells will activate telomerase so that telomere functions are restored, and cells become immortalized.⁴⁰

Telomerase is a specific DNA polymerase dependent on RNA. It solves the chromosome end replication problem, because telomerase can increase the number of repeating sequences and the length of telomere so that the cell will be immortalized.⁴¹ Telomerase activity is very high in an embryonic development; however, in mature somatic cells telomerase activity will be closed in order to regulate the growth, differentiation and aging of cells. However, according to the statistical analysis in tumor tissues, the positive telomerase activity rate in malignant tissues is from 84% to 95%, whereas in benign tumors and normal tissues, the positive telomerase activity rate is only 4%.⁴² Cell immortalization is a prerequisite for the transformation from normal cells to malignant cells, and some mutant cells can be transformed into immortalized cells via the M2 period. A constant telomere length and an increasing telomerase activity will force cells to generate dominant tumor genes; thus normal cells will become cancer cells, suggesting that telomerase and cancer genes have a close

relationship and telomerase activities are intimately linked to the formation of cancer cells.⁴³ In addition, the interference of telomerase activity has no critical impact on normal cells.⁴⁴ This special relationship of telomerase activity and cancer cells makes a very important value in the diagnosis and treatment of cancer. So the research into drugs that target telomerase and its substrate telomere has aroused widespread concern.

1.2.3 The significance of designing ligands specifically targeting G-quadruplex

DNA is the most effective anticancer target, since drugs can fundamentally inhibit the reproduction of cancer cells. The current drugs in use are DNA alkylating agents as well as some anti-tumor antibiotics. These kinds of drugs have many toxic effects due to the non-selective binding with a double helical DNA. So it is very important to develop novel drugs specifically binding to cancer cells with less toxicity. The human telomere can form a G-quadruplex structure, resulting in the loss of a linear DNA structure required by telomerase reverse transcriptions, gene transcriptions and gene expressions;⁴⁵ therefore, small-molecule ligands can induce and stabilize a G-quadruplex structure so as to inhibit telomerase activities. As a result, these induced G-quadruplex structures can stimulate the apoptosis of cancer cells.⁴⁶

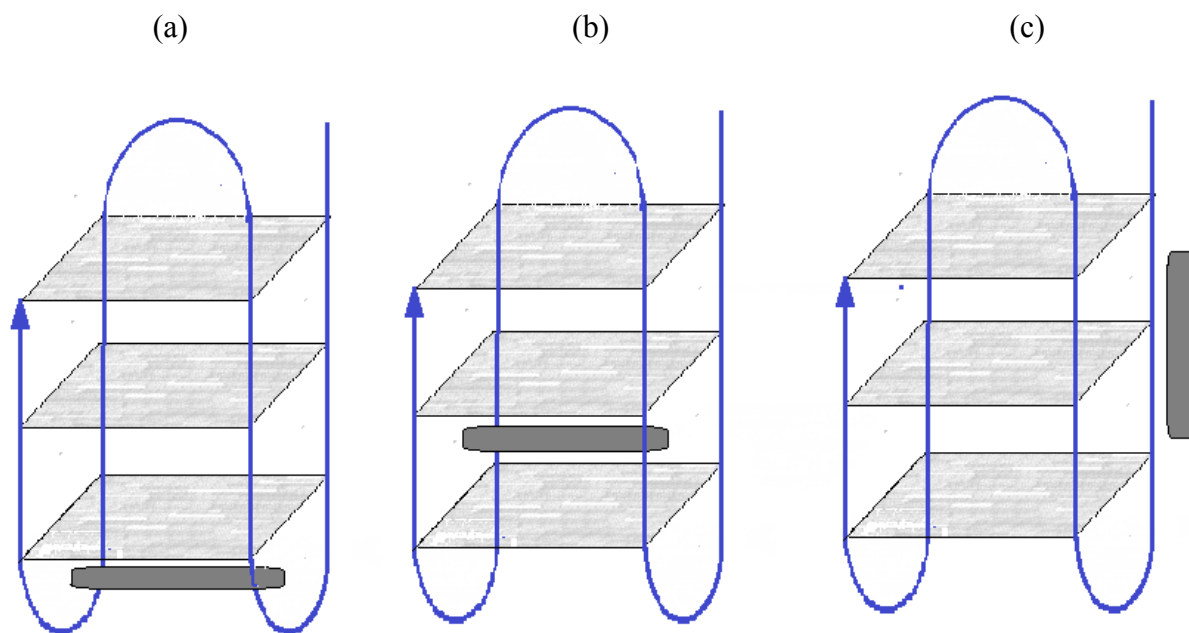
In addition, a G-quadruplex holds different structures (*e.g.* G-quartets, varieties of loops and grooves) from a DNA duplex. The special structure and biological functions mentioned above show the possibility to develop less toxic therapy by means of designing G-quadruplex targeted small ligands. In particular, the binding between small-molecule ligands and G-quadruplexes must be

selective; otherwise these drugs will affect normal DNA cells and produce unwanted side effects.⁴⁷

1.3 The interaction models between G-quadruplexes and small-molecule ligands

G-quadruplex has a special geometric structure different from the ordinary double helix DNA so that small-molecule ligands can specifically recognize G-quadruplex templates through different binding sites and binding modes.⁴⁸ G-quadruplex/ligand binding sites include G-tetrads, grooves, loops and ion channels.⁴⁹ So G-quadruplex/ligand binding modes include: 1) external π - π stacking at the end of a G-quadruplex; 2) “threading” intercalation of small-molecule ligands into the body of a G-quadruplex; 3) non-specific interactions in grooves and loops through hydrogen bonds and electrostatic interactions (Fig 1.6).⁵⁰

Fig 1.6 G-quadruplex/ligands binding modes: (a) external π - π stacking; (b) intercalation; (c) non-specific interaction



1) External π - π stacking binding mode

From a NMR spectroscopic study, a porphyrin derivative (TMPyP4) and *c-myc* G-quadruplex DNA was binding through an external π - π stacking interaction.⁵¹

2) Groove binding mode

From a NMR spectroscopic study and theoretical computer model, the stoichiometry of distamycin A with G-quadruplex DNA d[*TGGGGT*]₄ was 4:1. Two distamycin A dimers had interactions with two opposite grooves of a G-quadruplex.⁵²

3) Loop binding mode

X-ray single crystal studies have shown that the formation of tetra-substituted naphthalene diimide and G-quadruplex DNA (d[*TAGGG(TTAGGG)*]₃) complexes had a stoichiometry of

3:1, suggesting one ligand was stacking on top of a G-quartet's surface and another two ligands were non-specifically binding to a TTA loop.⁵³

4) Ion channel electrostatic binding mode

Nuclear magnetic resonance spectroscopy and CD spectroscopy studies have shown that AR-DETA could induce a disordered G-single strand DNA (d[TTAGGG]₄) to form a propeller-type G-quadruplex structure in buffer solutions without any metal cations. The results suggested that the anthracene ring of AR-DETA can stack on top of a G-quartets surface, and the side chain was protonated to simulate the function of metal cations resulting in electrostatic interactions between the positively charged side chain of the ligand and the high electron density ion channel of a G-quadruplex.⁵⁴

5) Intercalation binding mode

Intercalation-binding modes play important roles in DNA duplex drugs; however, it is difficult for the agents to be inserted into the body of a G-quadruplex because of a stable and rigid tetraplex structure and a high-energy demand of conformational change. Therefore, potential binding ligands are always inclined to an external stacking mode. However, a computer modeling study has shown that a BSU-1051 and G-quadruplex complex was based on the “threading” intercalation binding mode.⁵⁵

1.4 The methods to investigate the interaction between G-quadruplexes and small-molecule ligands

A variety of biophysical methods (*e.g.* fluorescence spectroscopy, circular dichroism spectroscopy,

and nuclear magnetic resonance) to investigate the interactions of ligand and double helical DNA can be used to study G-quadruplex/ligand interactions.⁵⁶ By these methods, it is possible to obtain the binding model, binding constant, and stoichiometry of G-quadruplex/ligand complex.

1.4.1 Circular dichroism (CD)

CD spectroscopy is the most convenient and direct method to the investigation of DNA secondary structure, so it is widely used to study G-quadruplex conformational changes and its thermodynamic behavior. A parallel type G-quadruplex has maxima at 265 nm and minima at 240 nm; an anti-parallel type G-quadruplex has maxima at 295 nm and minima at 260 nm; a hybrid G-quadruplex has maxima at 290 nm, and a shoulder at 265 nm.⁵⁷ These special peaks can distinguish different DNA secondary structures. Furthermore, CD spectroscopy is a highly sensitive method. It is even feasible to obtain the spectrum of a sample at the concentration of micro molar level.⁵⁸ When small-molecule ligands bind to a G-quadruplex, the characteristic absorption of CD spectra can show the structural influence of ligands and their binding modes.

1.4.2 Fluorescence emission spectroscopy

Fluorescence emission spectroscopy is a primary means for study of small molecules and nucleic

acid interactions. The excitation light can excite fluorescent materials. The electron will be transitioned from a ground state to a higher energy level (excited state). After this process, part of the energy will be consumed by an internal conversion so that the electron can reach the lowest vibrational state of the higher electronic energy level. And then, the electron goes back to the ground state and photons will be ejected to form the fluorescence at the same time. When a ligand binds to a DNA, its luminous intensity will generally increase due to an inhibited vibration mode, less water molecule quenching, and the protection from the environment of hydrophobic bases. Binding abilities can be determined by fluorescence intensity changes. Moreover, Ethidium bromide (EB) competition experiments can be done at room temperature for non-fluorescent compounds. EB itself has very weak fluorescence intensity. Once EB is inserted into a DNA molecule, the fluorescence intensity will be greatly increased; however, after adding ligands, the enhanced fluorescence will be partially or all quenched.⁵⁹ The degree of quenching determines the ligand binding ability compared with EB.⁶⁰ EB and DNA binding fulfills a Scatchard equation: $\gamma / C = K (n - \gamma)$, where γ is the average number of binding EB molecules; n is the number of binding sites for each DNA; k is binding constants; C is the concentration of free EB molecules.⁶¹ A Scatchard plot can be obtained by plotting γ/C versus γ .

1.5 The small-molecule ligands based on G-quadruplexes

In 1997, Sun reported the first small telomerase inhibitor based on a G-quadruplex target, and since then multiple research groups have synthesized various types of potential anticancer drugs

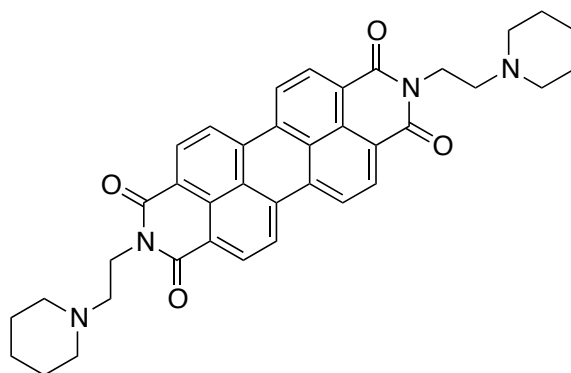
targeting G-quadruplexes.⁶² In order to design specific G-quadruplex ligands, it is critical to consider G-quadruplex/ligand interaction modes. For the majority of small-molecule ligands, the binding mode is established on π - π stacking and electrostatic interactions, so aromatic and charged ligands have been widely discussed. Meanwhile, ligands binding with quadruplex grooves, convex loops, and negatively charged ion channels have also aroused widespread attention. In recent years, the field of G-quadruplex binding ligands has achieved significant development, followed by several important small-molecule ligands. These small molecules can be divided into three main categories according to their structural characteristics: 1) fused ring aromatic system; 2) macro-ring system; 3) non-coplanar molecule system. Herein, some representative ligands will be introduced.

1.5.1 PIPER

As illustrated in Fig 1.7, the fused ring perylene derivative PIPER (*N,N'*-Bis[2-(1-piperidino)-ethyl]-3,4,9,10-perylenetetracarboxylic diimide) has a strong interaction with G-quadruplexes. PIPER was found by the application of computer-aided drug design with a half-inhibition rate (IC₅₀) lower than 1000 nM.⁶³ PIPER can stack on the plane of a G-tetrad, and its selectivity is related to PIPER's own self-aggregation. Perylene compounds with two-molecule aggregation bind poorly to double helical DNA, and thus have better selectivity to G-quadruplexes.⁶⁴ Another notable feature of PIPER is that PIPER can facilitate the rate of formation of hairpin bimolecular G-quadruplex by about 100 times,⁶⁵ and PIPER is able to induce the transition in the *c-myc* promoter region from DNA duplex strands to G-quadruplex structures.⁶⁶ In addition, pH has an influence on the selectivity

of PIPER. Under a low pH condition, PIPER exists as a single molecule and has similar binding constants with a double-stranded DNA and a tetraplex DNA; however, under a high pH condition, PIPER can aggregate so as to have a better selectivity with G-quadruplex structures.⁶⁷ In addition, the side chains of PIPER have an influence on its ability to induce a G-quadruplex structure, and also have an influence on stoichiometry and binding complex conformation due to the electrostatic interaction with the grooves of G-quadruplexes.⁶⁸

Fig 1.7 PIPER

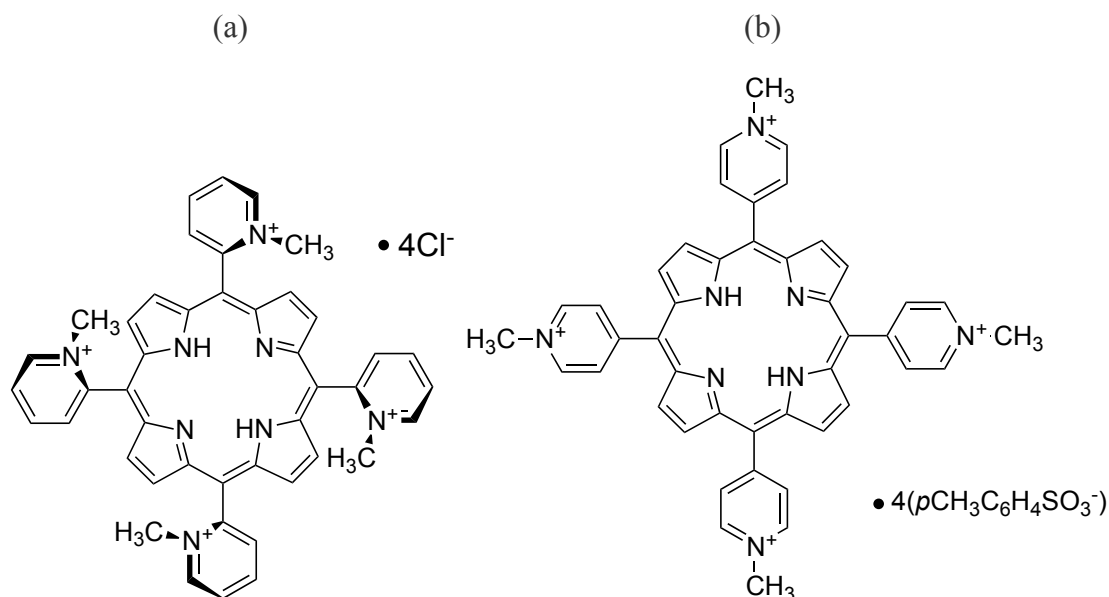


1.5.2 Porphyrin derivatives

Porphyrin compounds as double-stranded DNA ligands have been extensively studied, and also the aromatic ring of porphyrins can stack on top of G-quartets.⁶⁹ A representative porphyrin compound is TMPyP4 (*meso*-5,10,15,20-tetrakis-(*N*-methyl-4-pyridyl) porphine tetratosylate) (Fig 1.8 a) which can stabilize the human telomeric G-rich sequence, thereby effectively inhibiting

telomerase activity.^{70,71} As reported, TMPyP4's isomer, TMPyP2 (Fig 1.8 b), has a weaker activity of the mutual recognition of a G-quadruplex due to the steric hindrance resulting from the location of methyl groups. Because TMPyP4 has a typical symmetrical macrocyclic aromatic plane, it is widely used as special molecular probes to study a variety of different target sequences of G-quadruplexes. The crystal structure of a complex composed of TMPyP4 and d[TAGGGTTAGGG] showed that TMPyP4 only stacked on the 5' end region of a TTA loop, and had no direct contact with G-quartets. From a NMR spectroscopic study, TMPyP4 had an external π - π stacking interaction with the *c-myc* G-quadruplex DNA.⁷²

Fig 1.8 (a) TMPyP2; (b) TMPyP4

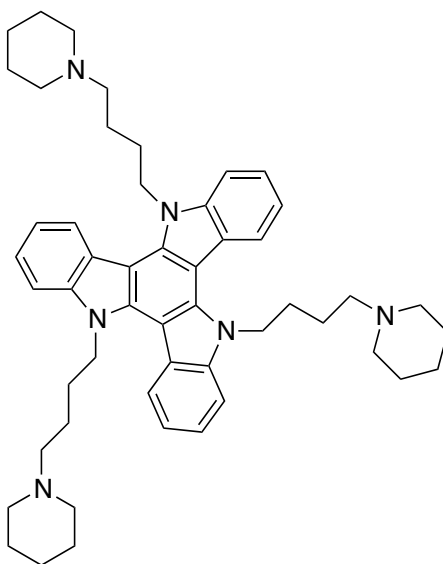


1.5.3 Triazatruxene derivatives

As illustrated in Fig 1.9, the first hydrophilic triazatruxene derivative, AZATRUX (5,10,15-*tris*[4-(1-piperidino)butyl]diindolo[3,2-a:3',2'-c]carbazole), has a tricyclic aromatic core and three positively charged side chains. This compound is fluorescent both in DMSO and water systems;⁷³ therefore it is feasible to investigate its binding properties via a high sensitive fluorescence spectroscopy. Under crowding conditions, AZATRUX can bind to the human telomeric sequence with a stoichiometry of 1:1 by an external end-stacking mode, and can bind to a parallel-stranded quadruplex [d(TGGGGT)]₄ with a stoichiometry of 2:1 by a π - π accumulation on G-quartet surfaces. Two side chains can reside in the grooves of a tetraplex; however, the third side chain is so flexible

as to be positioned over G-quartet surfaces.⁷⁴ In diluted conditions, spectroscopic and calorimetric experiments showed that AZATRUX can bind to a quadruplex monomer ([d(AG3TT)₄]), a quadruplex dimer ([d(TTAGGG)₈TT]), and a quadruplex trimer ([d(TTAGGG)₁₂TT]) with stoichiometries of 1:1, 3:1, and 4:1 respectively, revealing an external interaction between AZATRUX and quadruplex-quadruplex interfaces.⁷⁵

Fig 1.9 AZATRUX

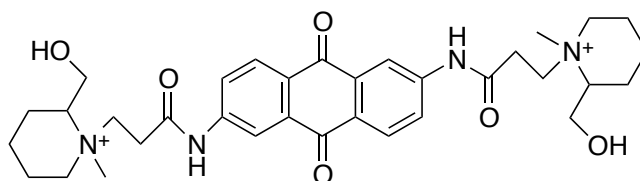


1.5.4 Amidoanthracene quinone derivatives

Tricyclic coplanar amidoanthraquinone derivatives were initially developed as small molecules interacting with a double helical DNA.⁷⁶ Since the discovery of BSU 1051 (2,6-diaminoanthraquinone) (Fig 1.10), about 100 substituted (1,4-, 1,5-, 1,8-, 2,6-, 2,7-) derivatives were successively synthesized, followed by their screening of cytotoxicity.⁷⁷ Most of them have very high inhibition

telomerase activities.⁷⁸ A subsequent structure-activity relationship showed the cytotoxicity of the ligand was not related to its telomerase inhibitory activity or its binding ability with a G-quadruplex, but positively correlated to its binding ability with a double helical DNA; therefore, the interaction between amidoanthraquinone derivatives and a double-stranded DNA causes the cytotoxicity.⁷⁹ Although two amide groups introduced in side chains improve the length of the fused ring plane from 7.5 to 12 Å, closer to the size of G-tetrad, and protonated amino side chains can also bring an external interaction with phosphate groups, the combination of such structure still cannot selectively identify a G-quadruplex over a double helix DNA.⁸⁰ The poor selectivity of amidoanthraquinone ligand limits its further development and application.

Fig 1.10 BSU 1051

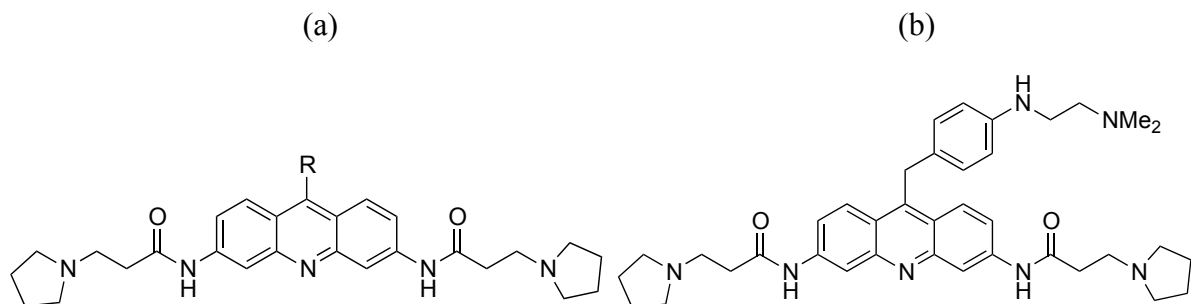


1.5.5 Acridine analogues

Disubstituted acridine compounds (Fig 1.11 a) share a similar tricyclic coplanar structure with anthraquinone derivatives, whereas their inhibition telomerase activities are higher than anthraquinone derivatives. This is mainly due to the nitrogen atom in the acridine fused ring, which can be protonated and positively charged so that it can more readily accumulate in the center of a G-tetrad with larger electrostatic interactions between nitrogen and the G-quartet center of high

electron density.^{81,82} However, the binding constants of disubstituted acridine derivatives with DNA duplex and G-quadruplex are almost the same.⁸³ So Martin designed and synthesized a series of 3, 6, 9-trisubstituted acridine analogues with a computer-aided model. The introduction of the third side chain can intercalate into G-quadruplex groove regions and increase the basicity of the pyridine ring nitrogen atom so as to make it more easily ionized.⁸⁴ Therefore, these compounds can better identify a telomeric sequence and inhibit telomerase activity. As illustrated in Fig 1.11 b, the most representative acridine analogue is BRACO-19 (*N,N'*-(9- {[4-(dimethylamino)phenyl]amino}-acridine-3,6-diyl)bis(3-pyrrolidin-1-ylpropanamide) trihydrochloride) showing a 30-fold higher binding affinity with G-quadruplex over duplex.⁸⁵

Fig 1.11 (a) disubstituted acridine compound; (b) BRACO-19

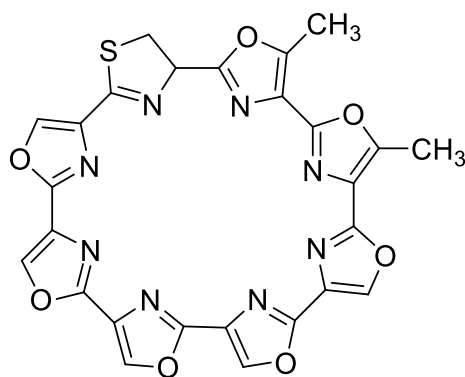


1.5.6 Telomestatin

As illustrated in Fig 1.12, telomestatin is a natural product isolated from *streptomyces* 3533-SV4.⁸⁶ The compound can promote the stabilization of G-quadruplexes, thereby inhibiting

telomerase activity. Because the size of the ligand and G-tetrad is very similar, telomestatin can occupy an entire tetrad plane with strong interactions resulting in its 70-fold binding selectivity to G-quadruplex over a double helical DNA.⁸⁷ In addition, telomestatin is the strongest telomerase inhibitor ($IC_{50} = 5 \text{ nM}$) without affecting the function of reverse transcriptase and polymerase due to the selective binding with intramolecular G-quadruplexes.⁸⁸ Telomestatin can also combine with a telomere overhang and change its single-stranded conformation. The cells treated with telomestatin for a long time have a shortened length of G-overhang.⁸⁹ An acute cellular toxicity and a long-term cell proliferation assay showed that telomestatin can inhibit cell growth and proliferation, especially in cells with a strong telomerase activity and a short length of telomere.⁹⁰

Fig 1.12 Telomestatin



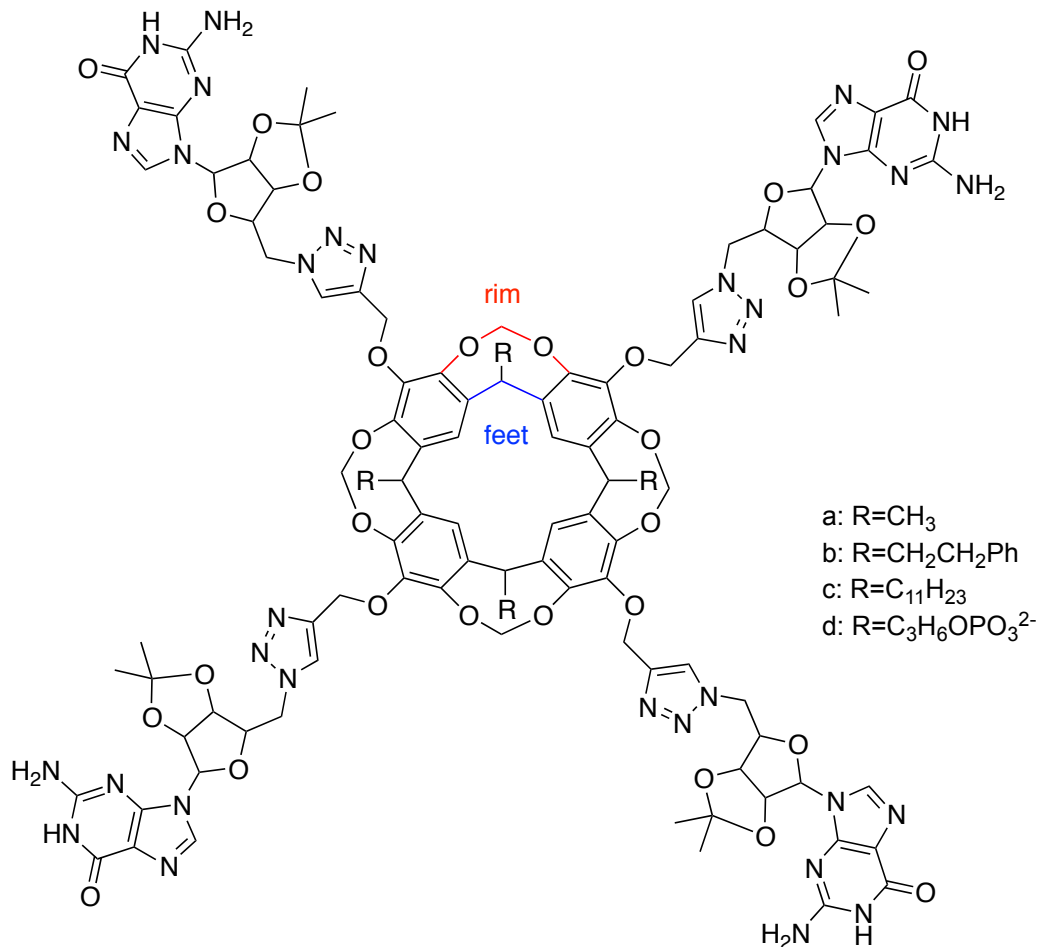
1.6 Template-assembled synthetic G-quartets (TASQs)

In 1994, George developed a molecular box probe containing crown ether as a host and several nucleotide bases as guests, to identify the Hoogsteen H-bonding, Watson-Crick H-bonding, and

some other kinds of interactions between nucleotide bases.⁹¹ Similar to this artificial molecular architecture concept, our group introduced guanines onto a rigid cavitand template and synthesized template-assembled synthetic G-quartets (TASQs) via a “click reaction”,⁹² a phosphite triester reaction,⁹³ and a phosphoramidite reaction.⁹⁴ Furthermore, our group characterized the topologies of complexes in various conditions, in order to further the study of their biological functions in lipophilic and hydrophilic systems and the extent they can imitate and replace the natural G-quartets or G-quadruplexes in the real world.

The first lipophilic TASQ (Fig 1.13 a-c) was synthesized by Mehran Nikan via a “click reaction”, forming a basket-like unimolecular G-quartet without the stabilization of cations, which suggests the critical role of the rigid cavitand host in inducing the self-assembly of four guanines to arrange in closer proximities on top of scaffolds in lipophilic systems.⁹⁵ With different selectivities of cations (Na^+ , Sr^{2+} , K^+ , Cs^+) in chloroform, NMR and CD studies showed that guanine-linked cavitands can be directed to form monomers and asymmetric dimers, thus encouraging conformational changes after cation competition experiments (Fig 1.14).⁹⁶

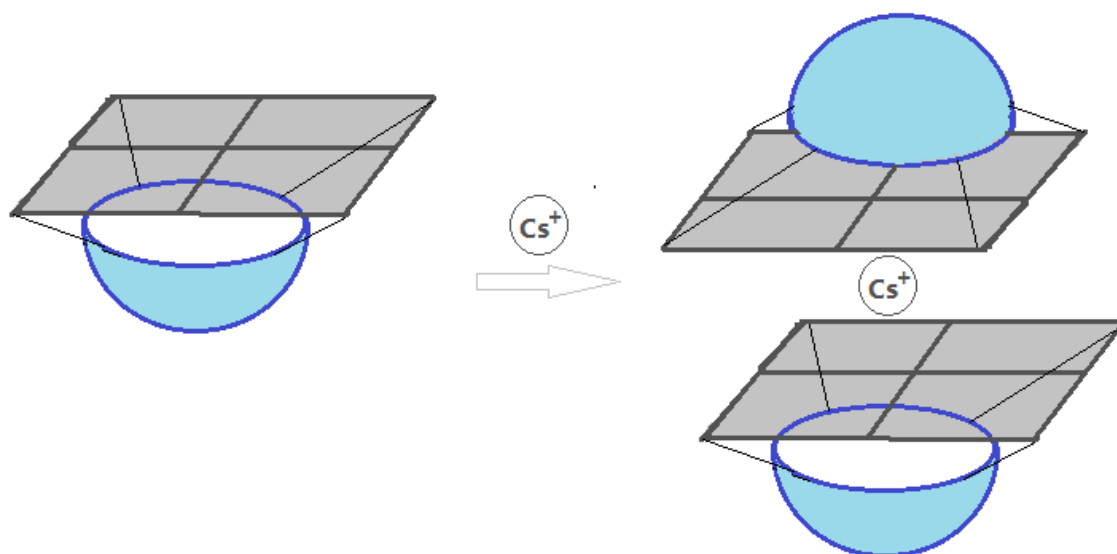
Fig 1.13 TASQs: (a-c) the first generation of lipophilic TASQ; (d) the first generation of hydrophilic TASQ.



The morphology of self-assembled guanines varies in different solvent systems. In order to simulate biological functions *in vivo*, a great deal of interest was raised in synthesizing hydrophilic TASQs to get them into water, the solvent of livings. The first generation of hydrophilic TASQ (Fig 1.13 d) was obtained by introducing a pendant alkyl phosphate group into the bottom feet of cavitaand, followed by a convergent coupling reaction of click chemistry.⁹⁷ The preliminary CD, UV-Visible absorbance and fluorescence studies of hydrophilic TASQ with binding ligands (*i.e.* PIPER and

TMPyP4) showed that PIPER can accumulate on top of G-quartet surfaces via π - π stacking; however TMPyP4 might have an electrostatic interaction with the phosphate feet of TASQ, suggesting such changes in the feet of cavitand might be problematic to screen and evaluate potential anticancer drugs.⁹⁸

Fig 1.14 Dimerization of first generation of lipophilic TASQ in chloroform in the presence of cesium cation.



Cation-free unimolecular phosphate linked cavitand-nucleotide conjugates where the linkage was at the feet rather than at rims, was synthesized via phosphite triester and phosphoramidite reactions (Fig 1.15) and these conjugates were characterized in methanol.⁹⁹ By the same methods, the second generation of hydrophilic TASQs (Fig 1.16) was obtained where the nucleotides were afforded at the rims of cavitands. This conjugate exists as a monomer in aqueous systems.¹⁰⁰

Fig 1.15 Phosphate linked TASQ in methanol

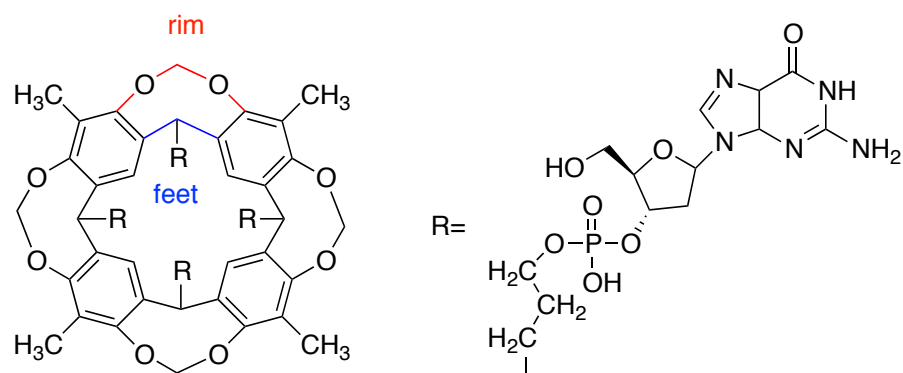
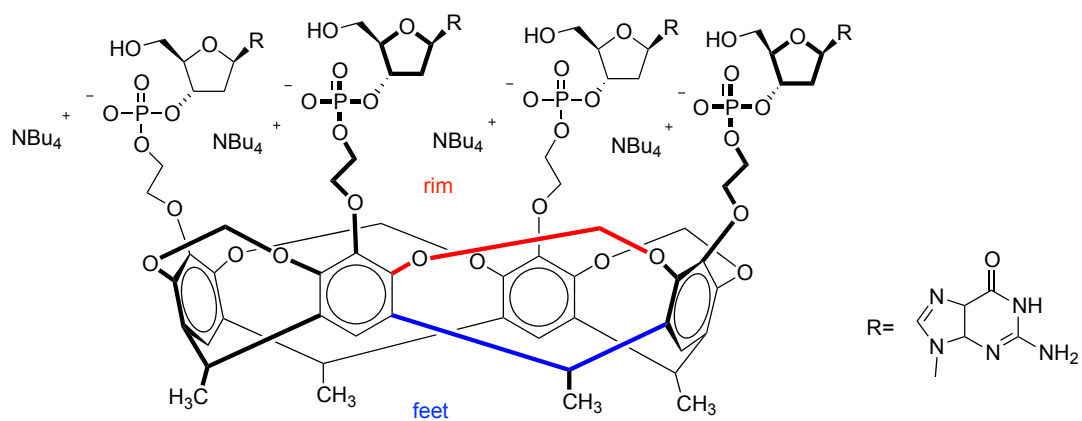


Fig 1.16 The second generation of hydrophilic TASQs



1.7 Thesis aims

The research into G-quadruplex based anticancer drugs are usually focused on the development and modification of various categories of small-molecule ligands. In contrast, little attention is paid to receptors. When a potential clinical drug is developed, they can only be tested with sophisticated and limited kinds of commercially available G-rich sequences. This imbalanced current situation has led to a time-consuming ligand study, or even worse led to the lack of understanding of binding mechanisms. The challenging problems are as follows: 1) the structures of natural G-quadruplexes are very complex, and the computer-aided molecular modeling is only theoretically correct on the premise of many assumptions; 2) the accurate methodology (*e.g.* NMR) requires high demand for valuable pharmaceutical products, resulting in time-consuming sample preparations; 3) ligand study is often based on a few specific commercially available G-quadruplexes, so it is difficult to form a comprehensive, general and convincing conclusion for all the natural G-quadruplex structures. Therefore, research into receptors is imminent and significant. Taking the above three challenges, binding modes, and the feasibility of organic synthesis into account, the imitation of a G-quadruplex structure needs to be simplified and focused specifically to the subunit structure G-quartet. If the artificiality of G-quartets can be proven successful, then the mimicking of a more complex G-quadruplex structure will be more promising and meaningful. Now here comes a question: is it possible to synthesize an artificial molecule with the same biological functions as the natural G-tetrad?

The rigid host template cavitand can be easily modified by the introduction of appropriate groups

on the upper or lower rim so as to recognize or bind to a ligand by means of hydrogen bonding, electrostatic interactions, as well as π - π interactions; therefore it is expected that the introduction of four fold guanine groups onto a cavitand upper rim will lead to the formation of G-tetrad organizations by the inducement of an inflexible template under physiological conditions. This functional macromolecule containing a cavitand skeleton may be able to recognize and coordinate with different classes of anticancer ligands. As mentioned above, our group has managed to synthesize two generations of hydrophilic template-assembled synthetic G-quartets (Fig 1.13 d, Fig 1.16) and characterize them in water.

However, to what extent could these artificial G-quartets imitate and replace the natural G-tetrad? The answer is still not clear. Firstly, all the potential applications of these two generations of hydrophilic TASQs are merely in the imaginary and hypothetical stage, and there are no solid experimental data to support those judgements. Secondly, the preliminary binding mechanism study between a triazole-linked TASQ (Fig 1.13 d) and TMPyP4 showed a positive induced CD signal, which was not consistent with the general stacking binding mechanism between TMPyP4 and G-quadruplexes since outside binding without stacking always had a positive induced CD signal.¹⁰¹ Moreover, the first generation of hydrophilic TASQ may form both intramolecular and intermolecular G-quartets due to a 25-fold weaker CD signal than triazole-linked lipophilic TASQ.¹⁰² Thus, not all artificial G-quartets can very well follow the examples of natural corresponding structures. Either the cavitand template, or the bridging structure between rims and guanines, plays an important role in the final biological functions.

The phosphate bridge in the second-generation hydrosoluble TASQ (Fig 1.16) is more similar to

the phosphate groups in the natural G-quadruplexes. As a result, the ligand study between the second generation hydrosoluble TASQ and varieties of small-molecule ligands is necessary and meaningful. If the binding mechanism of biomimetic receptor and ligands is similar to known mechanisms or computer-aided molecular simulation models, this artificial receptor will be promising to contribute to the screening of small-molecule anticancer drugs, helpful to understand the binding mechanism of new ligands, and worth being modified to simulate a more complex G-quadruplex structure.

CHAPTER 2 RESULTS AND DISCUSSION

2.1 Synopsis

TASQ **13**, PIPER, and AZATRUX were successfully obtained in order to study the interactions between TASQ **13** and ligands. Fluorescence spectroscopy and CD spectroscopy were used to investigate the changes of fluorescence intensity and chirality of TASQ **13**/ligand complex. The methodologies of Scatchard plot and Job plot were applied in the calculation of binding stoichiometries and binding constants. In addition, fluorescence binding plots were obtained to study the saturation numbers of [TASQ **13**]/[ligand] and the salt effects of KCl. The binding mechanisms between TASQ **13** and ligands were discussed with optical spectroscopy data and known mechanisms or molecular modeling. The ligand study herein was designed to show the potential of TASQ **13** as an artificial ligand binding receptor to imitate the natural terminal G-quartets of G-quadruplexes and to screen ligands with selectivities.

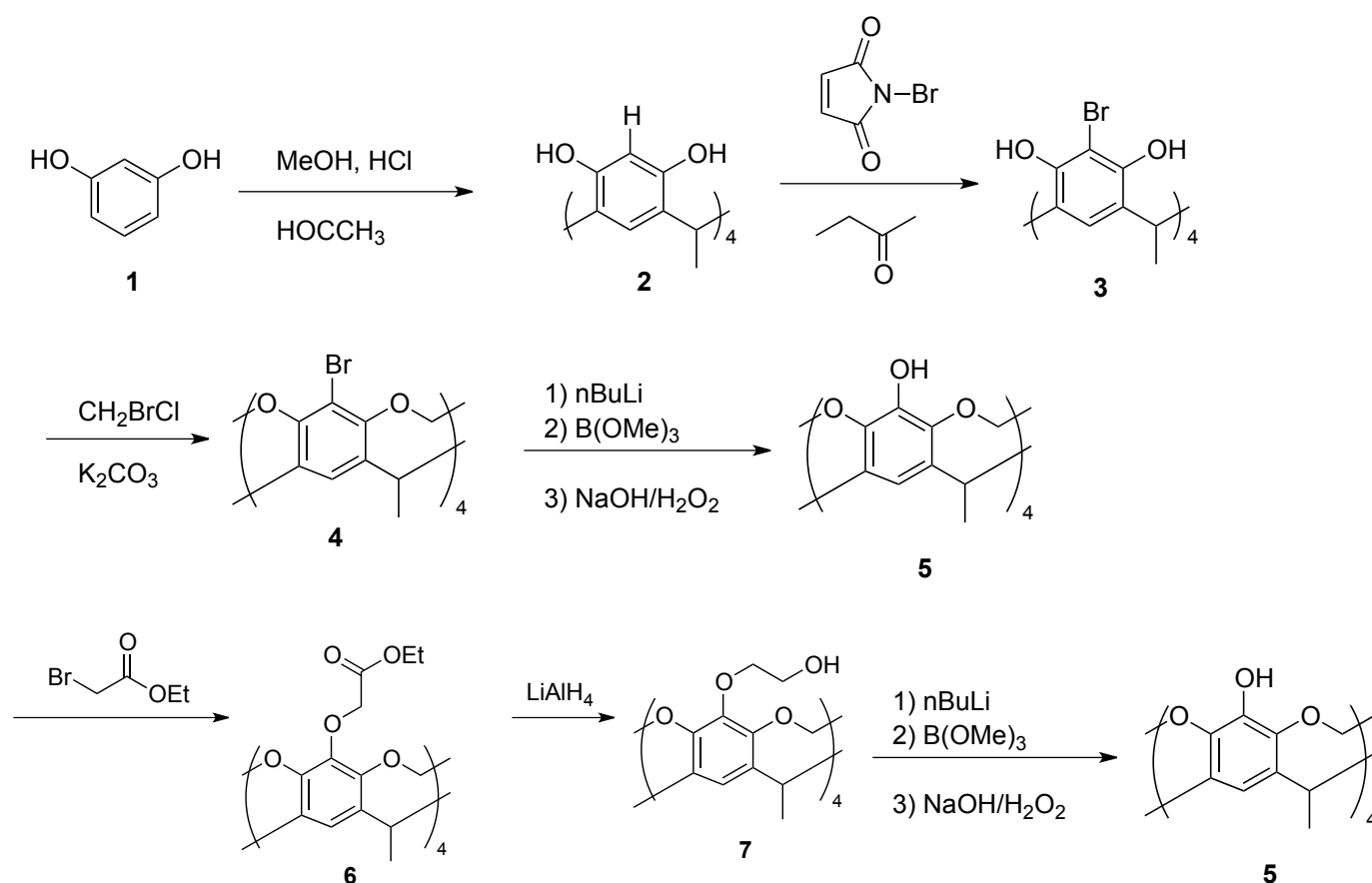
2.2 Synthesis of hydrophilic template-assembled synthetic G-quartet (TASQ) and ligands

2.2.1 Convergent synthetic routes for TASQ **13**

The synthesis of TASQ **13** was performed following by the synthetic routes and procedures

developed by a former Sherman group member Grant Bare; however, TASQ **13** was synthesized by the author starting from the first step. Every synthetic step has been tried by the author multiple times. All the yields and characterization reported below were obtained by the author and corresponded to previous results.

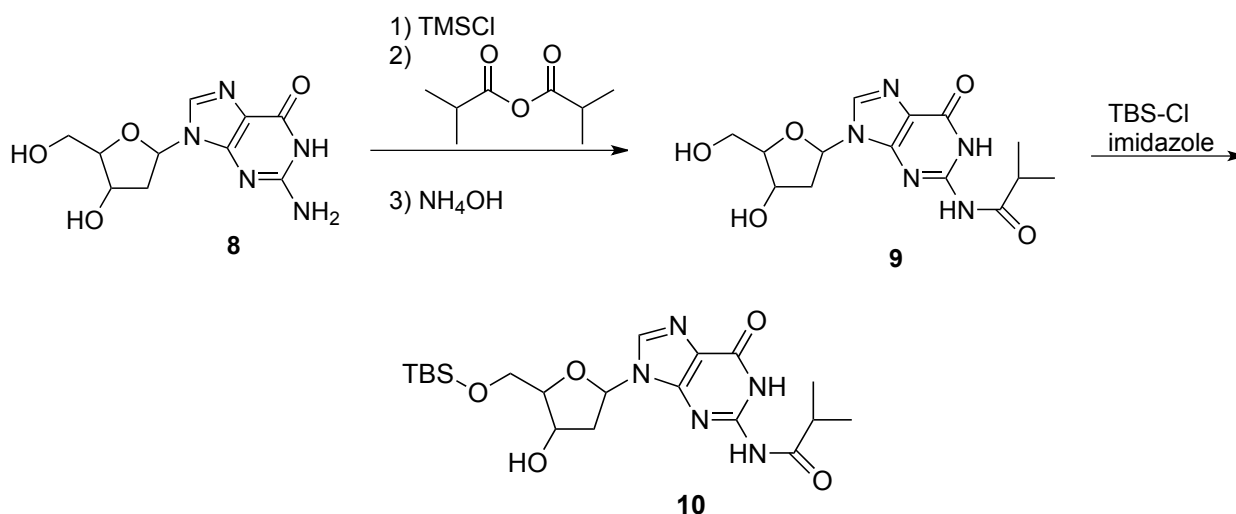
Scheme 2.1 Synthetic route for the tetraol cavitand **7**



As illustrated in Scheme 2.1, starting with resorcinols stirred with acetaldehyde in the presence of inorganic acid resulted in product **2** after a cyclocondensation reaction in 70% yield.¹⁰³ The

nucleophilic bromination of **2** at the *ortho* position of a phenolic hydroxyl group was performed by an addition of NBS at room temperature in 80% yield.¹⁰⁴ The next step was the nucleophilic substitution of CH₂BrCl to tetrabromo **3**, which can be achieved in two different ways. In the first way, **3** was refluxed with bromochloromethane and K₂CO₃ in DMSO at 70 °C for 24 h in 55% yield;¹⁰⁵ in the second route, a maximum of 5 g of **3** was treated with CH₂BrCl and Cs₂CO₃ in a sealed tube at 88 °C for only 3 h in 65.5% yield.¹⁰⁶ In both ways, the entropy change was less than 0, due to the rigidification of starting materials. The product **5** was obtained by lithium halogen exchange and hydroboration reaction in 35% yield.¹⁰⁷ Tetra-ethyl ester cavitand **6** was obtained by a Williamson ether reaction for 5 days in 70% yield.¹⁰⁸ And then, tetra-ester **6** was reduced by LiAlH₄ at 0 °C for 2 h to give tetra-ol **7** in 67% yield.¹⁰⁹

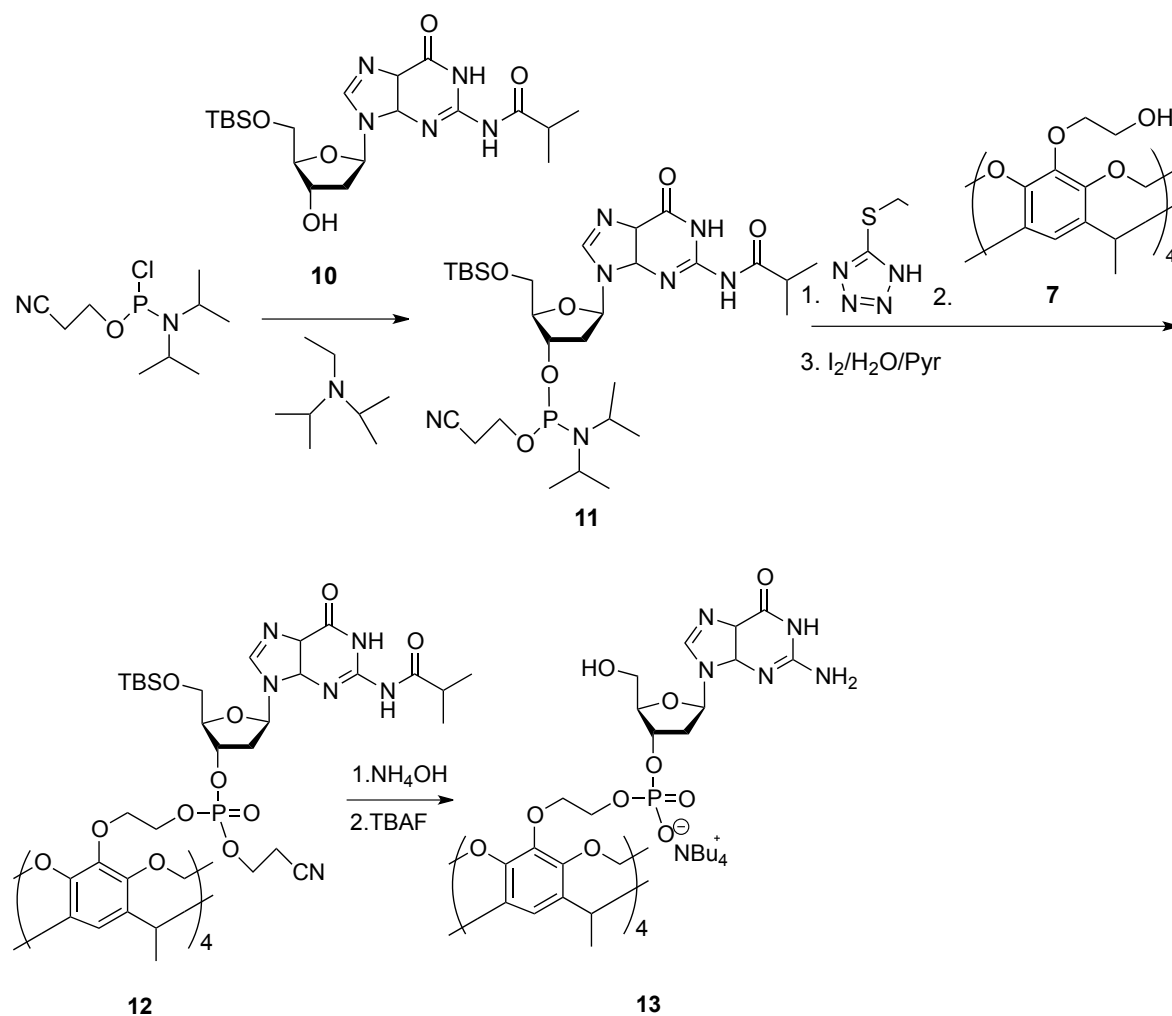
Scheme 2.2 Synthetic route for silyl deoxyguanine **10**



As illustrated in Scheme 2.2, deoxyguanosine was converted to TBS-protected *N*-acylation

nucleoside **10** in two steps. The hydroxyl moieties of the deoxyguanosines were protected by trimethylchlorosilane, followed by an *N*-acylation with isobutyric anhydride and a hydrolysis of protected groups in 75% yield.¹¹⁰ The next step is a selective monoprotection of diols **9** with *tert*-butyldimethylsilyl chloride at 0 °C for 45 minutes in 95% yield.¹¹¹

Scheme 2.3 Synthetic route for TASQ **13**



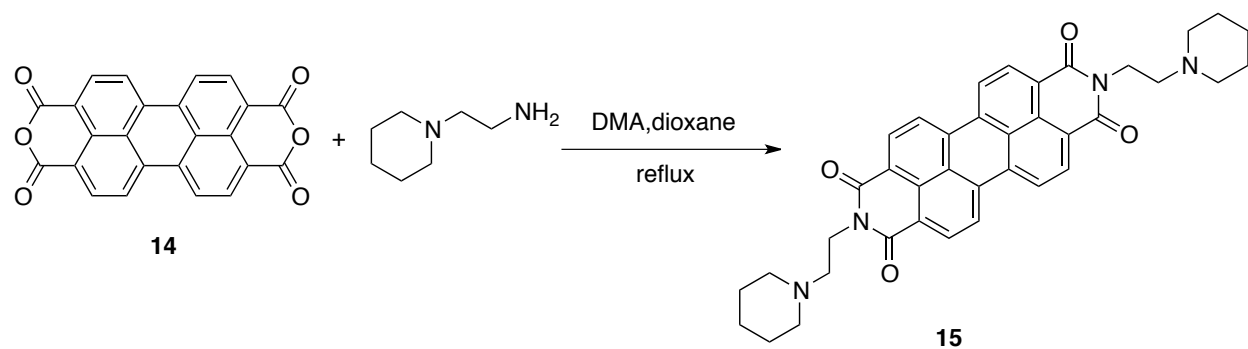
As illustrated in Scheme 2.3, to covalently attach guanosine **10** to cavitand **7**, a phosphoramidite

reaction was utilized. The unprotected hydroxyl group of **10** was reacted with 2-cyanoethyl-*N,N*-diisopropylchlorophosphoramidite by a nucleophile reaction to achieve **11**. After purification, the dry phosphoramidite **11** was mediated with 5-(ethylthio)tetrazole, and then linked to cavitand **7** in dry THF for 4 h, followed by an oxidation with iodine to obtain crude **12**. The completion of the phosphoramidite reaction was confirmed by TLC visualized with UV light. Without any further purification, crude **12** was treated with ammonia and TBAF in two steps to deprotect the hydroxyl and amino groups. Reverse-phase chromatography was used for the purification of final crude products with gradient elutions of water/methanol mixtures. Both preparative C-18 HPLC and C18 Sep-Pak cartridge were successfully used to obtain pure TASQ **13**, which gave clear signals by ¹H-NMR spectroscopy in D₂O at 400 MHz.

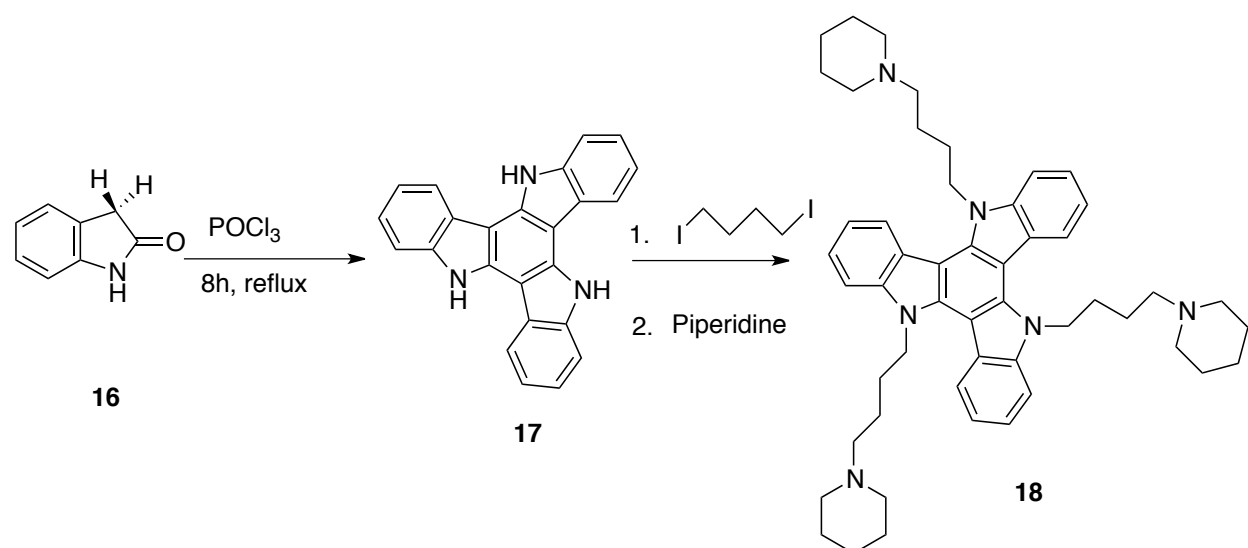
2.2.2 Synthetic routes for PIPER and AZATRUX

As for small-molecule ligands, the author prepared PIPER and AZATRUX according to literature procedures. Every synthetic step was performed by the author multiple times. All the yields and characterization reported below were obtained by the author, and corresponded to previous results. TMPyP4 was purchased from Sigma Aldrich. BSU-1051 and BRACO 19 were both donated from the group member Grant Bare.

Scheme 2.4 Synthetic route for PIPER 15



Scheme 2.5 Synthetic route for AZATRUX 18



As illustrated in Scheme 2.4, starting from tetracarboxylic acid dianhydride **14**, PIPER **15** was synthesized by adding 1-(2-aminoethyl)piperidine and treating with concentrated HCl to give the corresponding hydrochloride salt in 80% yield.¹¹²

As illustrated in Scheme 2.5, AZATRUX was synthesized in three steps. 2-indolone **16** was

utilized as a starting material. The cyclotrimerization of 2-indolone **16** in POCl₃ under heating led to the unsubstituted aromatic triazatruxene core **17** in 50% yield.¹¹³ An *N*-alkylation was achieved under basic conditions, followed by the substitution of iodide with piperidine to give AZATRUX **18** in 36% yield in total.¹¹⁴ The hydrochloride salt of AZATRUX **18** was obtained by dissolving **18** in a methanol/HCl mixture and adding diethyl ether.¹¹⁵

2.3 Ligand-binding studies

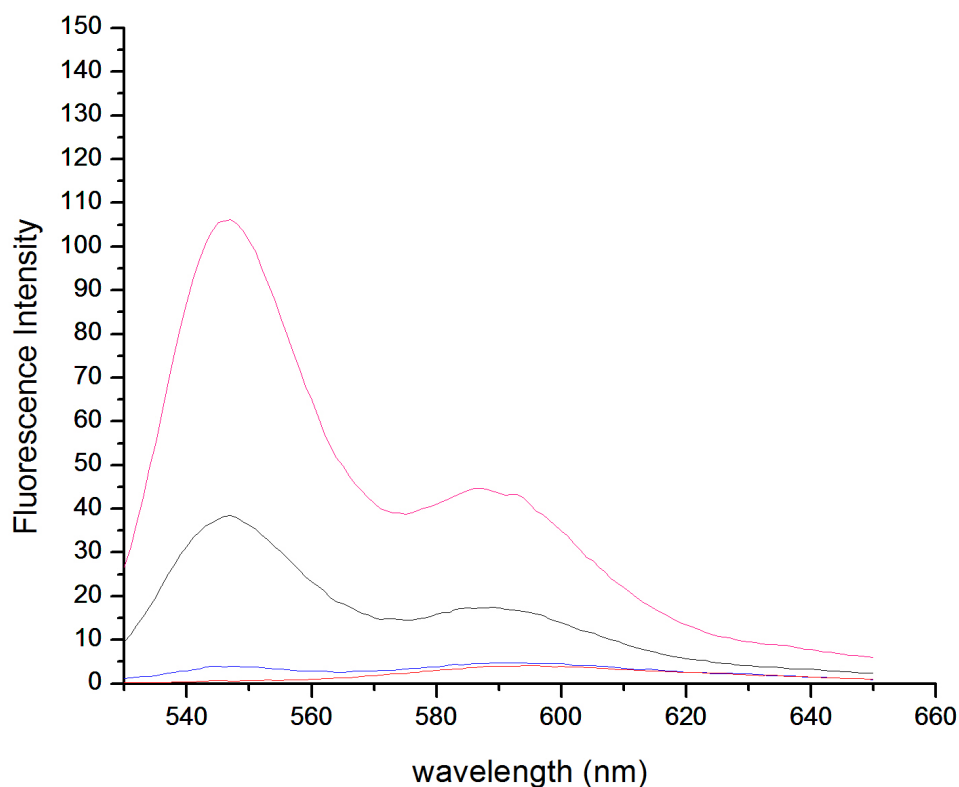
Before performing ligand-binding experiments, the fluorescence intensities of a variety of small-molecule ligands were initially studied at different pH values in order to select the best solution systems. When the preparative work above was completed, fluorescence emission spectra were achieved between TASQ **13** and small ligands (*i.e.* PIPER, TMPyP4, AZATRUX, BSU-1051, and BRACO 19) to qualitatively and quantitatively characterize their interactions. Scatchard plots and Job plots (See section 2.4.2.2 for more details) were drawn to evaluate binding constants and stoichiometries ([TASQ **13**] : [ligand]). Also, stoichiometric numbers ([TASQ **13**] : [ligand]) for fully saturated ligands and salt effects of KCl were obtained by drawing fluorescence binding plots (See section 2.4.2.2 for more details). In the end, binding mechanisms were analyzed and proposed by fluorescence spectroscopy data, CD studies, salt-affected experiments, and previously published models. Some ligands did not have interactions with TASQ **13** according to qualitative fluorescence and CD studies. These phenomena were also rationalized.

TASQ **13** should have CD signals in the range of 230-300 nm because of the proximity of its

aromatic rings to the chiral elements of guanosines. This feature has been confirmed by Grant Bare, a former member of our group. He not only characterized the CD spectrum of TASQ **13**, but also found that there was no intensity change by adding potassium or sodium cations, suggesting TASQ **13** was the first monomeric cation-free G-tetrad exposed in aqueous solutions.¹¹⁶ This unique open face template-assembled G-quartet was an ideal artificial minimal model of terminal G-quartets in G-quadruplexes. In addition, TASQ **13** had no fluorescence signal when excited at the wavelengths to observe fluorescence emission spectra of ligands.

2.3.1 Interactions of PIPER with TASQ 13

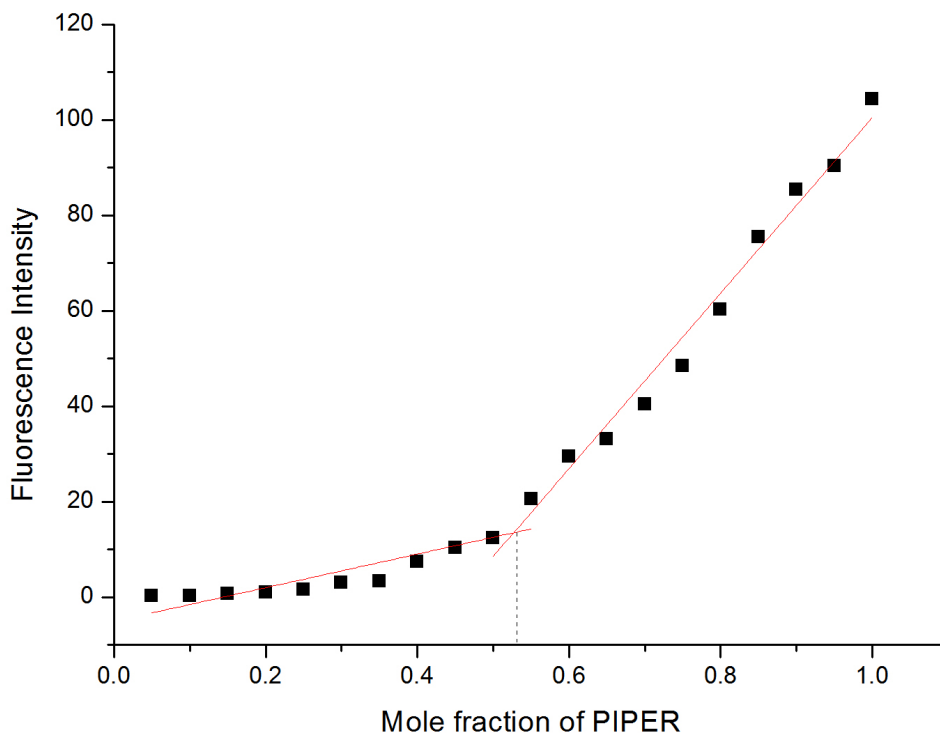
Fig 2.1 Fluorescence spectrum of PIPER alone (0.5 μM) at pH 6.5 (pink), 7 (black), 7.5 (blue), and 8 (red).



As illustrated in Fig 2.1, the fluorescence intensity of PIPER (0.5 μM) gradually increased as pH decreased. This phenomenon may be due to the difficult self-aggregation of PIPER at low pH, resulting from a strong electronic repulsion between protonated side chains in acidic conditions. This result was consistent with solubility profiles of perylene derivatives showing PIPER was completely dissolved in water below pH 6.5,¹¹⁷ and also consistent with the opinion that solutions of PIPER were fluorescent at pH < 7.¹¹⁸ It was reported that the fluorescence quantum yield of monomeric

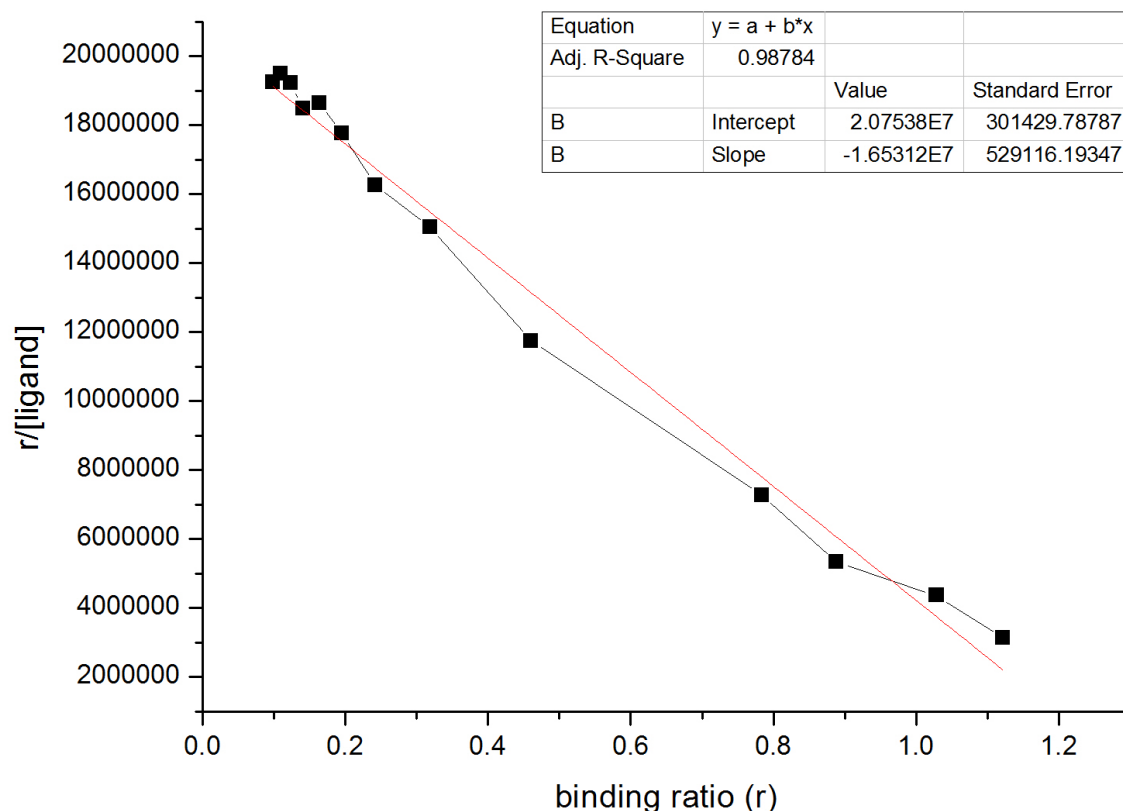
PIPER was about 1, while the fluorescence quantum yield of a PIPER dimer was less than 0.02 (non-fluorescent).¹¹⁹ So it can be speculated that at pH 6.5, PIPER mostly exists in the form of monomer. In addition, according to research by Vivian, a former member of our group, the ratio of [monomer] : [dimer] in an aqueous solution was related to the concentration of PIPER.¹²⁰ When PIPER was 0.5 μM , at least 85% of PIPER existed in the monomeric form. Moreover, many previous PIPER experiments were done at the concentration of 0.5-1 μM .¹²¹ In order to have a better comparison with previous results, the measuring concentration of PIPER was set as 0.5 μM in pH 6.5 aqueous solutions.

Fig 2.2 Job plot analysis of fluorescence binding data for PIPER and TASQ 13. The total molar concentration ($[\text{PIPER}] + [\text{TASQ 13}]$) was 0.5 μM .



A Job plot (Fig 2.2) and a Scatchard plot (Fig 2.3) were achieved by fluorescence titration experiments. From the Job plot, the binding stoichiometry between PIPER and **13** was obtained as 1:1, which was consistent with the x-axis intercept (=1.26) of the Scatchard plot (Fig 2.3). The result also verified that only one face of PIPER was needed in an end-stacking binding mode with G-quadruplexes.¹²² Also, a stoichiometry of 1:1 ruled out the possibility of external π - π stacking between PIPER and aromatic rings of the cavitand template.

Fig 2.3 Scatchard plot analysis of fluorescence binding data for PIPER (0.5 μ M) in absence and presence of successive additions of TASQ **13** in the range of 0-5 μ M at 25 $^{\circ}$ C.



As illustrated in Fig 2.3, the slope of the Scatchard plot between PIPER and TASQ **13** gave a binding constant (K_{PIPER}) of $1.65 \times 10^7 \text{ M}^{-1}$ within the previous reported range ($=10^5\text{-}10^7 \text{ M}^{-1}$) of PIPER/G-quadruplex binding.¹²³ It is the first time to evaluate a binding constant between an isolated G-quartet and ligands excluded from the effects of G-quadruplex grooves and loops.

Fig 2.4 Fluorescence spectrum of PIPER (0.5 μM) in absence and presence of successive additions of TASQ **13** in the range of 0-5 μM at 25 °C. Arrows indicate the increasing TASQ **13** concentrations.

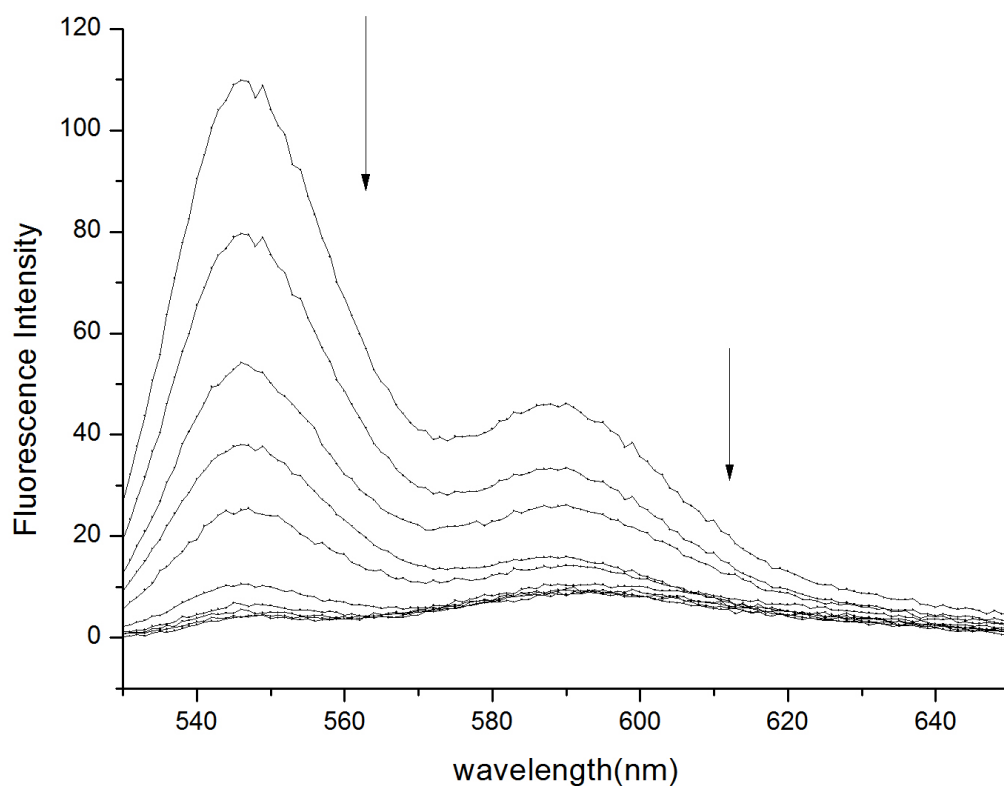
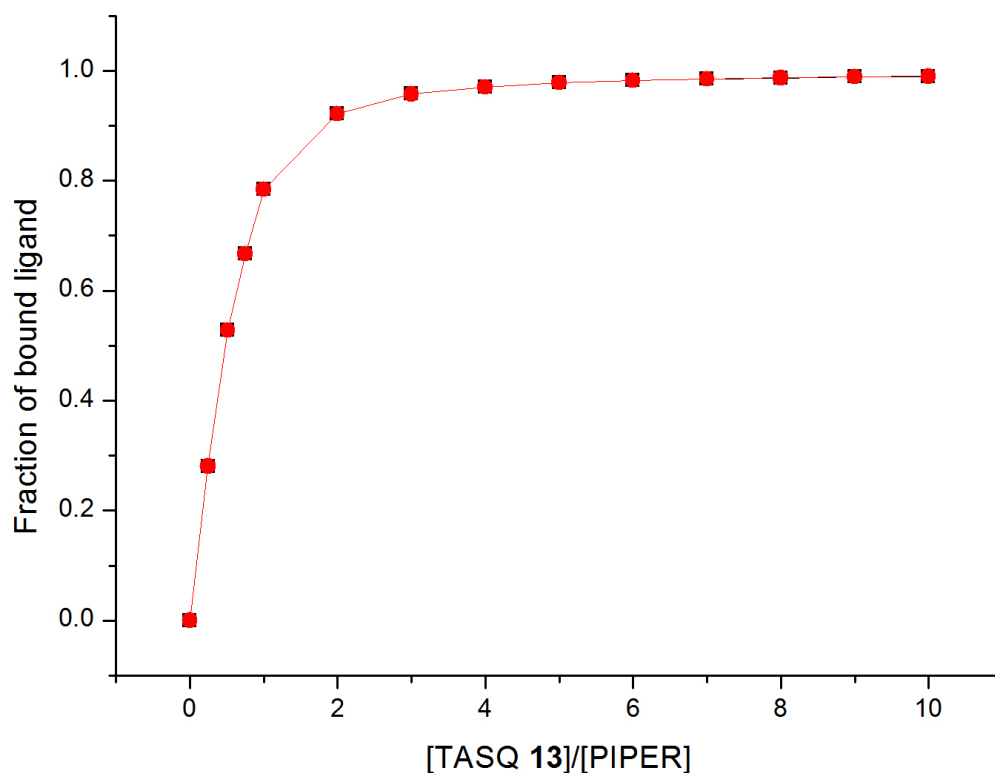


Figure 2.4 shows that the fluorescence intensity of PIPER gradually decreased by additions of TASQ **13**, which was consistent with the fluorescence quenching upon additions of G-quadruplex

DNA.¹²⁴ When stability constants of self-aggregations of closely related perylene bisimides were smaller than binding affinities with nucleotides, fluorescence intensities were enhanced because more perylene bisimides existed in monomeric forms rather than aggregation forms.¹²⁵ This theory was also consistent with fluorescence emission spectra of PIPER with TASQ **13**. The binding constant of PIPER with **13** ($K_{\text{PIPER}}=1.65 \times 10^7 \text{ M}^{-1}$) was close to the aggregation constant ($K_{\text{dimer}}=1.0 \times 10^7 \text{ M}^{-1}$) of PIPER dimer.¹²⁶ Therefore, there were no more PIPER monomers induced by additions of **13** so that fluorescence intensities did not increase. Moreover, no significant peak shift was observed, suggesting that there was only one kind of fluorescent species existing in solutions. Therefore, PIPER only stacked on top of TASQ **13** with a stoichiometry of 1:1 similar to the end-stacking binding mode of terminal G-quartets in G-quadruplexes.

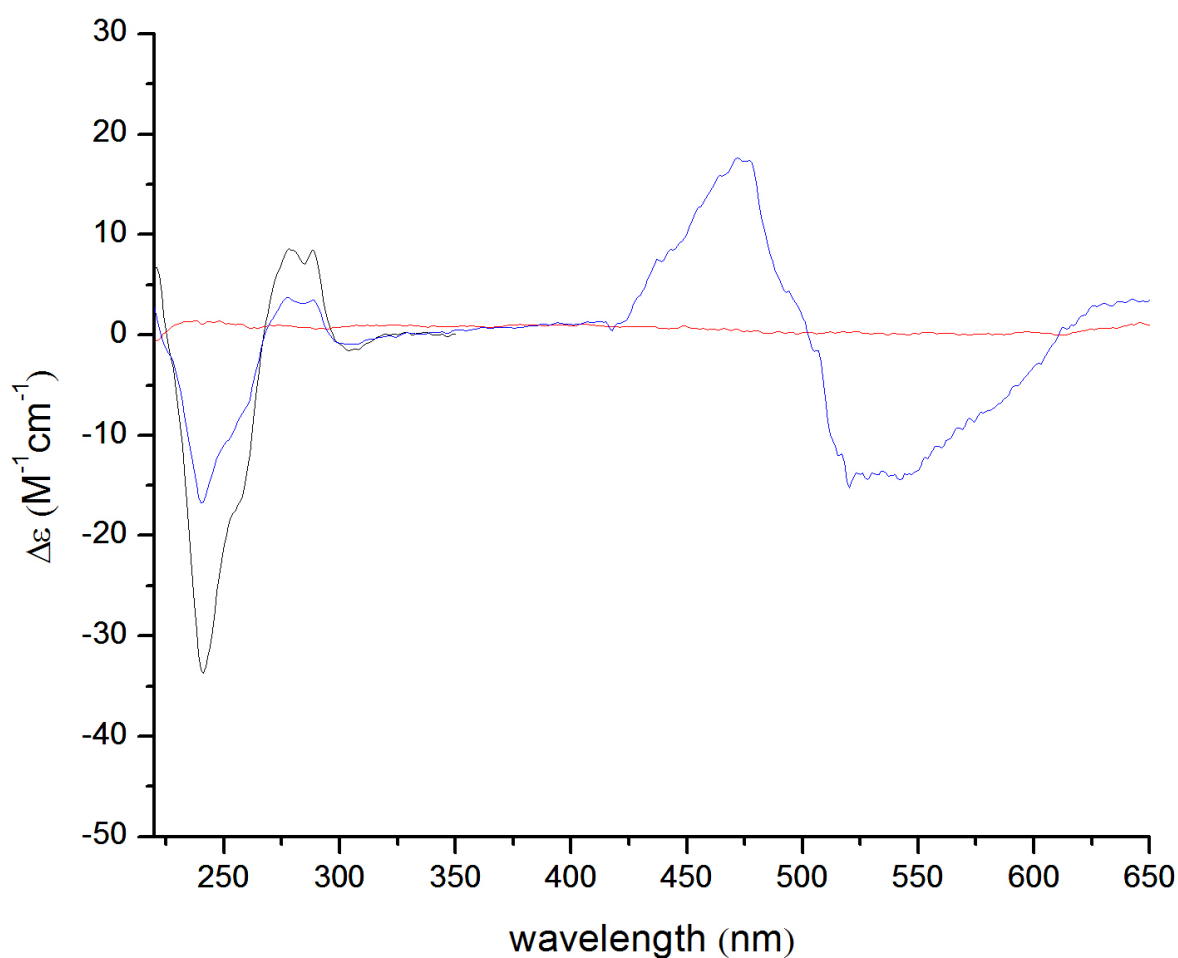
Fig 2.5 (a) Fluorescence binding plot of PIPER (0.5 μM) on increasing TASQ **13** concentrations in the range 0-5 μM in 0.1 mM EDTA, 10 mM Tris-HCl (black); (b) Salt-affected fluorescence binding plot of PIPER (0.5 μM) on increasing TASQ **13** concentrations in the range 0-5 μM in 0.1 mM EDTA, 10 mM Tris-HCl, 100 mM KCl (red).



As illustrated in a fluorescence binding plot (Fig 2.5 a), PIPER was almost saturated when $[\text{TASQ } \mathbf{13}] : [\text{PIPER}]$ was greater than 2, and fully saturated when stoichiometry number was more than 4, thus suggesting that the Scatchard plot was drawn according to the appropriate maximum fluorescence intensity in saturated conditions. In addition, a corresponding salt-affected fluorescence binding plot (Fig 2.5 b) was drawn by additions of KCl (the final concentration of KCl was 100 mM) to the same series of titration samples. There was no change of the fraction of bound ligand, thus

excluding electrostatic interactions between PIPER and TASQ **13**. These experimental results were also consistent with a binding stoichiometry of 1:1 and an end-stacking binding mode.

Fig 2.6 (a) CD spectrum of PIPER alone (10 μM , red); (b) TASQ **13** alone (10 μM , black); (c) TASQ **13** and PIPER (10 μM and 10 μM , blue).



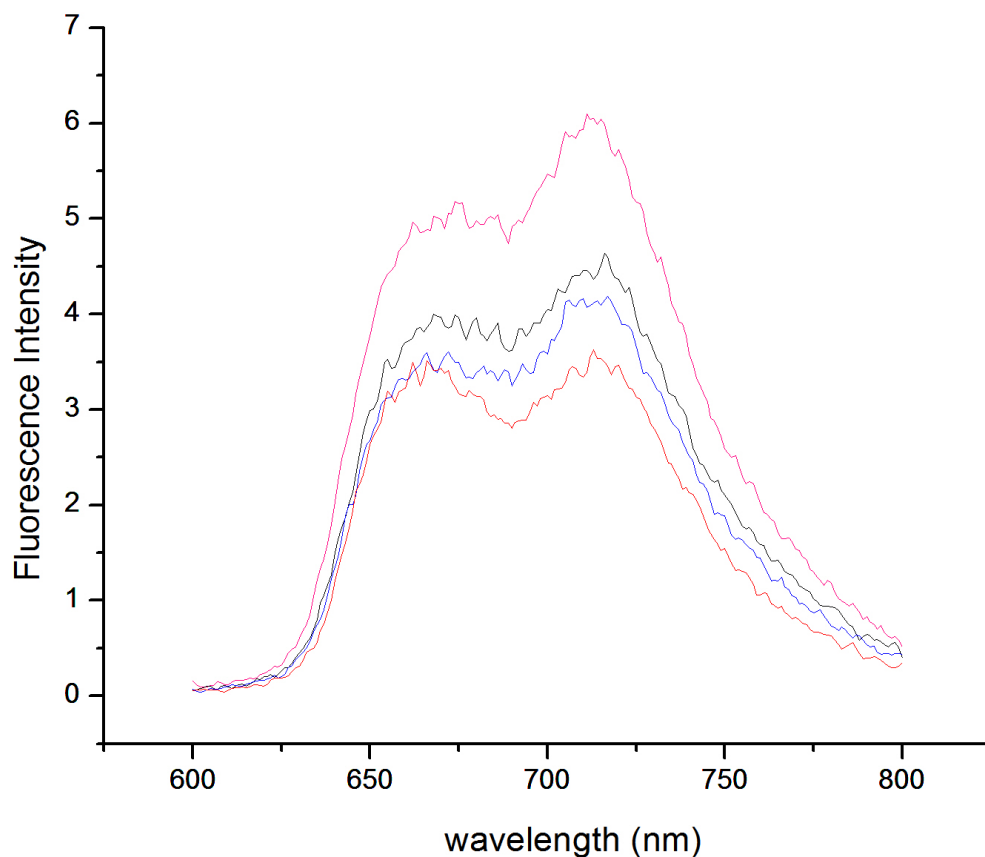
As illustrated in Fig 2.6, the CD spectrum of PIPER/TASQ **13** complexes with a stoichiometry of 1:1 showed a change in CD spectrum between 220-290 nm, suggesting a conformational change of

TASQ **13** upon PIPER binding. Since PIPER has no absorption under 400 nm,¹²⁷ this conformational change of nucleotides cannot be due to the contribution of the induced circular dichroism of PIPER in chiral conditions. For the same reason, the induced CD signal from 450 nm to 650 nm was entirely from the conformational change of PIPER, suggesting an interaction between PIPER and TASQ **13**. There was a strong negative peak at about 525 nm and a strong positive peak at about 475 nm in Fig 2.6. The CD spectrum of PIPER with intramolecular G-quadruplex was characterized by a positive peak increasing at 290 nm and a negative peak decreasing at 235 nm, which was consistent with our results.¹²⁸ The induced CD spectrum of PIPER with TASQ **13** can also be indirectly analyzed according to the CD spectra of PIPER with duplex DNA structures. In general, a strong induced CD reveals a groove-binding mode via π - π stacking while a weak induced CD is more congruent with intercalation binding mode.¹²⁹ So the theory of DNA duplex indirectly supports a face-stacking binding mode of PIPER with TASQ **13** via π - π interactions.

2.3.2 Interactions of TMPyP4 with TASQ **13**

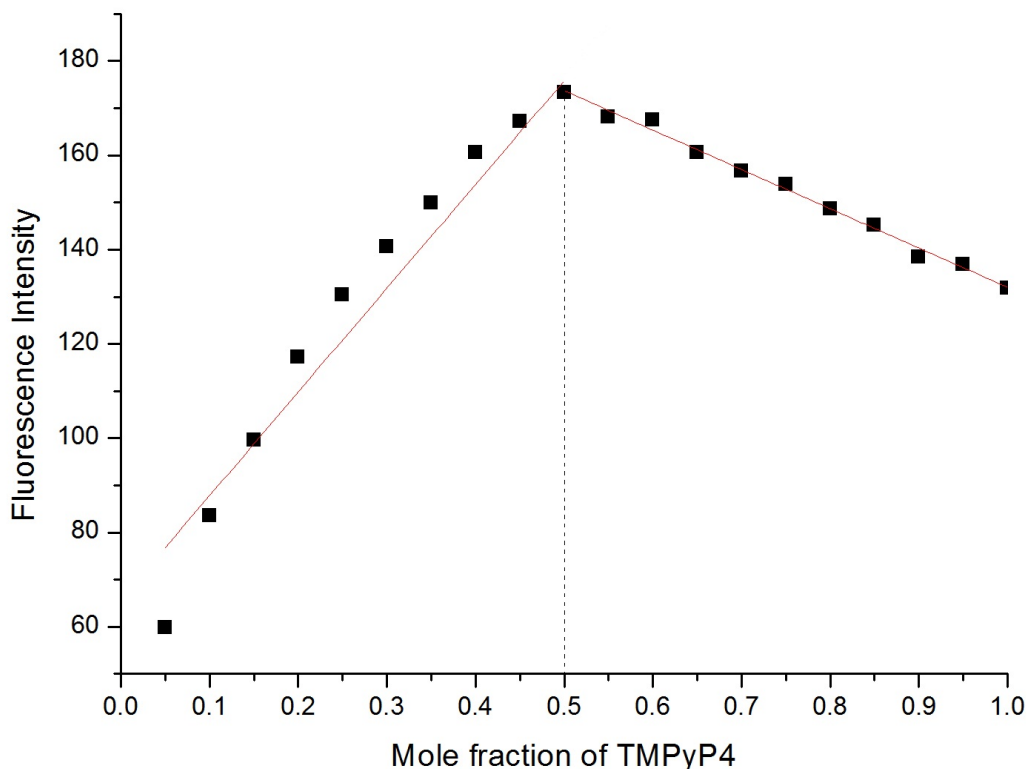
The ligand binding study of TMPyP4 to TASQ **13** has already been studied via UV-Vis spectroscopy by Grant Bare, a former member of our group.¹³⁰ The author tried to study their interactions in the perspective of fluorescence study. Fluorescence spectroscopy is more accurate and sensitive than UV-Vis spectroscopy, and the results will be more reliable if two series of data are consistent with each other.

Fig 2.7 Fluorescence spectrum of TMPyP4 alone (0.5 μM) at pH 6.5 (pink), 7 (black), 7.5 (blue), and 8 (red).



As illustrated in Fig 2.7, the fluorescence intensity of TMPyP4 slightly increased as pH decreased. This phenomenon may be due to the difficult self-aggregation of TMPyP4 under the concentration of 1 mM.¹³¹ Moreover, TMPyP4 obeys Beer's law in the range of 0-15 μM . And according to preliminary research by Grant Bare, TMPyP4 had interactions with TASQ **13** at pH 8 from their UV-Vis spectra.¹³² And many previous TMPyP4 experiments were performed at the concentration of about 8 μM .¹³³ In order to have a better comparison with previous results, the measuring concentration of TMPyP4 was set at 8 μM in pH 8 aqueous solutions.

Fig 2.8 Job plot analysis of fluorescence binding data for TMPyP4 and TASQ **13**. The total molar concentration ($[\text{TMPyP4}] + [\text{TASQ } \mathbf{13}]$) was $8 \mu\text{M}$.



A Job plot (Fig 2.8) and a Scatchard plot (Fig 2.9) were achieved by fluorescence titration experiments. From the Job plot, the binding stoichiometry between TMPyP4 and TASQ **13** was obtained as 1:1, which was consistent with the x-axis intercept ($=0.83$) of the Scatchard plot (Fig 2.9) and the previous result of UV-Vis spectra.¹³⁴ Also, a stoichiometry of 1:1 suggested that there was no external π - π stacking between TMPyP4 and the aromatic rings of the cavitand template and any electrostatic interactions between TMPyP4 and phosphate groups. The slope of the Scatchard plot (Fig 2.9) between TMPyP4 and TASQ **13** gave a binding constant (K_{TMPyP4}) of $5.53 \times 10^5 \text{ M}^{-1}$ in

accordance with the binding constant measured from UV-Vis spectra ($K_{\text{TMPyP4}}=8.5\times 10^5 \text{ M}^{-1}$).¹³⁵ K_{TMPyP4} was almost 100-fold weaker than K_{PIPER} , which is consistent with the coexistence of intercalation and end-stacking binding mechanisms of TMPyP4 to G-quadruplexes.¹³⁶

Fig 2.9 Scatchard plot analysis of fluorescence binding data for TMPyP4 (8 μM) in absence and presence of successive additions of TASQ 13 in the range of 0-80 μM at 25 $^\circ\text{C}$.

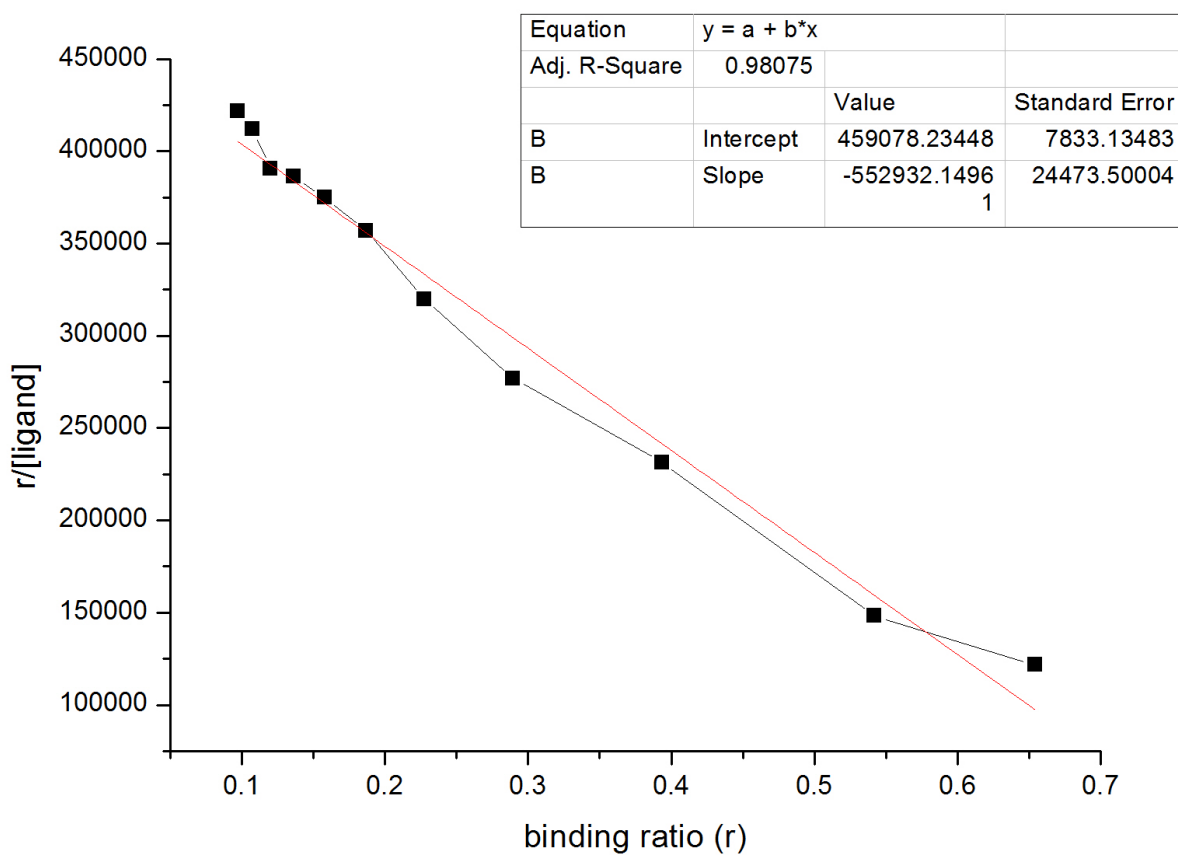


Fig 2.10 Fluorescence spectrum of TMPyP4 (8 μM) in absence and presence of successive additions of TASQ **13** in the range of 0-80 μM at 25 $^{\circ}\text{C}$. Arrows indicate the increasing TASQ **13** concentrations.

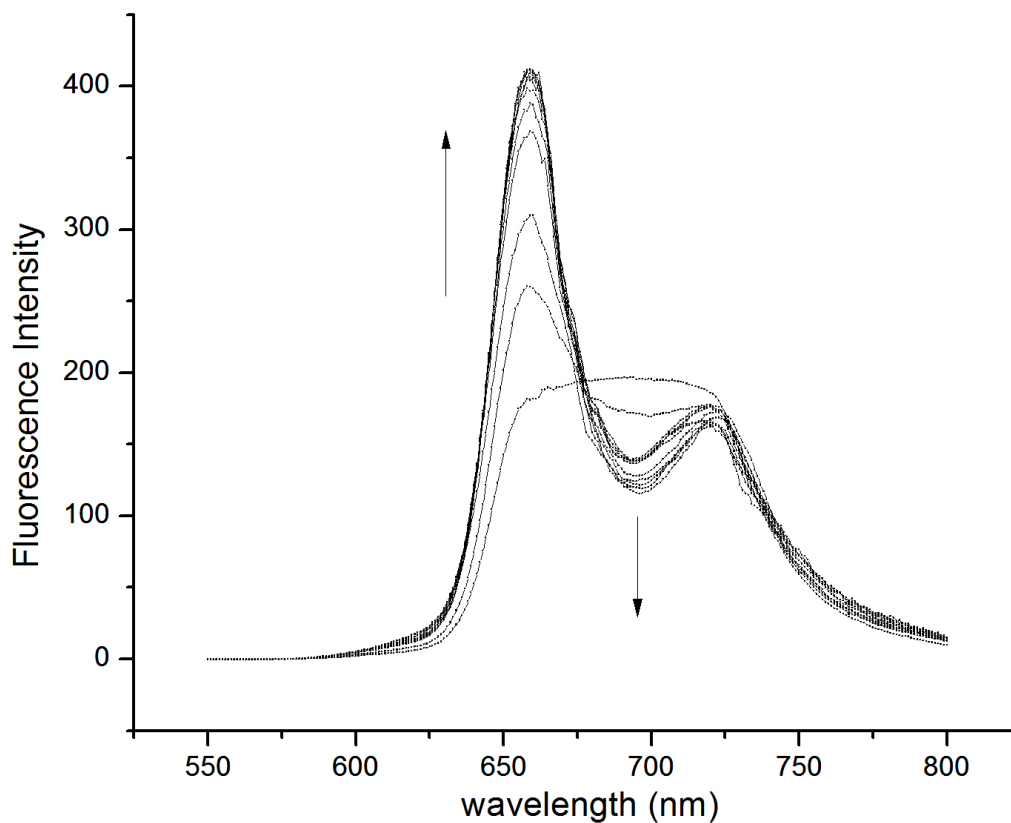
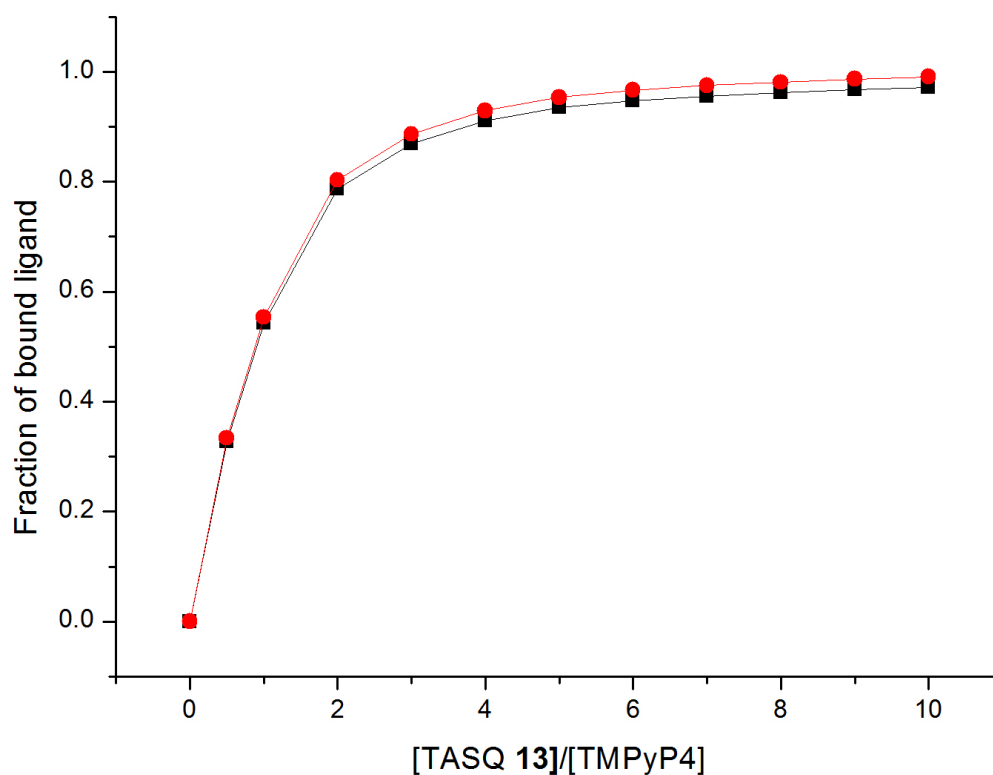


Figure 2.10 shows that the fluorescence spectrum of TMPyP4 was split from one peak to two peaks. The intensities at 660 nm gradually increased; however the intensities at 690 nm and 720 nm gradually decreased by additions of TASQ **13**. The increasing intensity at 660 nm was consistent with the fluorescence enhancement upon additions of G-quadruplex DNA due to the exclusion of water around TMPyP4.¹³⁷ Moreover, no significant peak shift was observed, suggesting that there was only one kind of fluorescent species existing in solutions. Therefore, TMPyP4 only stacked on top of TASQ **13** with a stoichiometry of 1:1 similar to the external end-stacking binding mode of

terminal G-quartets in a G-quadruplex.¹³⁸

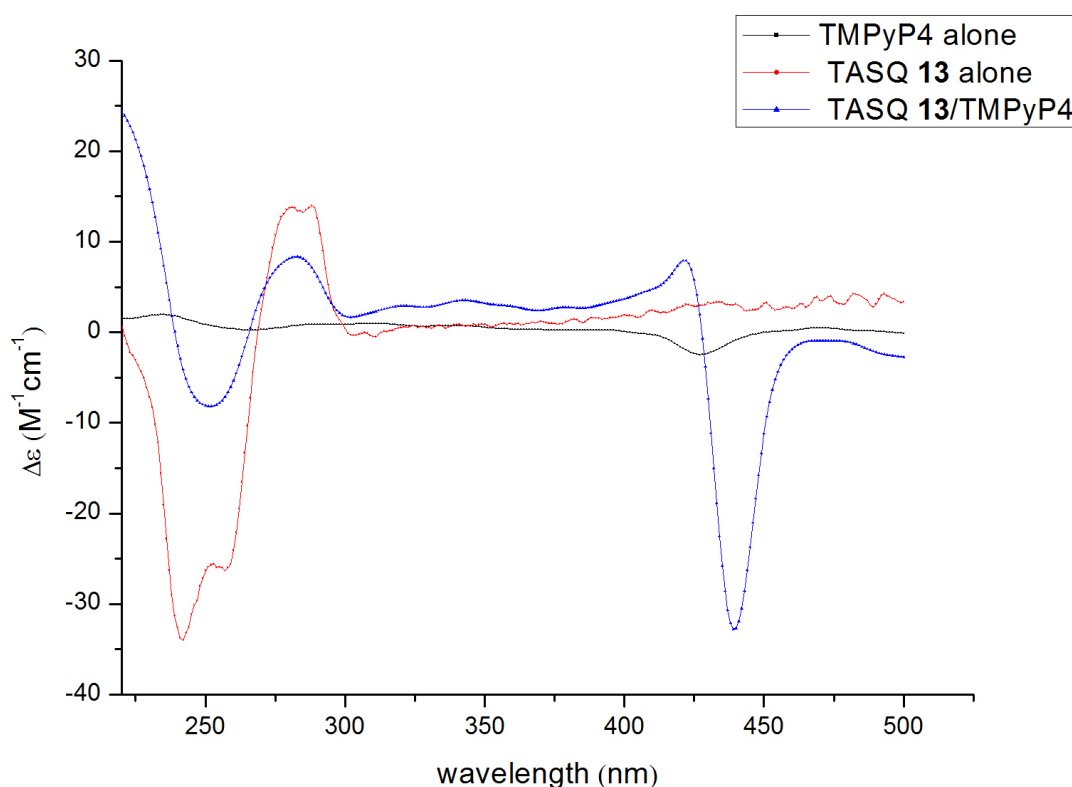
Fig 2.11 (a) Fluorescence binding plot of TMPyP4 (8 μM) on increasing TASQ **13** concentrations in the range 0-80 μM in 0.1 mM EDTA, 10 mM Tris-HCl (black); (b) Salt-affected fluorescence binding plot of TMPyP4 (8 μM) on increasing TASQ **13** concentrations in the range 0-80 μM in 0.1 mM EDTA, 10 mM Tris-HCl, 100 mM KCl (red).



As illustrated in the fluorescence binding plot (Fig 2.11 a), TMPyP4 was almost saturated when [TASQ **13**] : [TMPyP4] was greater than 4, and fully saturated when stoichiometry number was more than 6, thus suggesting that the Scatchard plot was drawn according to the appropriate maximum fluorescence intensity in saturated conditions. In addition, a corresponding salt-affected fluorescence binding plot (Fig 2.11 b) was drawn by additions of KCl (the final concentration of KCl

was 0.1 M) to the same series of titration samples. There was almost no change of the fraction of bound ligand, thus excluding electrostatic interactions between TMPyP4 and TASQ **13**. These experimental results were also consistent with a binding stoichiometry of 1:1 and an end-stacking binding mode. However, the previous study of TMPyP4 with the first generation hydrophilic TASQ (Fig 1.13 d) indicated a possible electrostatic interaction with TMPyP4.¹³⁹ This controversy can be explained by the steric hindrance around phosphate groups of TASQ **13** and the free arrangements of the three-carbon linked phosphate feet of the first generation hydrophilic TASQ (Fig 1.13 d).

Fig 2.12 (a) CD spectrum of TMPyP4 alone (10 μ M, black); (b) TASQ **13** alone (10 μ M, red); (c) TASQ **13** and TMPyP4 (10 μ M and 10 μ M, blue).



The CD spectrum (Fig 2.12) of TMPyP4/TASQ **13** complex at a stoichiometry of 1:1 showed a change in CD spectrum between 220-290 nm, similar to the CD spectrum of PIPER/TASQ **13**, revealing a similar conformational change of TASQ **13** upon TMPyP4 or PIPER binding. However, tosylate counterions of TMPyP4 have absorption in the range of 220-300 nm, so this conformational change may also result from the contribution of induced CD of tosylate anions. In contrast, nucleotides and tosylates have no absorption in the range of 450-650 nm, so the induced CD signal was entirely from the conformational change of TMPyP4 upon binding. Furthermore, there was a strong negative induced CD at about 435 nm. This signal can only be indirectly analyzed according to CD spectra of TMPyP4 with G-quadruplexes. In general, a negative induced CD reveals a stacking binding mode while a positive induced CD reveals an outside binding mode without stacking.¹⁴⁰ So this theory indirectly supports a stacking binding mode of TMPyP4 with TASQ **13**.

2.3.3 Interactions of AZATRUX with TASQ 13

Fig 2.13 Fluorescence spectrum of AZATRUX alone (0.5 μM) at pH 6.5 (pink), 7 (black), 7.5 (blue), and 8 (red).

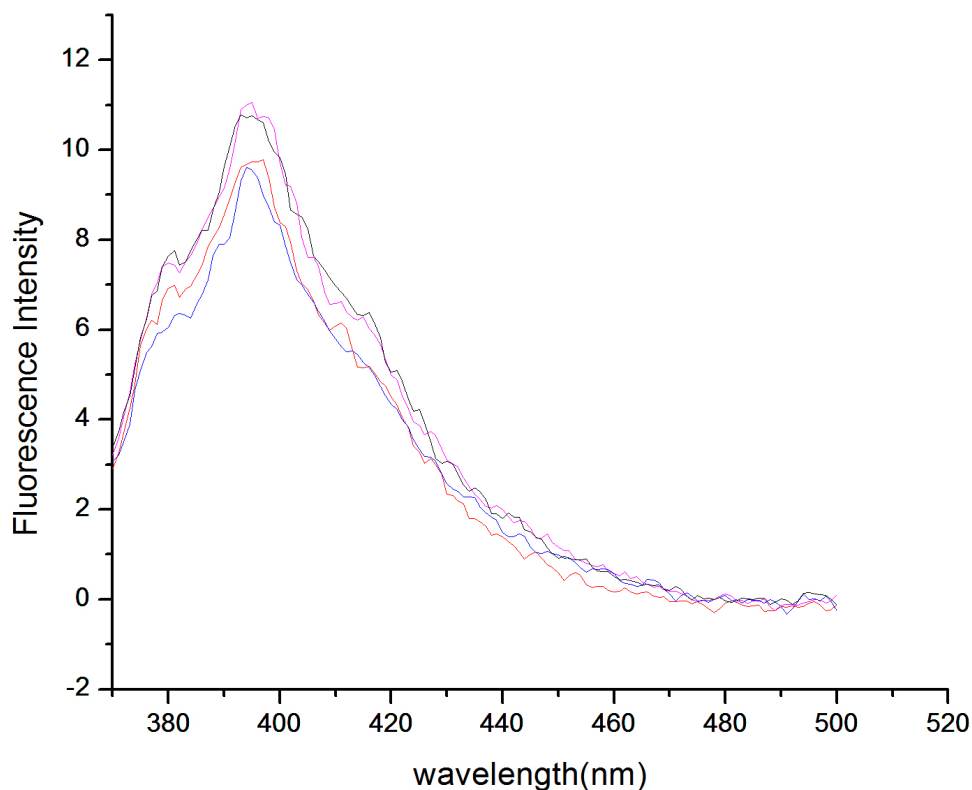


Fig 2.13 shows that the fluorescence intensity of AZATRUX had almost no change as pH decreased. This phenomenon matches previous $^1\text{H-NMR}$ results indicating AZATRUX existed in a monomeric form in water even in the micro molar concentration range at physiological pH, and previous UV-Vis spectra suggesting that AZATRUX obeyed Beer's law below the concentration of 20 μM at pH 6.5 or below.¹⁴¹ So the measuring concentration of AZATRUX was set at 3.6 μM at pH 8.

Fig 2.14 Job plot analysis of fluorescence binding data for AZATRUX and TASQ **13**. The total molar concentration ($[AZATRUX]+[TASQ\ 13]$) was $3.6\ \mu\text{M}$.

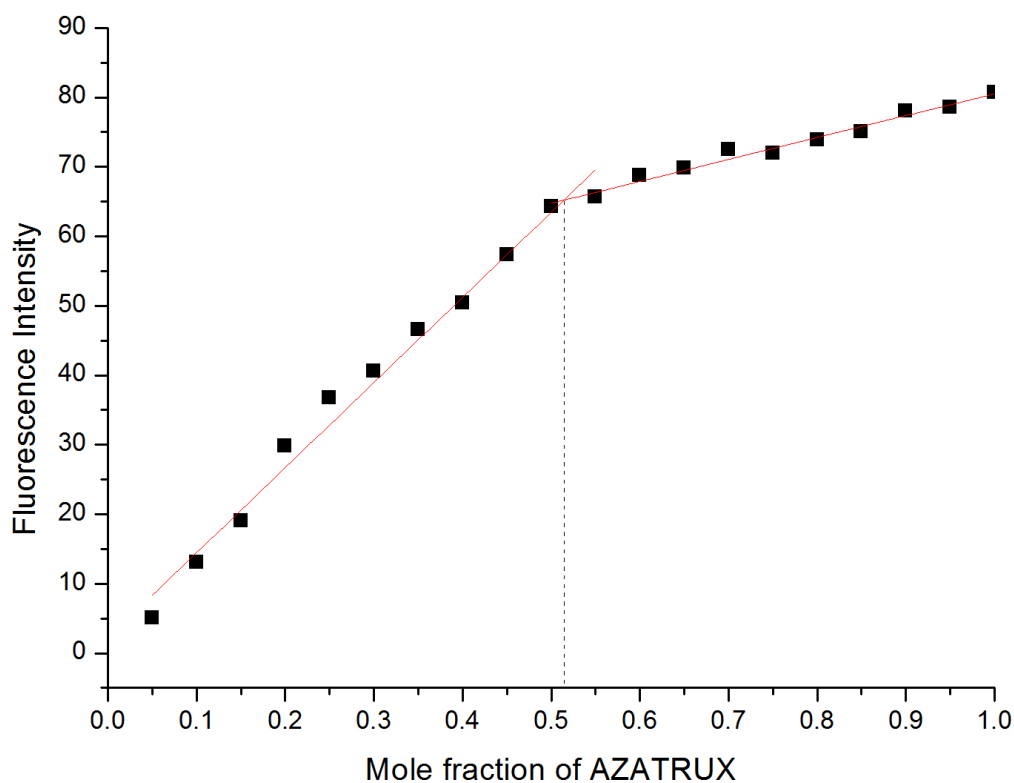


Fig 2.14 shows that the binding stoichiometry of AZATRUX to TASQ **13** was 1:1, which is consistent with the x-axis intercept ($=0.81$) of the Scatchard plot (Fig 2.15). The result also suggested that there was no external π - π stacking between AZATRUX and the aromatic rings of the cavitant template. The shape of the Job plot was also consistent with published results.¹⁴² Furthermore, the slope of the Scatchard plot between AZATRUX and TASQ **13** gave a binding constant ($K_{AZATRUX}$) of $2.55 \times 10^6\ \text{M}^{-1}$ within the previous reported range from $10^5\ \text{M}^{-1}$ to $10^8\ \text{M}^{-1}$ of G-quadruplex/AZATRUX binding.¹⁴³

Fig 2.15 Scatchard plot analysis of fluorescence binding data for AZATRUX (3.6 μM) in absence and presence of successive additions of TASQ **13** in the range of 0-36 μM at 25 $^{\circ}\text{C}$.

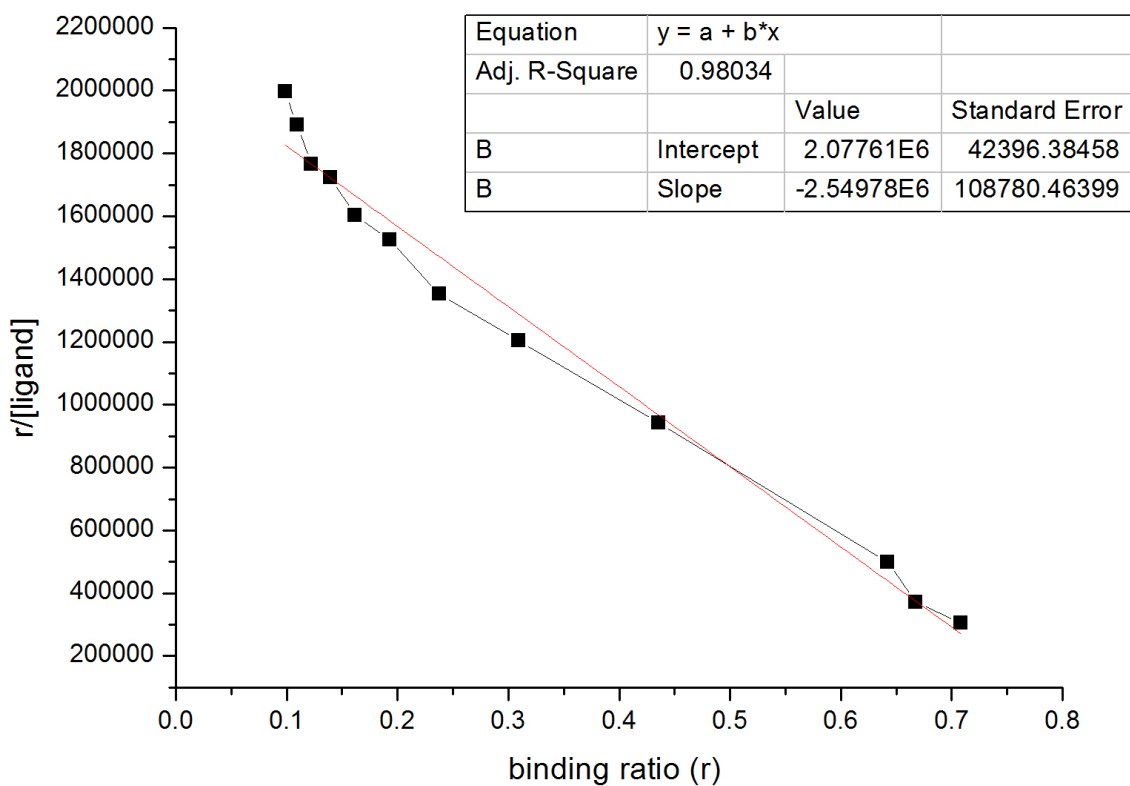
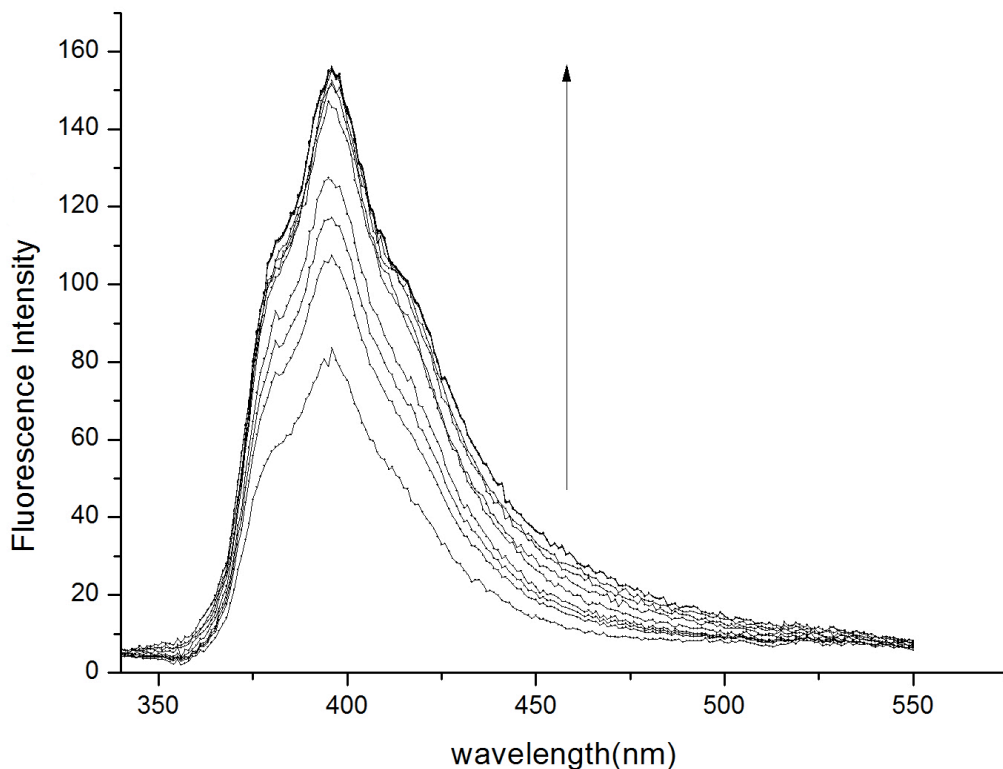


Fig 2.16 shows that the fluorescence intensity of AZATRUX gradually increased by additions of TASQ **13** mainly due to the exclusion of water molecules on the surface of AZATRUX; therefore the quenching of AZATRUX was reduced. Moreover, no significant peak shift was observed, suggesting that there was only one kind of fluorescent species existing in solutions. The previous fluorescence study of AZATRUX showed that the ligand can bind to a G-quadruplex via an external π - π stacking at terminal G-quartets, and no outside binding without stacking was found.¹⁴⁴ This result indirectly supports an end-stacking binding mode of AZATRUX to TASQ **13** with a stoichiometry of 1:1.

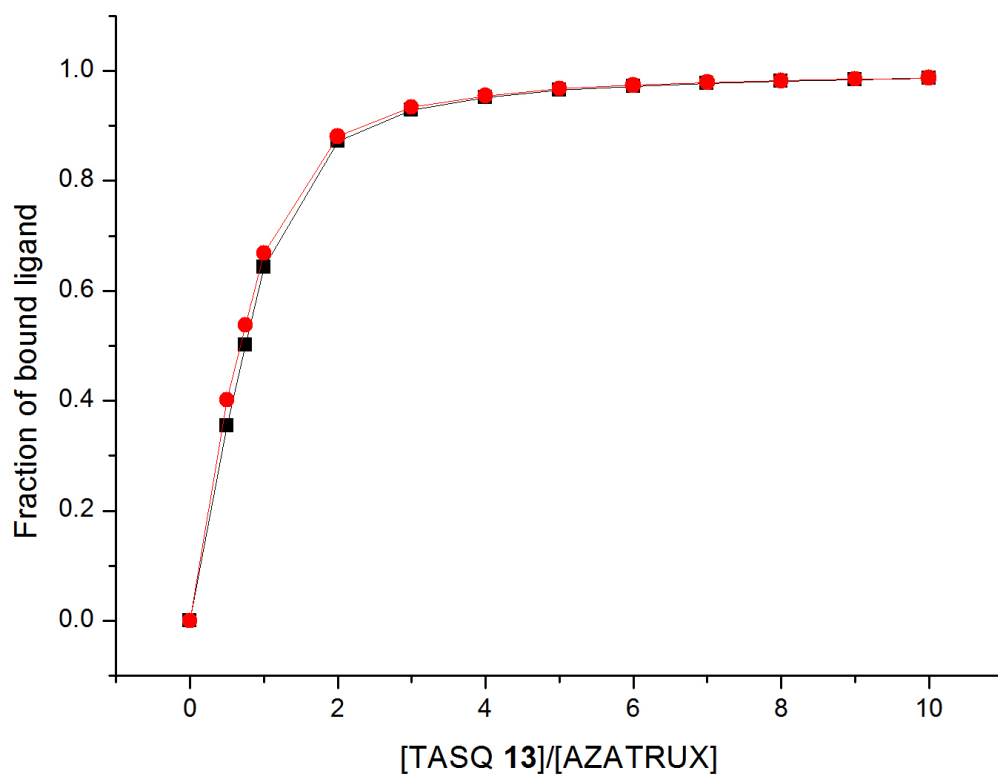
Fig 2.16 Fluorescence spectrum of AZATRUX (3.6 μM) in absence and presence of successive additions of TASQ **13** in the range of 0-36 μM at 25 $^{\circ}\text{C}$. Arrows indicate the increasing TASQ **13** concentrations.



A fluorescence binding plot (Fig 2.17 a) shows that AZATRUX was almost saturated when $[\text{TASQ } \mathbf{13}] : [\text{AZATRUX}]$ was greater than 2, and fully saturated when stoichiometry number was more than 4, thus suggesting that the Scatchard plot was drawn according to appropriate maximum fluorescence intensities in saturated conditions. In addition, a corresponding salt-affected fluorescence binding plot was drawn by additions of KCl (the final concentration of KCl was 0.1 M) to the same series of titration samples. There was no change of the fraction of bound ligand, thus

excluding electrostatic interactions between AZATRUX and TASQ 13. These experimental results were also consistent with the proposed binding mechanism mentioned above.

Fig 2.17 (a) Fluorescence binding plot of AZATRUX (3.6 μM) on increasing TASQ 13 concentrations in the range 0-36 μM in 0.1 mM EDTA, 10 mM Tris-HCl (black); (b) Salt-affected fluorescence binding plot of AZATRUX (3.6 μM) on increasing TASQ 13 concentrations in the range 0-36 μM in 0.1 mM EDTA, 10 mM Tris-HCl, 100 mM KCl (red).



2.3.4 Interactions of BSU 1051 with TASQ 13

Fig 2.18 Fluorescence spectrum of BSU 1051 alone (1 μM) at pH 6.5 (pink), 7 (black), 7.5 (blue), and 8 (red).

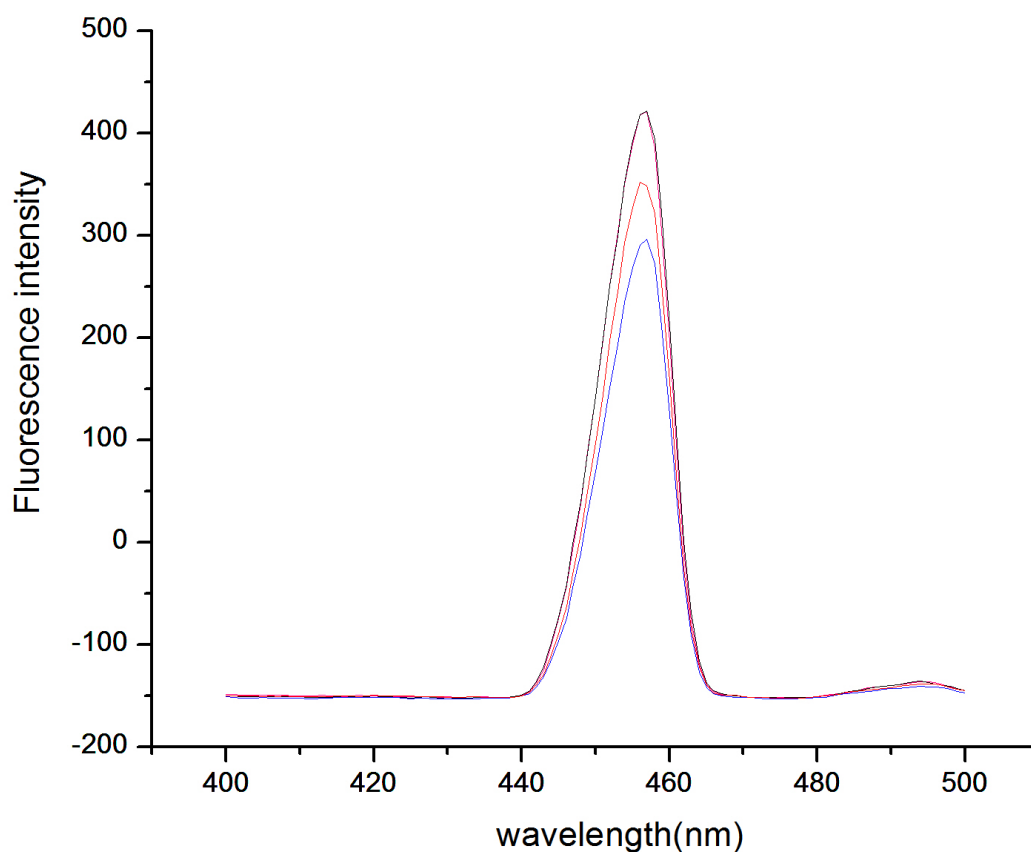
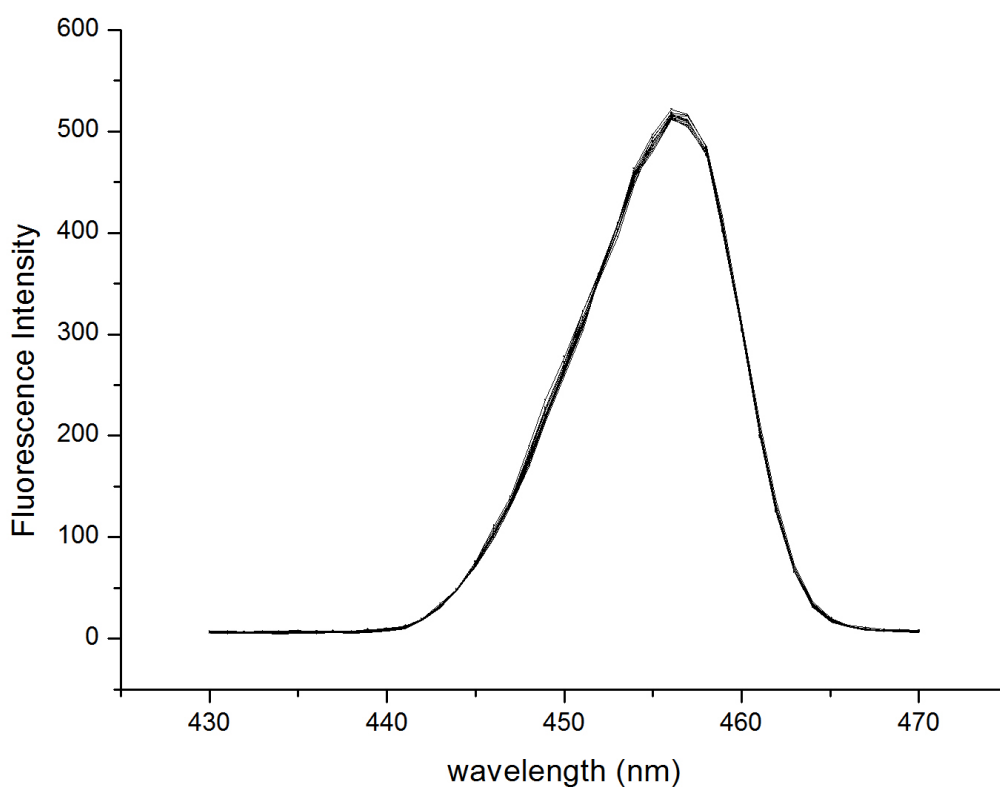


Fig 2.18 shows that the fluorescence intensity of BSU 1051 has almost no change from pH 6.5 to pH 7 due to a strong electrostatic repulsion between protonated side chains in acidic conditions; however, the intensity gradually decreases as pH increased from 7 to 8, which is consistent with the self-aggregation ability of BSU 1051 in a previous literature.¹⁴⁵ So the measuring concentration of

BSU 1051 was set at 1 μM at pH 7.

The binding mechanism of BSU 1051 to a G-quadruplex is not clear and is controversial. Neidle *et al.* proposed an external end-stacking binding mode by $^1\text{H-NMR}$ study;¹⁴⁶ in contrast, Hurley *et al.* proposed an intercalation-binding mode with NOSEY spectra,¹⁴⁷ which was also verified by Jenkins with molecular model study.¹⁴⁸

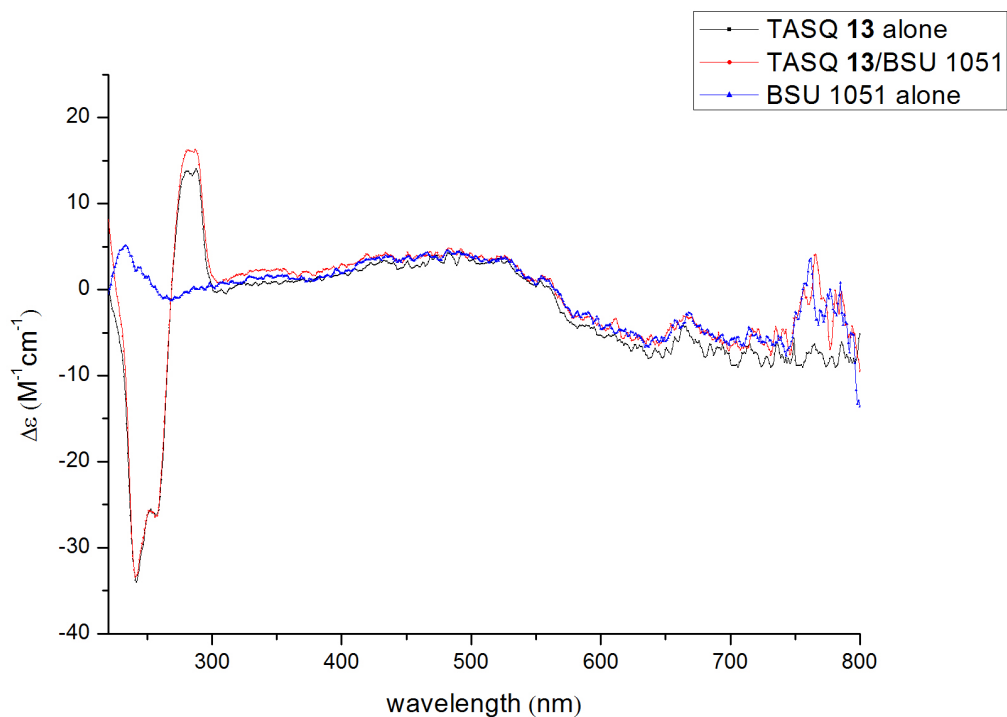
Fig 2.19 Fluorescence spectrum of BSU 1051 (1 μM) in absence and presence of successive additions of TASQ **13** in the range of 0-10 μM at 25 $^\circ\text{C}$.



A fluorescence spectrum of BSU 1051 (Fig 2.19) showed no fluorescence change upon additions of TASQ **13**, matching the proposed intercalation-binding mode of BSU 1051 to a G-quadruplex. A

CD spectrum (Fig 2.20) also showed no conformational change of TASQ **13** and no induced CD for BSU 1051, suggesting there was no interaction between TASQ **13** and BSU 1051. Since the stability constant of self-aggregation of BSU 1051 was about 10^3 M^{-1} and there was no enhanced fluorescence,¹⁴⁹ it indicated that the potential binding constant of BSU 1051 to TASQ **13** was less than 10^3 M^{-1} which might be too low for BSU 1051 to aggregate on top of terminal G-quartets of G-quadruplexes. In addition, previous studies showed critical roles of two side chains of BSU 1051, suggesting the binding behavior was mainly contributed from the residing of side chains in grooves or strong electrostatic interactions of side chains with G-quadruplexes rather than the weak interactions between the aromatic chromophore of BSU 1051 and the G-tetrad plane.¹⁵⁰ So it is reasonable that there was no interaction between BSU 1051 and TASQ **13**.

Fig 2.20 (a) CD spectrum of BSU 1051 alone (10 μM , blue); (b) TASQ **13** alone (10 μM , black); (c) TASQ **13** and BSU 1051 (10 μM and 10 μM , red).



2.3.5 Interactions of BRACO-19 with TASQ 13

Fig 2.21 Fluorescence spectrum of BRACO-19 alone (1 μM) at pH 6.5 (pink), 7 (black), 7.5 (blue), and 8 (red).

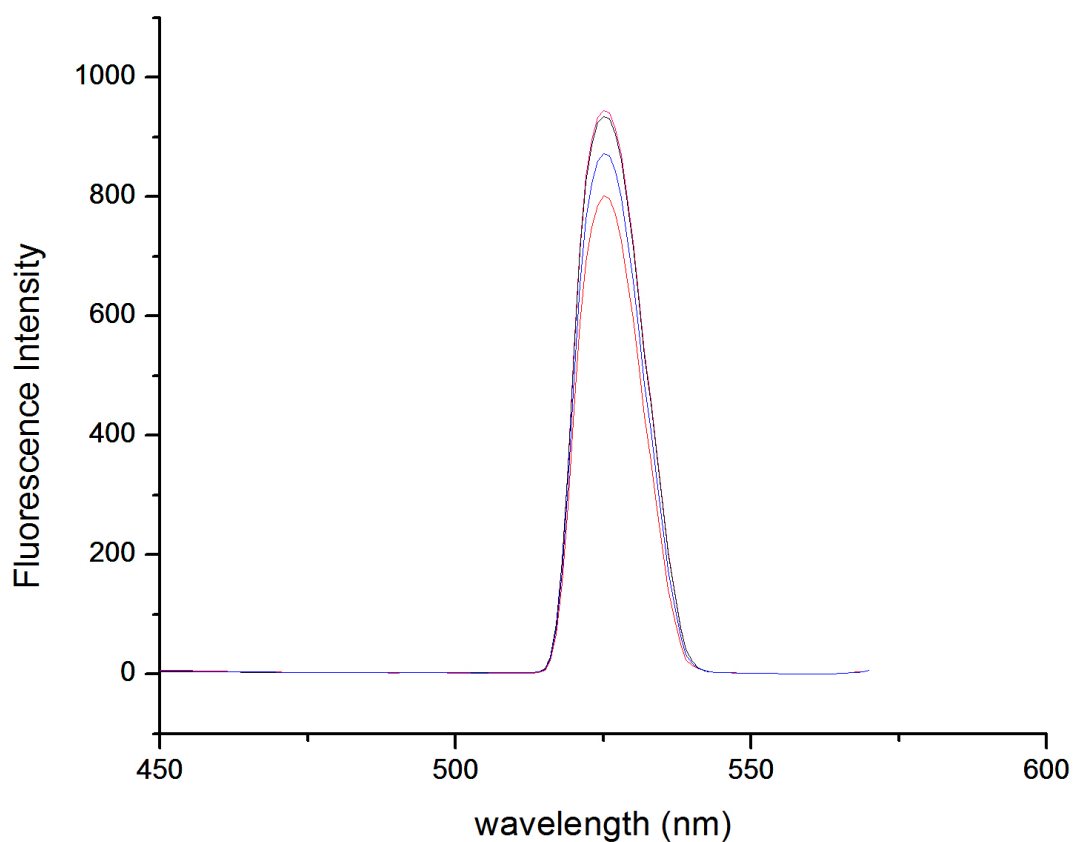
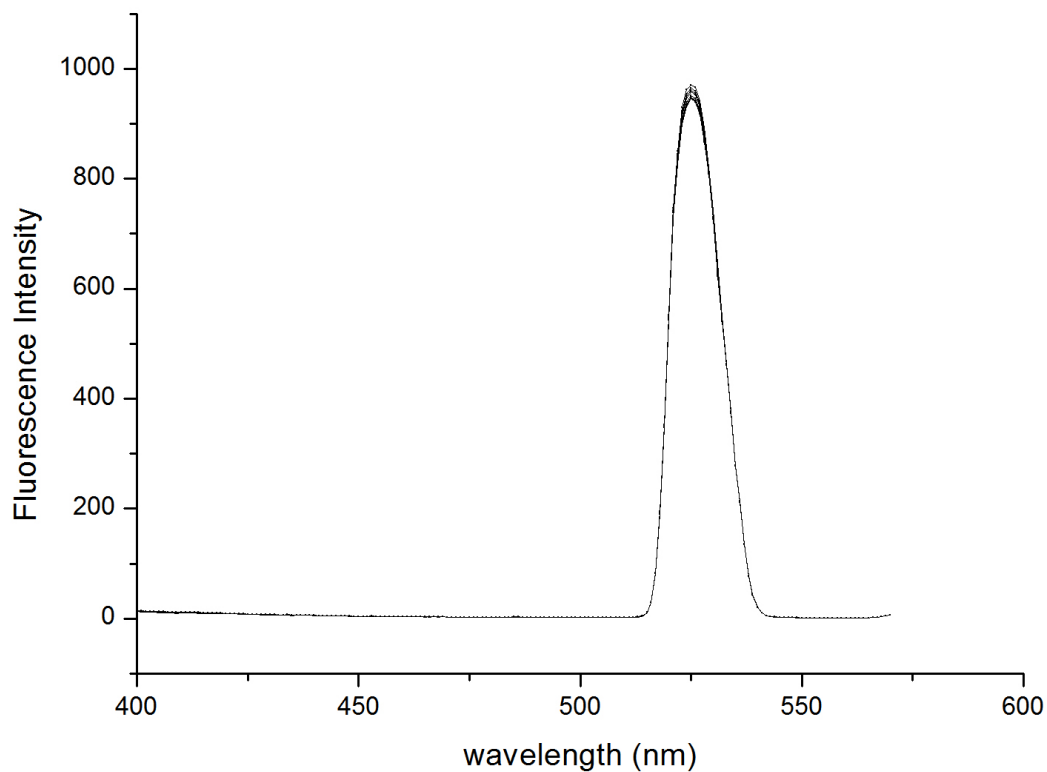


Fig 2.21 shows that the fluorescence intensity of BRACO-19 has almost no change from pH 6.5 to pH 7 due to a strong electronic repulsion between protonated side chains in acidic conditions; however, the intensity slightly decreases as pH increased from 7 to 8. This result is similar to the result of BSU 1051, maybe due to their similar central cores and the same 3,6-disubstituted side chains. So the measuring concentration of BRACO-19 was set at 1 μM at pH 7.

Fig 2.22 Fluorescence spectrum of BRACO-19 (1 μM) in absence and presence of successive additions of TASQ **13** in the range of 0-10 μM at 25 $^{\circ}\text{C}$.



The binding mechanism of BRACO-19 to a G-quadruplex has not been well studied and no fluorescence spectrum has been obtained before. Martin Read *et al.* performed a molecular modeling study showing that the acridine chromophore of BRACO-19 stacked on the surface of terminal G-quartets and all side chains resided in different grooves of G-quadruplexes.¹⁵¹ Mekala Gunaratnam *et al.* proposed that the acridine chromophore of BRACO-19 resided asymmetrically on top of the half surface of terminal G-quartets and the protonated nitrogen of acridine sit above the ion channel at the center of G-quadruplexes from a molecular modeling study.¹⁵² Campbell *et al.* proposed an intercalation-binding mode of BRACO-19 between a G-quartet and a TTAA tetrad by

the crystal structure of BRACO-19/biomolecular human telomeric G-quadruplex complexes, suggesting that BRACO-19 was not only stabilized by strong side-chain electrostatic interactions, but also by the thymine of TTAA tetrad and surrounding water molecules through H-bond.¹⁵³ In summary, the binding of BRACO-19 to a G-quadruplex is proposed to be via sophisticatedly three-dimensional interactions including feasible π - π stackings, electrostatic interactions, and hydrogen bonds. The absence of any of these interactions may result in weak binding affinities. So it is reasonable that the fluorescence spectrum of the Scatchard plot (Fig 2.22) showed no fluorescence change upon additions of TASQ **13**. Our template-assembled synthetic G-quartets can only resemble an isolated minimal G-quartet surface rather than grooves, loops and a TTAA tetrad.

2.4 Experimental

2.4.1 Synthesis of hydrophilic template-assembled synthetic G-quartets (TASQs) and ligands

General Procedures. All reagents and chemicals were purchased from standard suppliers and utilized without any further purification, except for the recrystallization of *N*-bromosuccinimide. THF was all freshly dried with sodium by distillation under nitrogen atmosphere. Pyridine was freshly dried by distillation under nitrogen atmosphere for the synthesis of **9**. DCM, DMSO, DMF, and ethyl acetate were all dried over 3 Å molecular sieves except that in the synthesis of **11** and **12**, ethyl acetate and hexane were purged with argon gas for 30 minutes prior to reactions. Methanol,

THF, and hexane were HPLC grade. Deuterated solvents were purchased from Cambridge Isotope Laboratories. All syringes were pre-dried in an 80 °C oven, and then flushed with argon gas at least three times. Reactions were monitored by TLC on 0.2 mm silica 60 F254 nm aluminum sheets. Silica gel (230-400 mesh, BDH) was used for flash chromatography. ¹H-NMR was performed on a Bruker AV-300 or AV-400 inv spectrometer. ¹H-NMR spectra were all referenced to a deuterium solvent signal. MALDI spectra were collected on a Bruker Biflex IV.

2,8,14,20-tetramethylpentacyclo[19.3.1.1^{3,7}.1^{9,13}.1^{15,19}]octacos-1(25),3,5,7(28),9,11,13(27),15,17,19(26),21,23-dodecaen-4,6,10,12,16,18,22,24-octol stereoisomer (2)¹⁵⁴

Resorcinol (100.00 g) was dissolved in 181 mL of H₂O, 181 mL of EtOH, and 90 mL of concentrated HCl. The mixture was cooled to 0 °C in an ice bath, and then 51 mL of CH₃CHO was added over 30 min by dropping funnel. The reaction was heated to 85 °C overnight. The crude products were filtered, and separated yellow needles were washed with cold 1:1 water/ethanol solvent until the filtrate was light yellow. The solid was dried under vacuum at 80 °C overnight. (C₃₂H₃₂O₈, 86.70 g, 70%)

5,11,17,23-tetrabromo-2,8,14,20-tetramethylpentacyclo-[19.3.1.1^{3,7}.1^{9,13}.1^{15,19}]octacos-1(25),3,5,7(28),9,11,13(27),15,17,19(26),21,23-dodecaene stereoisomer (3)¹⁵⁵

In a flame dried round bottom flask with a stir bar under an argon atmosphere, 1.00 g of crude **2**

and 2.62 g of freshly recrystallized dry NBS were added, followed by 25 mL of 2-butanone. After 10 min, the product started to crystallize. Stirring was continued for 4 h. The crude product was collected, washed with hot dichloromethane, and then dried under vacuum at 100 °C overnight. (C₃₂H₂₈O₈Br₄, 1.26 g, 80%)

7,11,15,28-tetrabromo-1,21,23,25-tetramethyl-2,20:3,19-dimetheno-1*H*,21*H*,23*H*,25*H*-bis[1,3]dioxocino[5,4-*i*:5',4'-*i*']benzodioxocin stereoisomer (4)

In the first way, a flame dried round bottom flask with a stir bar under an argon atmosphere was charged with 1.00 g of **3**, 6.00 g of K₂CO₃, and 0.64 mL of bromochloromethane. The reaction mixture was refluxed in 50 mL of DMSO under an argon atmosphere at 70 °C for 24 h. The crude product was cooled to room temperature, and carefully poured into 10% diluted HCl (100 mL). The crude product was filtered and dried overnight. The crude product was dry loaded onto silica gel and eluted with DCM. (C₃₆H₂₈O₈Br₄, 0.58 g, 55%)¹⁵⁶

In the second way, a flame dried sealed tube with a stir bar under an argon atmosphere was charged with 3.00 g of **3**, 9.00 g of K₂CO₃, 3.00 mL of bromochloromethane and 40 mL of dry DMSO. The mixture was stirred homogenously at 88 °C for 3 h. The crude product was cooled to room temperature, and carefully poured into 10% diluted HCl (100 mL). The crude product was filtered, dried overnight, dry loaded onto silica gel, and eluted with DCM. (C₃₆H₂₈O₈Br₄, 2.07 g, 65.5%)¹⁵⁷

MS (ESI) m/z: calculated: 908.2 for C₃₆H₂₉O₈Br₄ (M+H); found: 908.2

1,21,23,25-tetramethyl-2,20:3,19-dimetheno-1*H*,21*H*,23*H*,25*H*-bis[1,3]dioxocino[5,4-*i*:5',4'-*i'*]benzo[1,2-*d*:5,4-*d'*]-bis[1,3]benzodioxocin-7,11,15,28-tetrol (5)¹⁵⁸

Freshly dried HPLC grade THF by distillation under nitrogen atmosphere. In a flame dried round bottom flask with a stir bar under an argon atmosphere, 1.50 g of pure **4** was dissolved in 10 mL of dry THF and evaporated under vacuum three times. A suspension of **4** in 350 mL of dry warm THF was stirred until **4** was fully dissolved under Ar. The solution was then cooled to -78 °C in a dry ice/acetone bath. 8.8 mL of *n*-BuLi was syringed under an argon atmosphere balloon, and then added quickly to the solution. After 1 min, 1.70 mL of B(OMe)₃ was syringed and added. Then, the reaction mixture was warmed to ambient temperature gradually. After 3 h, the solution was cooled to -78 °C again, and 45 mL of 1.5 M NaOH-15% H₂O₂ was added. The mixture was warmed to room temperature gradually, and stirred overnight. 10 g of Na₂S₂O₅ was slowly added under an ice bath, and THF was removed *in vacuo*. The residue was acidified with 40 mL of 10% HCl, and then extracted with 40 mL of EtOAc three times. The organic layers were combined, washed with 50 mL of brine, dried with MgSO₄, and concentrated to 10 mL. The crude product was eluted by flash chromatograph with EtOAc : hexane (3:1), and then dried under vacuum overnight. (C₃₆H₃₂O₁₂, 380 mg, 35%)

MS (ESI) m/z: calculated: 656.6 for C₃₆H₃₃O₁₂ (M+H); found: 656.6

tetraethyl ester cavitand (6)¹⁵⁹

In a flame dried condenser linked round bottom flask with a stir bar under an argon atmosphere, 0.70 g of **5**, 0.94 mL of ethyl bromoacetate, and 0.88 g of potassium carbonate were suspended in acetone, and the mixture was refluxed under an argon atmosphere at 80 °C for 4 days. The mixture was cooled to room temperature, and the solvent was removed *in vacuo*. The residue was then washed with 20 mL of 10% HCl, and extracted with 20 mL of DCM three times. Organic layers were combined, washed with 50 mL of brine, dried with MgSO₄, concentrated to 10 mL, embedded onto silica gel, and then eluted with DCM: methanol (50:1) to yield pure **6** as a white solid. (C₅₂H₅₆O₂₀, 0.75g, 70%)

MS (ESI) m/z: calculated: 1023.3 for C₅₂H₅₆O₂₀Na (M+Na); found: 1023.3

tetraol cavitand (7)¹⁶⁰

In a flame dried round bottom flask with a stir bar under an argon atmosphere, 0.70 g of **6** was dissolved in 10 mL of dry THF, and coevaporated three times. Then, dry **6** was dissolved in 40 mL of dry THF and 0.32 g of LiAlH₄ was added to a round bottom flask very quickly under an argon atmosphere. After 4 h, the mixture was quenched with 1 mL of EtOAc, 1 mL of H₂O in an ice bath, followed by adding another 15 mL of 6N H₂SO₄. The aqueous layer was extracted three times with

20 mL of EtOAc. Organic layers were combined, washed with 50 mL of brine, dried with MgSO₄, concentrated to 10 mL, embedded on silica gel, and then eluted with DCM: methanol (50:1) to yield pure **7**. (C₄₄H₄₈O₁₆, 0.39 g, 67%)

MS (ESI) m/z: calculated: 856.3 for C₄₄H₄₉O₁₆ (M+H); found: 856.3.

2-*N*-isobutyryl-2'-deoxyguanosine (9**)¹⁶¹**

In a flame dried round bottom flask with a stir bar under an argon atmosphere, 1.34 g of **8** was coevaporated three times with dry pyridine, and then stirred in 50 mL of dry pyridine under argon atmosphere. 6.4 mL of trimethylchlorosilane was stirred with **8** for 15 min, followed by adding 8.2 mL of isobutyric anhydride. After 3 h, the reaction mixture was quenched with 10 mL of water in an ice bath. Then, another 10 mL of 29% ammonia was added. After 15 min, the solvent was removed *in vacuo*. The residue was re-dissolved in 50 mL of water and extracted with 50 mL of EtOAc: ether (1:1) once. The organic layer was reversely extracted with 50 mL of water twice. The combined aqueous layers were concentrated to 30 mL, and filtered to give **9**. (C₁₄H₁₉N₅O₅, 2.50g, 75%)

9-(5-*O*-*tert*-Butyldimethylsilyl-2-deoxy-β-*L*-*threo*-pentofuranosyl) guanine (10**)¹⁶²**

In a flame dried round bottom flask with a stir bar under an argon atmosphere, 0.60 g of **9** was

stirred with 0.60g of imidazoles in 22 mL of dry DMF at room temperature. The reaction mixture was then cooled to 0 °C in an ice bath under argon atmosphere, followed by adding 0.37 g of *tert*-butyldimethylsilyl chloride very quickly. After 45 minutes, the crude products were quenched with 0.5 mL of methanol, and the solvent was removed *in vacuo*. The residue was dissolved in 10 mL of DCM, embedded on silica gel, and then eluted with DCM:Methanol (10:1) to yield pure **10**. (C₁₆H₂₇N₅O₄Si, 0.80 g, 95%)

MS (ESI) m/z: calculated: 451.2 for C₁₆H₂₇N₅O₄Si (M+H); found: 451.6

phosphoramidites (11)

In a flame dried round bottom flask with a stir bar under an argon atmosphere, 1.49 g of **10** was dissolved in 6 mL of dry THF, and then coevaporated three times under an argon atmosphere. **10** residue was re-dissolved in 15 mL of dry THF, followed by adding *N,N*-diisopropylethylamine (2.3 mL) under an argon atmosphere. The reaction mixture was added dropwise with 2-cyanoethyl-*N,N*- diisopropylchlorophosphoramidite (0.9 mL) at room temperature. After 4 h, the solvent was removed *in vacuo*. The residue was re-dissolved in 50 mL of pre-purged ethyl acetate, extracted very quickly with 50 mL of saturated NaHCO₃ once, 50 mL of brine once, and dried with MgSO₄. The solvent was then quickly removed *in vacuo*. The residue was re-dissolved in 3 mL of pre-purged ethyl acetate, and then added dropwise into 400 mL of stirring cold hexanes at -78 °C under an argon atmosphere. The filtration funnel was dried under an argon atmosphere in advance.

The solution was quickly poured into a filtration funnel, and filtered after the filtration funnel was warmed to room temperature. Precipitate **11** was then coevaporated with dry THF three times, dried under vacuum, and stored under an argon atmosphere at -20 °C. (C₂₉H₅₀N₇O₆PSi, 1.90 g, 88%)

MS (ESI) m/z: calculated: 652.3 for C₂₉H₅₁N₇O₆PSi (M+H); found: 652.3

Template-assembled synthetic G-quartets (**13**)

In a flame dried round bottom flask with a stir bar under an argon atmosphere, **11** (0.65 g), (ethylthio)tetrazole (0.19 g), and tetraol cavitand **7** (50 mg) were all coevaporated with dry THF three times respectively. 5-(Ethylthio)tetrazole was dissolved in 6 mL of THF and then added dropwise to **11** in 6 mL of THF. After 5 min, **7** in 4 mL of THF was added dropwise to the solution at room temperature. After 4 h, the reaction mixture was cooled to 0 °C in an ice bath, and quenched with 1 mL of water, followed by adding 14 mL of 0.1 M iodine in THF: pyridine: water (80 : 20 : 2). After 5 min, the solvent was removed *in vacuo*. The residue was dissolved in DCM (40 mL), and extracted with 5% sodium metabisulfite (100 mL). The aqueous layer was reversely extracted two times with DCM (40 mL). Dichloromethane layers were combined, washed with 100 mL of saturated NaHCO₃ once, 100 mL of brine once, dried with MgSO₄, concentrated to 10 mL, embedded onto silica gel, and then eluted with DCM: methanol (20:1) to yield pure **12**. And then 6 mL of methanol and 6 mL of concentrated ammonia were stirred with **12** in a sealed falcon tube at 55 °C. After 16 h, the solvent was carefully removed *in vacuo* at 20 °C, and the residue was dried under vacuum

overnight. Then, the residue was stirred in 3 mL of 1M TBAF at room temperature. After 24 h, the reaction mixture was added to 15 mL of water, loaded onto a Sep-Pak Vac 12cc (2g) C18 cartridge, and then eluted with pure deionized water to pure methanol in 10% increments. Fractions in different solvents were analyzed by UV-Vis spectroscopy at 252 nm. Also, the reaction mixture can be concentrated to 10 mL, and then purified by HPLC with the same elution gradients. The desired fractions were coevaporated with water three times in order to remove the methanol. And then, the solution was lyophilized to yield desired pure **13** as white powders. (C₈₄H₉₄N₂₀O₄₀P₄, 5mg, 2.65%)

MS (MALDI-TOF) m/z: calculated: 2147.5 for C₈₄H₉₅N₂₀O₄₀P₄ (M-H); found: 2149.2.

***N, N'*-bis[2-(1-piperidino)ethyl]-3,4,9,10-perylenetetracarboxylic diimide (PIPER) (**15**)**¹⁶³

14 (0.20 g) was suspended in water (5 mL), followed by adding 1-(2-aminoethyl)piperidine (0.9 g). The reaction mixture was stirred at room temperature overnight. Then, the solution was filtered, washed with water, and dried under vacuum overnight to give **15**. PIPER (89 mg) was dissolved in concentrated HCl (4 mL), and treated with ultra sonication. The solution was added with 1 mL of water, filtered, washed with ether and dried to give hydrochloride salt PIPER as a purple solid. (C₂₄H₈O₆, 80 mg, 80%)

10,15-dihydro-5H-diindolo[3,2-a:3',2'-c]carbazole (17)¹⁶⁴

2.0 g of **16** were transferred to a flame dried round bottom flask with a stir bar under an argon atmosphere. POCl₃ (10 mL) was added through a condenser, and the mixture was refluxed at 100 °C under an argon atmosphere. After 8 h, the reaction mixture was quenched with ice in an ice bath, and then neutralized with a strong basic KOH solution until pH 7. The solution was filtered and washed thoroughly with water. The precipitate was dissolved in methanol, dry loaded onto silica gel, and then eluted with EtOAc: hexane (15:85) to give pure product **17** as a pale yellow solid. (C₂₄H₁₅N₃, 0.86 g, 50%)

MS (ESI) m/z: calculated: 346.4 for C₂₄H₁₆N₃ (M+H); found: 346.4

5,10,15-tris[4(1-piperidino)butyl]diindolo[3,2-a:3',2'-c]carbazole (AZATRUX) (19)¹⁶⁵

17 (355 mg) and KOH (576 mg) were dissolved in dry THF (20 mL) and coevaporated three times. The residue was dissolved in dry THF and 1,4-diiodobutane (2.0 mL) was added. The reaction mixture was refluxed at 72 °C under argon atmosphere. After 6 h, the solvent was removed *in vacuo*. The residue was dissolved in EtOAc (20 mL), washed with 10% aqueous HCl (20 mL), extracted with brine (20 mL), dried with MgSO₄, concentrated to 5 mL, embedded on silica gel, and then eluted with EtOAc: hexane (5:95) to yield pure **18** as a dark yellow viscous oil. **18** (209 mg) and piperidine (0.69 mL) were refluxed at 70 °C in dry THF under an argon atmosphere. The solvent was

removed *in vacuo*, and the residue was purified by flash chromatography with EtOAc saturated with 30% ammonia to give **19**. AZATRUX was then dissolved in a minimum amount of methanol/37% HCl (95:5), and then 2 mL of diethyl ether was added. The solution was stored at -20 °C overnight and filtered to give the hydrochloride salt of AZATRUX as a white solid. (C₅₁H₆₆N₆, 161 mg, 36%)

MS (ESI) m/z: calculated: 763.5 for C₅₁H₆₇N₆ (M+H); found: 763.5

2.4.2 Ligand binding studies

2.4.2.1 Preparation of the sample

Stock solutions of TASQ **13** (0.1 mM and 0.01 mM), PIPER (0.01 mM), TMPyP4 (0.01 mM), AZATRUX (0.01 mM), BSU 1051 (0.01 mM), and BRACO-19 (0.01 mM) were prepared in deionized water and stored at 4 °C in the dark to prevent decomposition. 10 mM Tris-HCl (at pH 6.5, 7, 7.5, and 8) and 0.1 mM EDTA buffers were selected according to the needs of different optical ligand studies. 10 mM Tris-HCl (at pH 6.5, 7, 7.5, and 8), 0.1 mM EDTA, 0.1 M KCl buffers were selected according to the needs of different salt-affected fluorescence binding plot studies. Titration samples were prepared by diluting an appropriate amount of ligands and TASQ **13** in buffer solutions to a total volume of 1000 µL, according to the final concentration of ligands and the ratio of [TASQ **13**] : [ligand]. All samples were heated at 90 °C for 5 minutes, slowly cooled to room

temperature, and then incubated overnight to anneal at 4 °C. All titration samples were prevented from light during the preparation and warmed up to room temperature before measuring.

2.4.2.2 Fluorescence emission spectroscopy

All fluorescence emission spectra of titration samples were collected on a Varian Eclipse fluorescence spectroscopy with a 1 mm × 1 cm quartz cell (excitation path length is 1 cm) for at least three times separate scans. All excitation and emission slits were set at 5 nm and the voltage was set at 800 V. PIPER was excited at 520 nm, and emission spectra were collected between 530 nm and 650 nm;¹⁶⁶ TMPyP4 was excited at 435 nm, and emission spectra were collected between 550 nm and 800 nm;¹⁶⁷ AZATRUX was excited at 320 nm, and the emission spectra were collected between 360 nm and 500 nm;¹⁶⁸ BSU 1051 was excited at 226 nm, and the emission spectra were collected between 400 nm and 500 nm; BRACO-19 was excited at 264 nm, and the emission spectra were collected between 500 nm and 600 nm.

To study the influence of pH on the fluorescence intensities of ligands, the concentrations of ligands were prepared as follows: [PIPER]=0.5 μM, [TMPyP4]=0.5 μM, [AZATRUX]=0.5 μM, [BSU 1051]=1 μM, [BRACO-19]=1 μM.

Job plots were used to analyze the stoichiometries between ligands and TASQ **13**. The concentrations of ligand and TASQ **13** were varied, while the sum of reactant concentrations was kept constant at 0.5 μM for PIPER, 8 μM for TMPyP4, 3.6 μM for AZATRUX. Maximum fluorescence intensities at 550 nm for PIPER, 660 nm for TMPyP4, and 394 nm for AZATRUX

were plotted versus the ligand initial mole fraction ($[\text{ligand}]_0 : [\text{TASQ } \mathbf{13}]_0$) to gain Job plots. Linear regression analysis of data was performed by using the software of Origin 8.0.

For the Scatchard plots and fluorescence binding plots, all ligand initial concentrations were kept constant at 0.5 μM for PIPER, 8 μM for TMPyP4, 3.6 μM for AZATRUX, 1 μM for BSU 1051 and BRACO-19. The ratios of $[\text{TASQ } \mathbf{13}] : [\text{ligand}]$ were increasing as 0, 0.5, 1, 2, 3, 4, 5, 6, 7, 8, 9, and 10. The maximum fluorescence intensities were collected at 550 nm for PIPER, 660 nm for TMPyP4, and 394 nm for AZATRUX. Fluorescence binding plots were performed to show the saturation of ligands, and obtained by plotting the fraction of bound ligand (γ) against the ratio of $[\text{TASQ } \mathbf{13}] : [\text{ligand}]$.¹⁶⁹ The fraction of bound ligand (γ) was obtained by a formula: $\gamma = (A_{\text{free}} - A_{\text{obs}}) / (A_{\text{free}} - A_{\text{sat}})$, where A_{free} is the maximum intensity of free ligand, A_{obs} is the maximum intensity of bound ligand, A_{sat} is the maximum intensity of saturated ligand. Scatchard plots were performed to show the stoichiometries and binding constants between the ligands and TASQ **13**, and obtained by plotting the binding ratio r against $r/[\text{ligand}]_{\text{bound}}$, where $[\text{ligand}]_{\text{bound}} = [\text{ligand}]_0 (1 - \gamma)$, $r = ([\text{ligand}]_0 - [\text{ligand}]_{\text{bound}}) / [\text{TASQ } \mathbf{13}]_0$. The analysis of data was performed by using the software of Origin 8.0. The standard errors of Scatchard plots were automatically generated by performing a regular linear fitting of original data without any customizations in Origin 8.0.

2.3.2.3 Circular dichroism (CD)

All CD spectra of titration samples were collected on a JASCO J-710 spectroscopy with a 1 cm path length quartz cell at room temperature, and only one series of samples were prepared. The ratio

of [ligand] : [TASQ 13] was 1:1. The concentrations of PIPER, TMPyP4, and BSU 1051 were all 10 μ M. CD Spectra were collected from 210 nm to 800 nm in 1 nm increments and averaged over 3 accumulations. The CD spectra of corresponding buffer solutions were collected so as to subtract the baselines. The analysis of data was performed by using the software of Origin 8.0.

2.5 Supplementary ^1H -NMR spectra

Fig 2.23 ^1H -NMR Spectrum of TASQ 13 in D_2O at 400 MHz

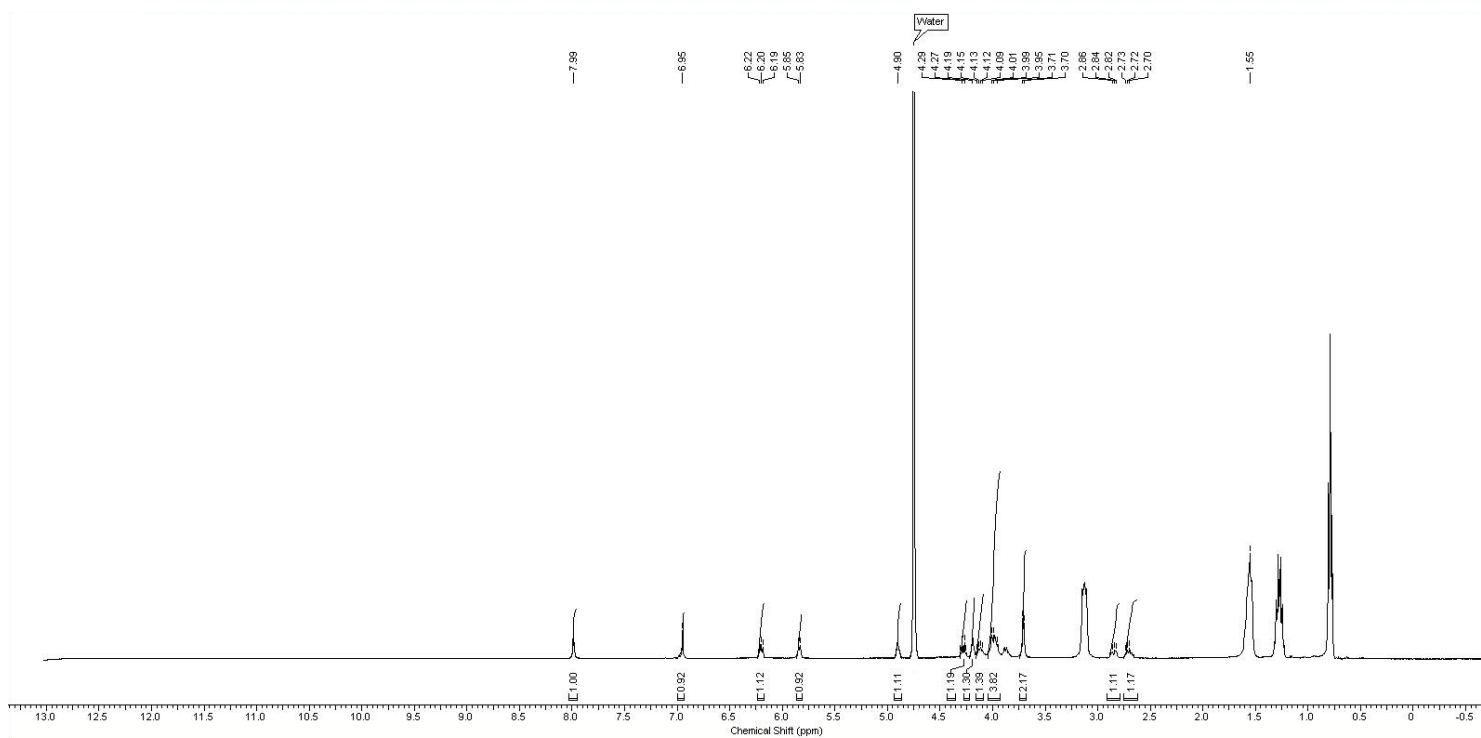


Fig 2.24 ^1H -NMR Spectrum of PIPER **15** in D_2O at 300 MHz

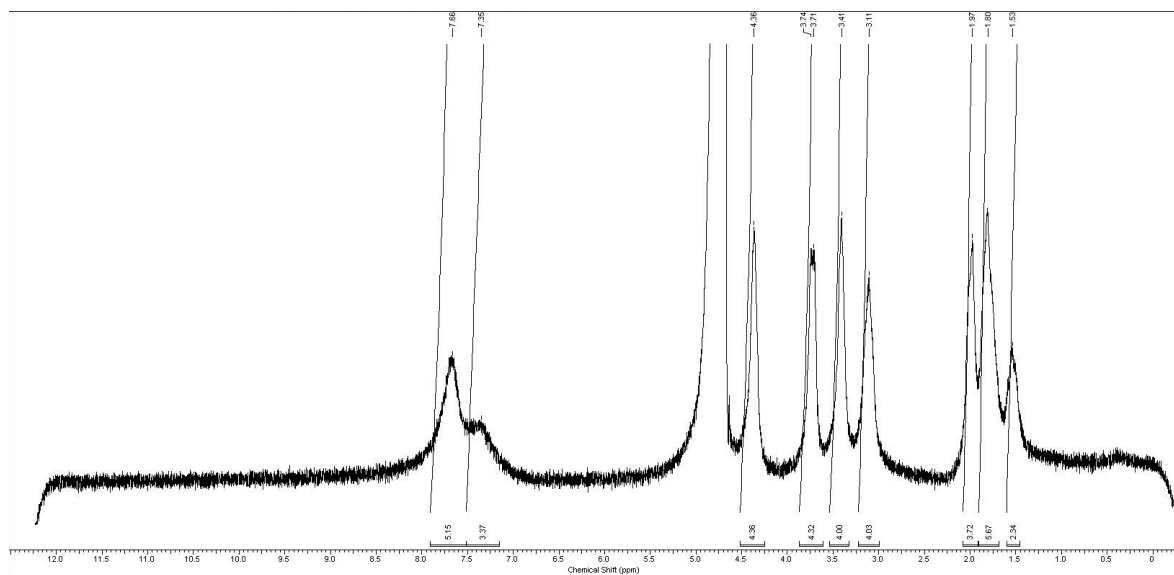
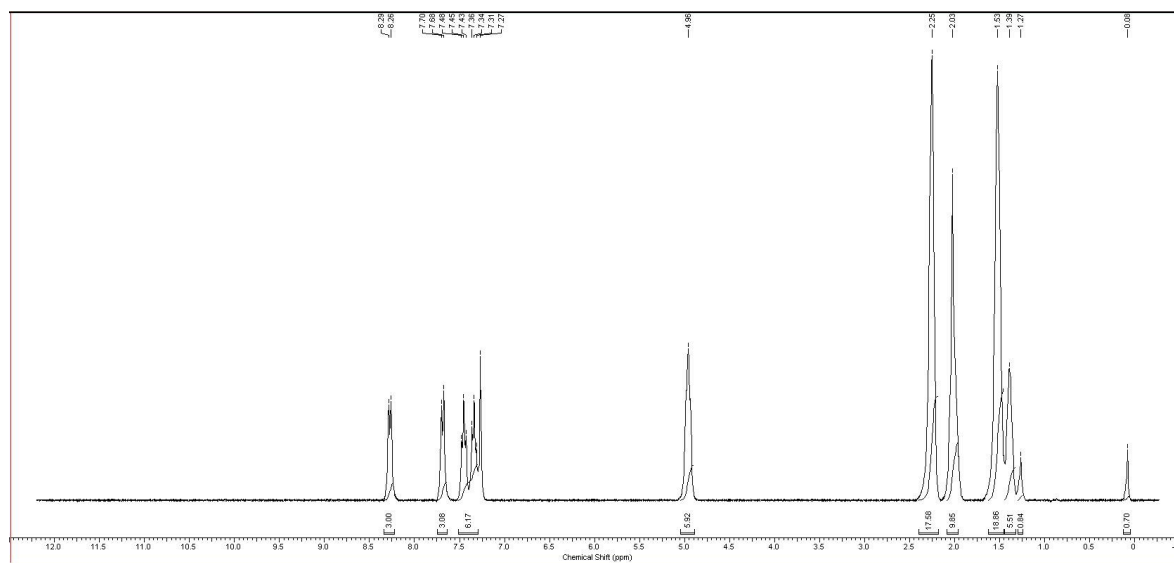


Fig 2.25 ^1H -NMR Spectrum of AZATRUX **19** in CDCl_3 at 300 MHz



CHAPTER 3 CONCLUSIONS AND FUTURE WORK

In order to investigate the biological functions of TASQ **13**, the author successfully synthesized TASQ **13**, PIPER, as well as AZATRUX, and then prepared a variety of ligand samples (*i.e.* PIPER, TMPyP4, AZATRUX, BSU 1051, and BRACO-19) so as to study interactions of TASQ **13**/ligand by fluorescence spectroscopy and CD spectroscopy. The conclusions are as follows:

1. PIPER can bind to TASQ **13** with a stoichiometry of 1:1 and an affinity of $1.65 \times 10^7 \text{ M}^{-1}$ on top of a G-tetrad plane via π - π stacking at pH 6.5, consistent with a qualitative CD study.
2. TMPyP4 can bind to TASQ **13** with a stoichiometry of 1:1 and an affinity of $8.5 \times 10^5 \text{ M}^{-1}$ on top of a G-tetrad plane via π - π stacking at pH 8, consistent with the model proposed by Grant Bare.¹⁷⁰
3. AZATRUX can bind to TASQ **13** with a stoichiometry of 1:1 and an affinity of $2.55 \times 10^6 \text{ M}^{-1}$ on top of a G-tetrad plane via π - π stacking at pH 8.
4. BSU 1051 has no interactions with TASQ **13**.
5. BRACO-19 has no interactions with TASQ **13**.
6. The binding mechanisms of biomimetic receptor TASQ **13** and ligands are similar to known mechanisms or computer-aided molecular simulation models, and TASQ **13** shows different selectivities over different ligands. Indeed, TASQ **13** can imitate the natural terminal G-tetrads of G-quadruplexes. This artificial receptor has promise to contribute to the screening of small-molecule anticancer drugs and may be helpful to understand the binding mechanism of new ligands.

Future research can be done as follows:

1. $^1\text{H-NMR}$ spectroscopy, X-Ray Crystallography, and molecular modeling can be done to investigate the detailed atomic-level structural parameters and topological assignments for TASQ **13**/ligand interactions.
2. TASQ **13** is worth being modified to simulate a more complex three-dimensional natural G-quadruplex structure.
3. TASQ **13** can be studied as a ligand to interact with human telomeric sequences or telomerase in different conditions.

REFERENCES

- (1) Watson, J. D.; Crick, F. H. C. *Nature*, **1953**, *171*, 737-738.
- (2) Bansal, M. *Curr. Sci.* **2003**, *85*, 1556-1563.
- (3) B-DNA double helix structure was drawn by Richard Wheeler in the public domain:
[http://en.wikipedia.org/wiki/File: A-DNA,_B-DNA_and_Z-DNA.png](http://en.wikipedia.org/wiki/File:A-DNA,_B-DNA_and_Z-DNA.png) (accessed June 6, 2012)
- (4) Bansal, M. *Curr. Sci.* **2003**, *85*, 1556-1563.
- (5) Franklin, R. E.; Gosling, R. G. *Nature*, **1953**, *171*, 740-741.
- (6) Franklin; Gosling, *Acta Cryst.* **1953**, *6*, 673-677.
- (7) Fuller, W.; Wilkins, M. H. F.; Wilson, H. R.; Hamilton, L. D. *J. Mol. Biol.* **1965**, *12*, 60-76.
- (8) Cheatham, T. E. *J. Am. Chem. Soc.* **1997**, *119*, 4805-4825.
- (9) Jones, S.; Van, Heyningen P.; Berman, H. M.; Thornton, J. M. *J. Mol. Biol.* **1999**, *287*, 877-896.
- (10) Ban, C.; Ramakrishnan, B.; Sundaralingam, M. *I. Biophys. J.* **1996**, *71*, 1215-1221.
- (11) Drawn by Richard Wheeler in the public domain: [http://en.wikipedia.org/wiki/File: A-DNA,_B-DNA_and_Z-DNA.png](http://en.wikipedia.org/wiki/File:A-DNA,_B-DNA_and_Z-DNA.png) (accessed June 6, 2012)
- (12) Gellert, M.; Lipsett, M. N.; Davies, *Proc. Nat. Acad. Sci.* **1962**, *48*, 2013-2018.
- (13) Ban, C.; Ramakrishnan, B.; Sundaralingam, M. *I. Biophys. J.* **1996**, *71*, 1215-1221.
- (14) Burge, S.; Parkinson, G. N.; Hazel, P.; Todd, A. K.; Neidle, S. *Nucleic Acids Res.* **2006**, *34*, 5402-5415.
- (15) Williamson, J. R. *Cell*, **1989**, *59*, 871-880.
- (16) Huppert, J. L. *Nucleic Acids Res.* **2007**, *35*, 2, 406-413.
- (17) Qin, Y.; Hurley, L. H. *Biochimie*, **2008**, doi: 10.1016.
- (18) Wilson, W. D. *Chem. Biol.* **2007**, *2*, 589-594.
- (19) Wilson, W. D. *Chem. Biol.* **2007**, *2*, 589-594.

- (20) Bates, P.; Mergny, J. L.; Yang, D. *EMBO Rep.* **2007**, *8*, 1003-1010.
- (21) Tian-mia, Ou; Lu, Yujing; Tan, Jiaheng; Huang, Z. S. *ChemMedChem*, **2008**, *3*, 690 – 713.
- (22) Tian-mia, Ou; Lu, Yujing; Tan, Jiaheng; Huang, Z. S. *ChemMedChem*, **2008**, *3*, 690 – 713.
- (23) Pendino, F.; Tarkanyi, I.; Dudognon, C.; Hillion, J.; Lanotte, M.; Aradi, J. *Curr. Cancer. Drug Targets*, **2006**, *6*, 147-180.
- (24) Liu, D. O.; Connor, M. S.; Safari, A.; Song, Yang Z. *J. Biol. Chem.* **2004**, *279*, 51338-51342.
- (25) Bryan, T. M.; Cech, T. R. *Curr. Opin. Cell. Biol.* **1999**, *11*, 318-322.
- (26) Wang, Y.; Patel, D. J. *Structure*, **1993**, *1*, 263-282.
- (27) Ambrus, A.; Chen, D.; Dai, J.; Bialis, T.; Jones, R. A.; Yang, D. *Nucleic Acid Res.* **2006**, *34*, 2723-2735.
- (28) Dai, J.; Carver, M.; Punchihewa, C. *Nucleic Acids Res.* **2007**, *35*, 4927-4970.
- (29) Shay, J. W.; Bacchetti, S. *Eur. J. Cancer.* **1997**, *33*, 787-791.
- (30) Cuesta, J.; Read, M. A.; Neidle, S. *Mini. Rev. Med. Chem.* **2003**, *3*, 11-21.
- (31) Bates, P.; Mergny, J. L.; Yang, D. *EMBO Rep.* **2007**, *8*, 1003-1010.
- (32) Wilson, W. D.; Sugiyama, H. *Chem. Biol.* **2007**, *2*, 589-594.
- (33) V. M. Ingram, *Nature*, **1956**, 792-794.
- (34) Blackburn, E. H.; Gall, J. G. *J. Mol. Biol.* **1978**, *120*, 33-53.
- (35) Lingner, J. *Proc. Natl. Acad. Sci. U. S. A.* **1996**, *93*, 10712-10717.
- (36) Lingner, J. *Curr. Opin. Genet. Dev.* **1998**, *8*, 226-232.
- (37) Griffith, J. D. *Cell*, **1999**, *97*, 503-514.
- (38) Rezler, E. M. *Annu. Rev. Pharmacol. Toxicol.* **2003**, *43*, 359-379.
- (39) De, C. A. *Biochimie*, **2008**, *90*, 131-155.
- (40) Stewart, S. A.; Weinberg, R. A. *Annu. Rev. Cell Dev. Biol.* **2006**, *22*, 531-557.
- (41) Helder, M. N.; Wisman, G. B. A.; Van der Zee A. G. J. *Cancer Invest.* **2002**, *20*, 82-101.

- (42) Riou, J. F.; Morjani, H. *Ann. Pharm. Fr.* **2006**, *64*, 97-105.
- (43) De, C. A.; Lacroix, L. *Biochimie*, **2008**, *90*, 131-155.
- (44) Rezler, E. M.; Bearss, D. J.; Hurley, L. H. *Curr. Opin. Pharmacol.* **2002**, *2*, 415-423.
- (45) Hurley, L. H. *Nat. Rev. Cancer*, **2002**, *2*, 188-200.
- (46) Tian-mia, Ou; Lu, Yujing; Tan, Jiaheng; Huang, Z. S. *ChemMedChem*, **2008**, *3*, 690 – 713.
- (47) Bates, P.; Mergny, J. L.; Yang, D. *EMBO Rep.* **2007**, *8*, 1003-1010.
- (48) Hazel, P.; Parkinson, G. N.; Neidle, S. *J. Am. Chem. Soc.* **2006**, *128*, 5480-5487.
- (49) Haq, I.; Ladbury, J. *J. Mol. Recognit.* **2000**, *12*, 188-197.
- (50) Monchaud, D.; Teulade-Fichou, M. P. *Org. Biomol. Chem.* **2008**, *6*, 627-636.
- (51) Wei, C.; Jia, G.; Yuan, J.; Feng, Z.; Li, C. *Biochemistry*, **2006**, *45*, 6681-6691.
- (52) Martino, L.; Virno, A.; Pagano, B.; Virgilio, A.; Micco, S. D.; Galeone, A.; Giancola, C.; Bifulco, G.; Mayol, L.; Randazzo, A. *J. Am. Chem. Soc.* **2007**, *129*, 16048-16056.
- (53) Parkinson, G. N.; Cuenca, F.; Neidle, S. *J. Mol. Biol.* **2008**, *381*, 1145-1156.
- (54) Rodriguez, R.; Dan, P. G.; Goncalves, D. P. N. *Angew. Chem. Int. Ed.* **2007**, *46*, 5405-5407.
- (55) L. H. Hurley; Wheelhouse, R. T.; Sun, D. *Pharmacology and Therapeutics*, **2000**, *85*, 141-158.
- (56) Neidle, S. *Methods*, **2007**, *43*, 245.
- (57) Masiero, S.; Trotta, R.; Pieraccini, S.; De Tito, S.; Perone, R.; Randazzo, A.; Spada, G. P. *Org. Biomol. Chem.* **2010**, *8*, 2683-2692.
- (58) Paramasivan, S.; Rujan, I.; Bolton, P. H. *Methods*, **2007**, *43*, 324-331.
- (59) Pasternack, R. F.; Caccam, M.; Keogh, B.; Stephenson, T. A.; Williams, A. P.; Gibbs, E. *J. Am. Chem. Soc.* **1991**, *113*, 6835-6840.
- (60) Pasternack, R. F.; Gibbs, E. J.; Villafranca, J. J. *Biochemistry*, **1983**, *22*, 2406-2414.
- (61) J. B. Lepecq; C. Paoletti. *J. Mol. Biol.* **1967**, *27*, 87-106.

- (62) Sun, D.; Thompson, B.; Cathers, B. E.; Salazar, M.; Kerwin, S. M.; Trent, J. O.; Jenkins, T. C.; Neidle, S.; Hurley, L. H. *J. Med. Chem.* **1997**, *40*, 2113-2116.
- (63) Fedoroff, O. Y.; Salazar, M.; Han, H. *Biochemistry*, **1999**, *38*, 6981-6986.
- (64) Kern, J. T.; Wang, T. P.; Kerwin, S. M. *Biochemistry*, **2002**, *41*, 11379-11389.
- (65) Han, H.; Cliff, C. L.; Hurley, L. H. *Biochemistry*, **1999**, *38*, 6981-6986.
- (66) Rangan, A.; Fedoroff, O. Y.; Hurley, L. H. *J. Biol. Chem.* **2001**, *276*, 4640-4646.
- (67) Han, H.; Langley, D. R.; Rangan, A. *J. Am. Chem. Soc.* **2001**, *123*, 8902-8913.
- (68) Kerwin, S. M.; Chen, G.; Kern, J. T. *Bioorg. Med. Chem. Lett.* **2002**, *12*, 447-450.
- (69) Wheelhouse, R. T.; Sun, D.; Han, H. *J. Am. Chem. Soc.* **1998**, *120*, 3261-3262.
- (70) Izbicka, E.; Wheelhouse, R. T.; Raymond, E. *Cancer Res.* **1999**, *59*, 639-644.
- (71) Han, H.; Langley, D. R.; Rangan, A. *J. Am. Chem. Soc.* **2001**, *123*, 8902-8913.
- (72) Wei, C.; Jia, G.; Yuan, J.; Feng, Z.; Li, C. *Biochemistry*, **2006**, *45*, 6681-6691.
- (73) Marco Franceschin, *Eur. J. Org. Chem.* **2010**, 134-141.
- (74) Luigi Petraccone, *Biochimie*, **2011**, *93*, 1318-1327.
- (75) Annunziata Cummaro; Iolanda Fotticchia; Franceschin, M.; Giancola Concetta; Luigi Petraccone, *Biochimie*, **2011**, *93*, 1392-1400.
- (76) Sun, D.; Thompson, B.; Cathers, B. E. *J. Med. Chem.* **1997**, *40*, 2113-2116.
- (77) Perry, P. J.; Gowan, S. M.; Reszka, A. P. *J. Med. Chem.* **1998**, *41*, 3253-3260.
- (78) Perry, P. J.; Reszka, A. P. *J. Med. Chem.* **1998**, *41*, 4873-4884.
- (79) Perry, P. J.; Jenkins, T. C. *Mini Rev. Med. Chem.* **2001**, *1*, 31-41.
- (80) Perry, P. J.; Jenkins, T. C. *Mini Rev. Med. Chem.* **2001**, *1*, 31-41.
- (81) Harrison, R. J.; Gowan, S. M.; Kelland, L. R. *Bioorg. Med. Chem. Lett.* **1999**, *9*, 2463-2468.
- (82) Read, M. A.; Wood, A. A.; Harrison, J. R. *J. Med. Chem.* **1999**, *42*, 4538-4546.

- (83) Harrison, R. J.; Cuesta, J.; Chessari, G.; Read, M. A.; Basra, S. K.; Reszka, A. P.; Morrell, J.; Gowan, S. M.; Incles, C. M.; Tanious, F. A.; Wilson, W. D.; Kelland, L. R.; Neidle, S. J. *J. Med. Chem.* **2003**, *46*, 4463-4476.
- (84) Read, M.; Harrison, R. J.; Romabnoli, B.; Tanious, F. A.; Gowan, S. H.; Reszka, A. P.; Wilson, W. D.; Kelland, L. R.; Neidle, S. *Proc. Natl. Acad. Sci. USA.* **2001**, *98*, 4844-4849.
- (85) Burger, A. M.; Dai, F.; Schultes, C. M. *Cancer Res.* **2005**, *65*, 1489-1496.
- (86) K. Shin-ya; K. Wierzba; K. I. Matsuo; T. Ohtani; Y. Yamada; K. Furihata; Y. Hayakawa; H. Seto, *J. Am. Chem. Soc.* **2001**, *123*, 1262-1263.
- (87) Kim, M. Y.; Gleason, G. M.; Izbicka, E.; Nishioka, D.; Hurley, L. H. *Cancer Res.* **2003**, *63*, 3247-3256.
- (88) Kim, M. Y.; Vankayalapati, H.; Shin-Ya, K. *J. Am. Chem. Soc.* **2002**, *124*, 2098-2099.
- (89) Gomez, D.; Aouali, N.; Renaud, A. *Cancer Res.* **2003**, *63*, 6149-6153.
- (90) Sumi, M.; Tauchi, T.; Sashida, G. *Int. J. Oncol.* **2004**, *24*, 1481-1487.
- (91) Otto, F. S.; George, W. G. *J. Am. Chem. Soc.* **1994**, *116*, 6089-6100.
- (92) Mehran Nikan; John Sherman, *Angew. Chem. Int. Ed.* **2008**, *47*, 4900-4902.
- (93) Grant Bare, Ph.D. thesis, **2012**, University of British Columbia.
- (94) Grant Bare, Ph.D. thesis, **2012**, University of British Columbia.
- (95) Mehran Nikan; John Sherman, *Angew. Chem. Int. Ed.* **2008**, *47*, 4900-4902.
- (96) Mehran Nikan; John Sherman, *J. Org. Chem.* **2009**, *74*, 5211-5218.
- (97) Mehran Nikan; Grant Bare; John Sherman, *Tetrahedron Letters*, *52*, **2011**, 1791-1793.
- (98) Vivian Mei-Yan Lau, Ligand-binding behavior of Templated-Assembled Synthetic G-Quartets, bachelor of science thesis, University of British Columbia, **2010**.
- (99) Grant Bare, Ph.D. thesis, **2012**, University of British Columbia.
- (100) Grant Bare, Ph.D. thesis, **2012**, University of British Columbia.

- (101) Anantha, N. V. *Biochemistry* 1998, 37, 2709-2714.
- (102) Vivian Mei-Yan Lau, Ligand-binding behavior of Templated-Assembled Synthetic G-Quartets, bachelor of science thesis, University of British Columbia, **2010**.
- (103) D. J. Cram; Stefan Karbach; Hye-Eun Kim; Carolyn, B. Knobler; Emily, F. Maverick; John, L. E.; Roger, C. H. *J. Am. Chem. Soc.* **1988**, 110, 2229-2237.
- (104) D. J. Cram; Stefan Karbach; Hye-Eun Kim; Carolyn, B. Knobler; Emily, F. Maverick; John, L. E.; Roger, C. H. *J. Am. Chem. Soc.* **1988**, 110, 2229-2237.
- (105) D. J. Cram; Stefan Karbach; Hye-Eun Kim; Carolyn, B. Knobler; Emily, F. Maverick; John, L. E.; Roger, C. H. *J. Am. Chem. Soc.* **1988**, 110, 2229-2237.
- (106) Esteban Roman; Carlos Peinador; Sandra Mendoza; Angel E. K. *J. Org. Chem.* **1999**, 64, 2577-2578.
- (107) Janet, R. Fraser; Bozena Borecka; James Trotter; John, C. S. *J. Org. Chem.* **1995**, 60, 1207-1213.
- (108) Francoise Arnaud-Neu; Elizabeth M. Collins; Mary Deasy; Ferguson, G.; Harris, S. J.; Kaitner, B.; Lough, A. J.; McKervey, M. A.; Marques, E.; Ruhl, B. L.; Marie, J. Schwing-Weill; Seward, E. M. *J. Am. Chem. Soc.* **1989**, 111, 8681-8691.
- (109) D. J. Cram; Karbach S.; Kim Y. H.; Baczynskyj L.; Marti, K.; Sampson, R. M.; Kalleymeyn, G. W. *J. Am. Chem. Soc.* **1988**, 110, 2554-2560.
- (110) G. S. Ti; B. L. Gaffney; Jones, R. A. *J. Am. Chem. Soc.* **1982**, 104, 1316-1319.
- (111) Arnaud Marchand; Christophe, M.; Jean, L. I.; Gosselin G. *Nucleosides, Nucleotides and Nucleic Acids*, **2000**, 19, 1, 205-217.
- (112) Claudia Sissi, *Biorganic & Medicinal Chemistry*, **2007**, 15, 555-562.
- (113) M. Franceschin, *Eur. J. Org. Chem.* **2010**, 134-141.
- (114) M. Franceschin, *Eur. J. Org. Chem.* **2010**, 134-141.

- (115) M. Franceschin, *Eur. J. Org. Chem.* **2010**, 134-141.
- (116) Grant Bare, PhD thesis, **2012**, University of British Columbia.
- (117) W. Tuntiwechapikul, *Bioorg. Med. Chem. Lett.* **2006**, *16*, 4120–4126.
- (118) S. M. Kerwin, *Bioorg. Med. Chem. Lett.* **2002**, *12*, 447–450.
- (119) William Ford, *Journal of Photochemistry*, **1987**, *37*, 189-204.
- (120) Vivian Mei-Yan Lau, Ligand-binding behavior of Templated-Assembled Synthetic G-Quartets, bachelor of science thesis, University of British Columbia, **2010**.
- (121) S. M. Kerwin, *Bioorg. Med. Chem. Lett.* **2002**, *12*, 447–450.
- (122) H. Dincalp, *Journal of Photochemistry and Photobiology A: Chemistry*, **2007**, *185*, 1–12.
- (123) Valentina, C.; Antonello, A.; Bianco, A.; Ortaggi, G.; Marco, F.;
J.Mass.Spectrom. **2009**, *44*, 530–54.
- (124) H. Dincalp, *Journal of Photochemistry and Photobiology A: Chemistry*, **2007**, *185*, 1–12.
- (125) H. Dincalp, *Journal of Photochemistry and Photobiology A: Chemistry*, **2007**, *185*, 1–12.
- (126) William Ford, *Journal of Photochemistry*, **1987**, *37*, 189-204.
- (127) W. Tuntiwechapikul, *Bioorg. Med. Chem. Lett.* **2006**, *16*, 4120–4126.
- (128) Claudia Sissi, *Biorganic & Medicinal Chemistry*, **2007**, *15*, 555-562.
- (129) Garbett, N. C. *Nat. Protoc.* **2007**, *2*, 3166-3172.
- (130) Grant Bare, Ph.D. thesis, **2012**, University of British Columbia.
- (131) Kano, K.; Minamizono, H.; Kitae, T.; Negi, S. *J. Phys. Chem. A*, **1997**, *101*, 6118-6124.
- (132) Grant Bare, Ph.D. thesis, **2012**, University of British Columbia.
- (133) Annunziata Cummaro; Iolanda Fotticchia; Franceschin, M.; Giancola Concetta; Luigi Petraccone, *Biochimie*, **2011**, *93*, 1392-1400.
- (134) Grant Bare, Ph.D. thesis, **2012**, University of British Columbia.

- (135) Grant Bare, Ph.D. thesis, **2012**, University of British Columbia.
- (136) Grant Bare, Ph.D. thesis, **2012**, University of British Columbia.
- (137) Ravi Jasuja, *J. Phys. Chem. B*, **1997**, *101*, 1444-1450.
- (138) Phan, A. *Nat. Chem. Biol.* **2005**, *1*, 167-173.
- (139) Vivian Mei-Yan Lau, Ligand-binding behavior of Templated-Assembled Synthetic G-Quartets, bachelor of science thesis, University of British Columbia, **2010**.
- (140) Narayanan, V. A.; Azam, M.; Sheardy, R. D. *Biochemistry*, **1998**, *37*, 2709-2714.
- (141) Marco Franceschin, *Eur. J. Org. Chem.* **2010**, 134-141.
- (142) Annunziata Cummaro; Iolanda Fotticchia; Franceschin M.; Giancola Concetta; Luigi Petraccone, *Biochimie*, **2011**, *93*, 1392-1400.
- (143) Annunziata Cummaro; Iolanda Fotticchia; Franceschin M.; Giancola Concetta; Luigi Petraccone, *Biochimie*, **2011**, *93*, 1392-1400.
- (144) Annunziata Cummaro; Iolanda Fotticchia; Franceschin M.; Giancola Concetta; Luigi Petraccone, *Biochimie*, **2011**, *93*, 1392-1400.
- (145) Ihtshamul Haq, *J. Am. Chem. Soc.* **1996**, *118*, 10693-10701.
- (146) Read, M. A.; Neidle, S. *Biochemistry*, **2000**, *39*, 13422-13432.
- (147) L. H. Hurley, *Pharmacology and Therapeutics*, **2000**, *85*, 141-158.
- (148) Ihtshamul Haq; John, E. L.; Babur, Z. C.; Terence, C. J. *J. Am. Chem. Soc.* **1996**, *118*, 10693-10701.
- (149) Ihtshamul Haq; John, E. L.; Babur, Z. C.; Terence, C. J. *J. Am. Chem. Soc.* **1996**, *118*, 10693-10701.
- (150) L. H. Hurley, *Pharmacology and Therapeutics*, **2000**, *85*, 141-158.
- (151) Martin Read, *PNAS*, **2001**, 4844-4849.

- (152) Mekala, G. *J. Med. Chem.* **2009**, *52*, 3774–3783.
- (153) N. H. Campbell, *J. Am. Chem. Soc.* **2008**, *130*, 6722–6724
- (154) D. J. Cram; Stefan Karbach; Hye-Eun Kim; Carolyn B. Knobler; Emily F. Maverick; John L. Ericson; Roger C. Helgeson. *J. Am. Chem. Soc.* **1988**, *110*, 2229-2237.
- (155) D. J. Cram; Stefan Karbach; Hye-Eun Kim; Carolyn B. Knobler; Emily F. Maverick; John L. Ericson; Roger C. Helgeson. *J. Am. Chem. Soc.* **1988**, *110*, 2229-2237.
- (156) D. J. Cram; Stefan Karbach; Hye-Eun Kim; Carolyn B. Knobler; Emily F. Maverick; John L. Ericson; Roger C. Helgeson. *J. Am. Chem. Soc.* **1988**, *110*, 2229-2237.
- (157) Esteban Roman; Carlos Peinador; Sandra Mendoza; Angel, E. K. *J. Org. Chem.* **1999**, *64*, 2577-2578.
- (158) Janet R. Fraser; Bozena Borecka; James Trotter; John C. S. *J. Org. Chem.* **1995**, *60*, 1207-1213.
- (159) Francoise Arnaud-Neu; Elizabeth M. Collins; Mary Deasy; Ferguson G.; Harris S. J.; Kaitner B.; Lough, A. J.; McKervey, M. A.; Marques, E.; Ruhl, B. L.; Marie J. Schwing-Weill; Seward, E. M. *J. Am. Chem. Soc.* **1989**, *111*, 8681-8691.
- (160) D. J. Cram; Karbach S.; Kim, Y. H.; Baczynskyj, L.; Marti, K.; Sampson, R. M.; Kallemeyn, G. W. *J. Am. Chem. Soc.* **1988**, *110*, 2554-2560.
- (161) G. S. Ti; B. L. Gaffney; Jones, R. A. *J. Am. Chem. Soc.* **1982**, *104*, 1316-1319.
- (162) Arnaud Marchand; Christophe M.; Jean, L. I.; Gosselin G. *Nucleosides, Nucleotides and Nucleic Acids*, **2000**, *19*, 1, 205-217.
- (163) Claudia Sissi, *Biorganic & Medicinal Chemistry*, **2007**, *15*, 555-562.
- (164) Luca Ginnari-Satriani, *Org. Biomol. Chem.* **2009**, *7*, 2513-2516.
- (165) Luca Ginnari-Satriani, *Org. Biomol. Chem.* **2009**, *7*, 2513-2516.
- (166) Claudia Sissi, *Biorganic & Medicinal Chemistry*, **2007**, *15*, 555-562.

- (167) Annunziata Cummaro; Iolanda Fotticchia; Franceschin M.; Giancola Concetta; Luigi Petraccone, *Biochimie*, **2011**, *93*, 1392-1400.
- (168) Annunziata Cummaro; Iolanda Fotticchia; Franceschin M.; Giancola Concetta; Luigi Petraccone, *Biochimie*, **2011**, *93*, 1392-1400.
- (169) Vivian Mei-Yan Lau, Ligand-binding behavior of Templated-Assembled Synthetic G-Quartets, bachelor of science thesis, University of British Columbia, **2010**.
- (170) Grant Bare, Ph.D. thesis, *2012*, University of British Columbia.